Energy Research and Development Division
FINAL PROJECT REPORT

ENABLING RENEWABLE FUELS THROUGH FLEXIBLE BURNERS

Prepared for: California Energy Commission
Prepared by: UCI Combustion Laboratory

UCI COMBUSTION LABORATORY
UNIVERSITY of CALIFORNIA • IRVINE

JUNE 2016
CEC-500-2016-041

PREPARED BY:

Primary Author(s):
Anthony Jordan
Andres Colorado
Zhixuan Duan
Dr. Vincent McDonell

UCI Combustion Laboratory
University of California, Irvine
131 Engineering Laboratory Facility
Irvine, California 92697-3550
Tel: (949) 824-5950 x121
Fax: (949) 824-7423

Contract Number: 500-10-048

Prepared for:

California Energy Commission

Anish Gautam, P.E.
Project Manager

Virginia Lew
Office Manager
Energy Efficiency Research Office

Laurie ten Hope
Deputy Director
Energy Research and Development

Robert P. Oglesby
Executive Director

DISCLAIMER

This report was prepared as the result of work sponsored by the California Energy Commission. It does not necessarily represent the views of the Energy Commission, its employees or the State of California. The Energy Commission, the State of California, its employees, contractors and subcontractors make no warranty, express or implied, and assume no legal liability for the information in this report; nor does any party represent that the uses of this information will not infringe upon privately owned rights. This report has not been approved or disapproved by the California Energy Commission nor has the California Energy Commission passed upon the accuracy or adequacy of the information in this report.

ACKNOWLEDGEMENTS

The support of Mr. Nathan Kirksey and Mr. Dimas Avila during the many hours of collecting data for the performance mapping portion of the project was very valuable and helpful.

PREFACE

The California Energy Commission Public Interest Energy Research (PIER) Program supports public interest energy research and development that will help improve the quality of life in California by bringing environmentally safe, affordable, and reliable energy services and products to the marketplace.

The PIER Program conducts public interest research, development, and demonstration (RD&D) projects to benefit California.

The PIER Program strives to conduct the most promising public interest energy research by partnering with RD&D entities, including individuals, businesses, utilities, and public or private research institutions.

PIER funding efforts are focused on the following RD&D program areas:

- Buildings End-Use Energy Efficiency
- Energy Innovations Small Grants
- Energy-Related Environmental Research
- Energy Systems Integration
- Environmentally Preferred Advanced Generation
- Industrial/Agricultural/Water End-Use Energy Efficiency
- Renewable Energy Technologies
- Transportation

Enabling Renewable Fuels Through Flexible Burners: Final Report is the final report for subaward POEFo2-V10 under CEC interagency agreement 500-10-048, conducted by University of California, Irvine Combustion Laboratory. The information from this project contributes to Public Interest Energy Research's (PIER) Industrial/Agricultural/Water End-Use Energy Efficiency Program.

For more information about the PIER Program, please visit the Energy Commission's website at www.energy.ca.gov/research/ or contact the Energy Commission at 916-654-4878.

ABSTRACT

The use of natural gas as an energy source has increased in popularity due to its economic, as well as its environmental benefits. However, defining a standard composition mixture for natural gas can be problematic. Consequently, burners must be able to adapt to changing fuel composition when meeting emission regulation standards, preventing hardware degradation caused by flame instability, and maintaining high combustion efficiency. The research team at the University of California, Irvine used a scaled version of a Coen Quantum Low NO_x™ burner to study the applicability of fuel flexible technology using optimization search algorithms. To satisfy the four main categories required to make burner fuel flexible, a variety of sensors were incorporated into the system: 1. fuel identification and properties; 2. flame stability; 3. emissions; and 4. efficiency. Two optimization search algorithms were used to investigate sensor information which generated detailed performance maps: Powell's Direction-Set method and Downhill Simplex method. The Powell's Direction-Set algorithm reliably found acceptable optimal operating conditions for a variety of simulated scenarios, but it also required a number of iterations to converge to a solution. Conversely, the Downhill Simplex algorithm was quick to converge, but it had a higher failure rate. This project demonstrated the burner's fuel-flexible capabilities using both the Powell's Direction-Set and Downhill Simplex algorithms. The simulation approach proved to successfully predict trends with the addition of higher hydrocarbons—namely, an increase in the oxides of nitrogen emissions levels. The research team at the University of California, Irvine also used the results from this project to compare emission trend predictions using a computational fluid dynamic and chemical reactor network model, which had already been developed in previous work

Keywords: Fuel interchangeability, industrial boiler, fuel composition, flame stability, NO_x emissions, oxides of nitrogen emissions, Powell's direction-set method, downhill simplex method

Please use the following citation for this report:

Jordan, Anthony, Colorado, Andres, Duan, Zhixuan and McDonell, Vincent. (University of California, Irvine). 2013. *Enabling Renewable Fuels Through Flexible Burners: Final Report.* California Energy Commission. Publication number: CEC-500-2016-041

TABLE OF CONTENTS

Acknowledgements ..... **i**

PREFACE ..... **ii**

ABSTRACT ..... **iii**

TABLE OF CONTENTS ..... **iv**

LIST OF FIGURES ..... **vi**

EXECUTIVE SUMMARY **1**

Introduction 1

Project Purpose 1

Project Results 2

Project Benefits 3

CHAPTER 1: Introduction **1**

CHAPTER 2: Background **2**

2.1 NO_x Formation and Control 2

2.1.1 Definition and Regulation of Oxides of Nitrogen 2

2.1.2 NO_x Formation Pathways 3

2.1.3 NOx Control Strategies 4

2.2 Natural Gas and Fuel Interchangeability 6

2.2.1 Natural Gas 6

2.2.2 Fuel Interchangeability 8

2.3 Control and Optimization 9

2.4 Direction-Set Algorithms 10

2.4.1 Powell's Method 10

2.4.2 Combustion Applications 12

2.5 Downhill Simplex Algorithm 14

2.5.1 Nelder and Mead 14

2.5.2 Combustion Applications 17

2.6 Current Project 18

CHAPTER 3: Experimental Apparatus **20**
3.1 Burner Geometry 20
3.1.1 Burner 20
3.1.2 Distribution Plate and Throat Area 20
3.1.3 Windbox 21
3.1.4 Core Fuel Injector 21
3.1.5 Radial Fuel Injectors 21
3.1.6 Outer Fuel Injectors 21
3.2 Test Facility 21
3.2.1 Test Stand 21
3.2.2 Furnace Enclosure 22
3.2.3 Water Cooling System 23
3.2.4 Flow Control System 24
3.3 Sensors 26
3.3.1 Fuel Identification and Properties 27
3.3.2 Flame Stability 30
3.3.3 Emissions 31
3.3.4 Efficiency 31
CHAPTER 4: Burner Performance Mapping **33**
4.1 Test Plan 33
4.2 Experimental Procedure 34
4.3 Burner Performance Mapping Database 34
4.3.1 Performance with No Sensor Feedback 34
4.3.2 Trends and Correlations with Sensor Feedback 35
4.3.3 Performance Mapping 41
CHAPTER 5: Closed Loop Control **44**
5.1 Simulations 44
5.1.1 5th Order Approximations 44

5.1.2 Types of Simulations 44
5.2 Cost Function 45
5.3 5th Order Approximation 47
5.4 Cost Function Maps 48
5.5 Simulation Results 51
5.5.1 No Fluctuations (NF) 51
5.5.2 With Fluctuations (WF) 59
5.5.3 Simulated Noise with No Fluctuations (SNNF) 61
5.5.4 Simulated Noise With Fluctuations (SNWF) 68
CHAPTER 6: Validation of Fuel Interchange Parameters 70
6.1 Computational fluid dynamics (CFD) 70
6.2 Chemical reactor network (CRN) 73
6.2.1 Ideal reactor 73
6.2.2 Construction of CRN model 74
6.3 Results 76
CHAPTER 7: Conclusions 78
Glossary 80
References 86
Appendix A: 5th Order Approximation Code (Approx.m) 1

LIST OF FIGURES

Figure ES- 1: Air SCFM vs NOx. Left 100-0, Right 95-5 NG-PG. No control 1
Figure 1: NOx Control Technologies. Adapted From (Turns, 2000) 5
Figure 2: First Iteration of Powell's Direction-Set Algorithm for Two Parameters (n=2) 10
Figure 3: First Iteration of Powell's Direction-Set Algorithm for Two Parameters (n=2) 14
Figure 4: Starting Simplex With Pperations Overlapped 16
Figure 5: Downhill Simplex Flowchart Modified (Jackson and Agrawal, 1999) 17
Figure 6:Scaled Quantum Low NO_x Burner (Adapted From (Demayo, 2001)) 20

Figure 7: (Top) Schematic of Test Stand (Adapted From (amuelsen and Miyasato, 2000)) and (Bottom) Furnace Enclosure 22

Figure 8: Water Cooling Configuration 23

Figure 9: Flow Control Schematic 25

Figure 10: Sonic Orifice Control Panel 26

Figure 11: Migatron RPS-409A-IS Intrinsically Safe Ultrasonic Sensor 28

Figure 12: Speed of Sound (SOS) Model and Physical Hardware 29

Figure 13: C/H ratio (left) and Wobbe (right) vs. C2/T 29

Figure 14: Side-wall Mounted Fiber Optic Probe 30

Figure 15: Horiba PG250 Analyzer (Left) and Emissions Probe (Right) 31

Figure 16: Air SCFM vs NO_x. Left 100-0, Right 95-5 NG-PG. No SOS Control 35

Figure 17: EA vs NO_x Corr 3%O2 (Blue: 100-0, Red: 95-5, Green: 92.5-7.5 NG-PG) 36

Figure 18: FS vs NO_x Corr 3%O2 (Blue: 100-0, Red: 95-5, Green: 92.5-7.5 NG-PG) 37

Figure 19: EA vs Light AVG (Blue: 100-0, Red: 95-5, Green: 92.5-7.5 NG-PG) 38

Figure 20: Light AVG vs NOx Corr 3%O2 (All Blends) 38

Figure 21: AFT vs NOx Corr 3%O2 (Blue: 100-0, Red: 95-5, Green: 92.5-7.5 NG-PG) 39

Figure 22: EA vs Light PkPk (Blue: 100-0, Red: 95-5, Green: 92.5-7.5 NG-PG) 40

Figure 23: EA vs Boiler Eff (Blue: 100-0, Red: 95-5, Green: 92.5-7.5 NG-PG) 41

Figure 24: 100-0 NG-PG Performance Maps 42

Figure 25: 95-5 NG-PG Performance Maps 42

Figure 26: 92.5-7.5 NG-PG Performance Maps 43

Figure 27: Cost Function: Sub-Functions 46

Figure 28: 100-0 NG-PG Approximation Maps 47

Figure 29: 95-5 NG-PG Approximation Maps 48

Figure 30: 92.5-7.5 NG-PG Approximation Maps 48

Figure 31: 100-0 NG-PG Cost Function Map 49

Figure 32: 95-5 NG-PG Cost Function Map 50

Figure 33: 92.5-7.5 NG-PG Cost Function Map 50

Figure 34: PDS NF Results: 100-0 NG-PG, FS/EA of -2/14 52

Figure 35: PDS NF Results: 95-5 NG-PG, FS/EA of -2/14 53

Figure 36: PDS NF Results: 92.5-7.5 NG-PG, FS/EA of -2/14 54

Figure 37: DHS NF Results: 100-0 NG-PG, FS/EA of -2/14..... 56

Figure 38: DHS NF Results: 95-5 NG-PG, FS/EA of -2/14..... 57

Figure 39: DHS NF Results: 92.5-7.5 NG-PG, FS/EA of -2/14..... 58

Figure 40: PDS SNNF Results: 100-0 NG-PG, FS/EA of -2/14 62

Figure 42: PDS SNNF Results: 92.5-7.5 NG-PG, FS/EA of -2/14 63

Figure 43: DHS SNNF Results: 100-0 NG-PG, FS/EA of -2/14 65

Figure 45: DHS SNNF Results: 92.5-7.5 NG-PG, FS/EA of -2/14 66

Figure 46 Geometry and Meshes of the CFD simulation. 70

Figure 47 Comparison of Simulated Results of NG Case Using 1) Eddy-Dissipation Model and 2) PDF Model 71

Figure 48 Comparison of temperature distribution in PG and NG flames 72

Figure 49 criteria of ideal reactor selection: (a) polar and sagittal angles of the velocity vectors belonging to a psr reactor. (b) polar and sagittal angles of the velocity vectors belonging to a pfr reactor.(faravelli et al., 2001)..... 74

Figure 50 Overview of pathlines passing through reaction region, colored by residence time (s) 75

Figure 51 Overview of the CRN Model for Diffusive Flame 76

Figure 52 Results of CRN Model in Terms of NO_x Emission, Compared to Measured Data..... 76

Figure 53 Data Correction by Changing Split Ratios 77

EXECUTIVE SUMMARY

Introduction

Fuel-flexible operation of burners is desirable in order to increase access to a larger number of potential fuels; however, emissions requirements for the operation of these burners have become increasingly stringent. These requirements have led to burners with a tendency to operate near their stability limits. When a burner operates near its stability limit and variation in fuel composition is required, challenges may arise, which can lead to possible operational safety issues. For example, if the reaction blows out and is reignited, it can cause a large pressure oscillation within the boiler and furnace chamber which can rupture the boiler shell or damage furnace walls. Operating near the stability limit also makes turndown, the ratio of the maximum burner load to minimum burner load, difficult to control when low emissions are desired over a range of loads.

Project Purpose

Thus, the research done within this project seeks to monitor changes in fuel composition regarding the modification of burner operation. The scope of the variation measured within fuel composition is similar to the expected variation in the makeup of natural gas. Figure ES- 1 compares the oxides of nitrogen (NO_x) emissions levels of a burner with different fuel flow splits and air flows. This comparison illustrates the contrasting differences of fuel composition without a specific control strategy. For example, the operating points on both graphs from a flow split of zero and 75 standard cubic feet per minute (scfm) of air illustrate that the NO_x levels increase by 15 to 20 percent. In this case, the burner's NO_x emission would exceed the allowable limit unless its operation was modified.

Figure ES- 1: Air SCFM vs NOx. Left 100-0, Right 95-5 NG-PG. No control

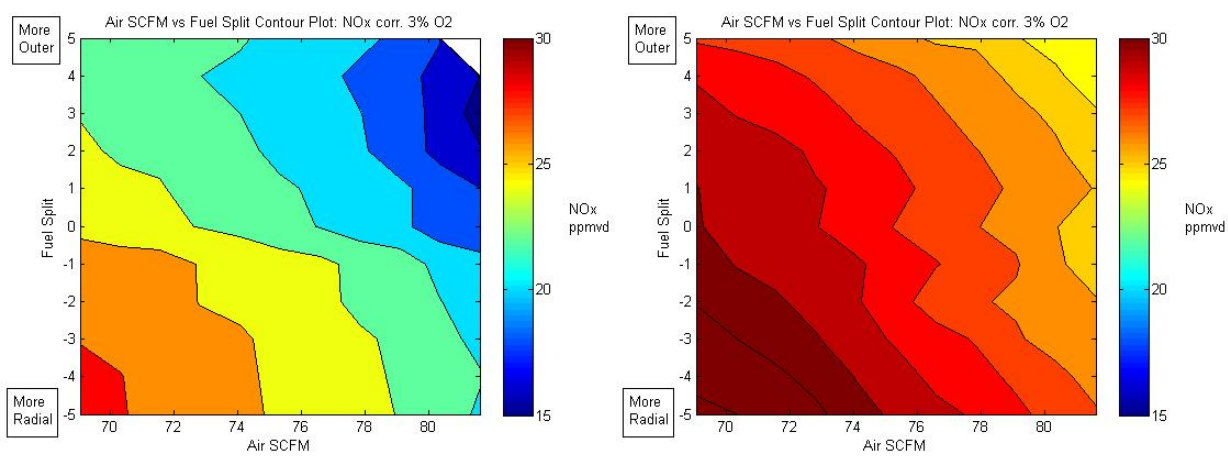

In addition to minimizing NO_x and maximizing the stability of the burner, overall performance must also be considered. Operating at higher excess air values tends to lower NO_x emissions,

but it also requires extra work to move the additional air. This reduces the overall efficiency of the system.

To accomplish stable operation and low emissions while accommodating varying fuel composition, an array of sensors and control algorithms were deployed using a 400 million British thermal unit per hour (MMBTU/hr) burner. This burner is based on a commercial advanced low emissions burner. Like many low emissions burners, it is fuel-staged with three separately controlled fuel circuits. These circuits allow the burner to attain reasonable turndown while still meeting emissions requirements. Certain combinations of fuel splits provided enhanced stability, but generally led to higher emissions levels. The fuel split is primarily used to help fulfill safe operation with low emissions; however, if the fuel composition changes, the burner's fuel schedule must also change accordingly. A low cost sensor that can infer the heating value of the fuel was developed to accomplish this. A stability sensor based on reaction luminosity, was also employed. As a reaction approaches blowoff, luminosity becomes increasingly irregular. Monitoring luminosity and looking for an increase in intensity fluctuations provides a means of establishing whether or not a reaction is approaching blowoff. The result determined how burner operation could be adjusted accordingly. In addition, the luminosity sensor was found to correlate NO_x emissions very well, displaying higher mean intensity levels that equate linearly with higher NO_x emissions. Even though a standard exhaust emission sampling system was used to monitor NO_x levels, a much lower cost luminosity sensor could also be used.

In order to simultaneously optimize the four parameters of interest (stability, NO_x emissions, and system efficiency), a "cost function" was developed, combining each of the parameters into a single value.

The sensor information is used in conjunction with fuel circuit operation to demonstrate that the burner could automatically provide a low emission and a stable operating point as fuel composition changes. Two control algorithms were evaluated, both with their strengths and weaknesses. Generally, the Powell's Direction Set optimization approach is favored, despite the fact that it takes longer to find the new optimal operation point compared to the Downhill Simplex Method. Nonetheless, it is more dependable than the Downhill Simplex method.

Project Results

Overall, the project demonstrated the benefits of adding sensors and controls as well as the burner's capability to adjust itself to account for fuel compositional variation. The applied controls allowed the burner to remain at NO_x emissions levels below the regulatory limit, even when as much as 7.5percent propane (by volume) was added. In the absence of controls, the burner would have exceeded the NO_x limits.

While the research within this project focused on the viability of actively controlling a burner at higher hydrocarbon rates, additional measures must be taken in order to gain maximum benefits. First, the technology applied to renewable fuels consisting largely of methane and carbon dioxide (like those produced by waste water plants or landfills) must be reevaluated while complying with Assembly Bill 32 (AB 32, Global Warming Solutions Act, Nunez, Statutes

of 2006). Second, a low NO_x burner with either no more than two fuel circuits or the ability to tune performance through air splits instead of fuel splits must be designed and implemented. Design and implementation of such a burner can begin immediately via arrangements with a burner manufacturer such as Maxon and Honeywell. Burners comprised of three separate fuel circuits, such as the one used in this project, are comparatively complex and costly to manufacture. Active monitoring of fuel flexible burners can directly benefit the public by reducing NO_x emissions and therefore formation of ozone.

Project Benefits

Generally, monitoring the flue gas of smaller scale combustion devices (like small package boilers and water heaters) is less cost effective than monitoring the flue gas of large scale combustion systems such as those found at power plants. However, as demonstrated by researchers at the University of California, Irvine, it is possible for a sustainable system to be implemented on a small scale burner without a substantial increase in cost. Ultimately, a burner with the ability to adapt to varying fuel composition (like that found in methane or with some carbon dioxide or natural gas and hydrogen mixtures) is better equipped to maintain overall safety and emissions requirements.

CHAPTER 1: Introduction

Combustion systems account for a large portion of California's energy usage and the various fuels being used are continuously shifting in order to meet regulation standards. Burners that operate on natural gas have increased in popularity due to several key factors. The first factor is the use of stringent environmental regulation standards, invoked at the local and state levels. Pollution, specifically NOx, have become a very important parameter when designing new burners or retrofitting preexisting burners with new technology. There are several geometric designs, burning methods, and sensor feedback control strategies that have been proposed and each one has their associated benefits and drawbacks. Another key factor is the lower environmental impact of burning natural gas compared to coal or diesel fuels. Natural gas, which is mainly comprised of methane (CH4), contains fewer carbon chains than coal and therefore produces less carbon based emissions. However, as will be shown shortly, natural gas has no standard composition and can vary drastically from region to region. These dynamic fuel composition fluctuations create new challenges for burners already operating on the edge of stable combustion trying to meet emission standards. Fuel composition fluctuation problems are going to continue in the future due to the beneficial economic and environmental aspects of burning natural gas and its variants. This project aims to address the two major issues outlined thus far: NOx control and fuel composition effects.

In order to solve and or counteract these two problems, a system of sensor feedback and optimization search algorithms will be used to find the most optimal operating condition given a desired load and sensed fuel composition. Optimization and control strategies have been selected for this task due to the ability to operate burners in conditions the burners were not originally designed for. Simply changing the operating conditions is a far easier and more robust system to add to a preexisting burner than altering the geometric design to accommodate all types of fuels. This project aims at modifying currently "dumb" burners by adding some intelligence to their operational capabilities in order to find an optimal and acceptable region to burn a variety of fuel blends.

CHAPTER 2: Background

There are three main topics in this project that must be discussed before proceeding and they are: NO_x formation and control, fuel composition and its effect on burners, and optimization search algorithms. The most important parameter in this experiment is the control of NO_x emissions. Therefore, how this chemical is formed, why it is important to regulate, and common strategies to mitigate its production will be discussed. It is also critical to understand how the performance of a burner changes with different blends of natural gas. Finally after discussing how the previous two parameters present issues to burners the remaining sections of this chapter will discuss how optimization algorithms have been used in previous work and how this project addresses some unanswered problems.

2.1 NO_x Formation and Control

2.1.1 Definition and Regulation of Oxides of Nitrogen

Combustion processes emit various pollutants that are harmful to the environment and its inhabitants. Pollutants of primary concern are particulate matter, sulfur oxides, unburned hydrocarbons, NO_x, carbon monoxide (CO), and carbon dioxide (CO_2). Of critical importance to boilers, furnaces, and stationary gas turbines are the production of $NO_x$and CO. NO_x is a catch all category associated with the chemicals nitric oxide (NO), nitrogen dioxide (NO_2), and nitrous oxide (N_2O) (Hill and Douglas Smoot, 2000). Collectively NO and NO_2 are most commonly referred to as NO_x due to their co-presence in the combustion process. While both NO_x and CO are important factors in the environment's health more emphasis will be put on NO_x particles due to its sizeable difference in difficulty to control and reduce concentration levels compared to CO.

The presence of NO_x in the atmosphere can cause many environmental problems, such as the formation of photochemical smog, acid rain, destruction of stratospheric ozone and the creation of tropospheric ozone (Turns, 2000)(Lefebvre and Ballal, 2010). Destruction of ozone by chemical reactions with NO in the stratosphere (the region between 12km to 51km above the earth's surface) can increase the amount of harmful solar radiation that can enter the earth's atmosphere which can result in various skin diseases. NO can also undergo a series of chemical reactions to produce ozone while constrained in the troposphere—the region from the surface of the earth to about 12 kilometers (km). Increased exposure to ozone can cause respiratory illness, impaired vision, and allergies.

For these reasons the regulation of NO_x emissions from combustion devices has been of critical importance to the federal and state levels of government. Due to the significant presence of smog encountered in the Los Angeles basin during the 1950s, California created laws regulating the emissions of automobiles in the 1960s. Then in 1963, the federal government passed the Clean Air Act which put restrictions on various pollutants (Turns, 2000). California has been a leader in setting strict emission regulation standards and is the primary force propelling research in the study of pollutant reduction and control. The South Coast and Bay Area Air

Quality Management Districts (SCAQMD and BAAQMD) have both enacted legislation lowering the previous allowable NO_x and CO concentrations for boilers of various load sizes to much more stringent levels. The SCAQMD promulgated Rule 1146.2 and BAAQMD Regulation 9 Rule 7, of which the key points are summarized in Table 1 (South Coast Air Quality Management District, 2006)(Bay Area Air Quality Management District, 2011). For this particular project the burner being investigated operates at 0.4 MMBtu/hr and therefore regulated by the less than 2 MMBtu/hr category. The previous NO_x standard was set at 30 parts per million volumetric dry (ppmvd) but is now 20 ppmvd corrected to 3 percent oxygen (O_2). As will be shown in later sections, the new NO_x standard is very difficult for the proposed burner to reach and causes it to operate within a very narrow band of allowable input parameters to maintain acceptable emissions.

Table 1: SCAQMD and BAAQMD Limits on NO_x and CO

Input (million Btu/hr)	NO_x limit (ppmvd, 3% O_2)	CO limit (ppmvd, 3% O_2)
<2	20	400
>2 to 5	30	400
>5 to <10	15	400
10 to <20	15	400

2.1.2 NO_x Formation Pathways

In order to control the levels of NO_x in the combustion exhaust stream, the various NO_x formation pathways must be understood first. There are four main recognized mechanisms that contribute to the production of NO_x: thermal or Zeldovich mechanism, prompt or Fenimore mechanism, N_2O-intermediate mechanism, and fuel bound nitrogen mechanism. Some mechanisms are more prevalent under one set of conditions versus another and are therefore dependent on the particular burner application and design. Furthermore, the primary form of NO_x is NO in most combustion processes with NO_2 being a small fraction of the overall NO_x concentration (Hill and Douglas Smoot, 2000).

2.1.2.1 Thermal or Zeldovich Mechanism

Thermal NO_x is formed from oxidation of atmospheric nitrogen at high temperatures (>1800 degrees Kelvin [°K]) in fuel-lean environments (Hill and Douglas Smoot, 2000). The thermal NO_x formation pathway was first proposed by Zeldovich and can be represented by the following set of chemical reactions:

1) $O + N_2 \Leftrightarrow NO + N$
2) $N + O_2 \Leftrightarrow NO + O$
3) $N + OH \Leftrightarrow NO + O$

This set of reactions are most commonly referred to as the extended Zeldovich model. The activation energy in reaction 1 to produce a forward reaction is very large and therefore heavily dependent on temperature. It is generally seen that flame temperatures below 1800 °K have

very low thermal NO_x production (Turns, 2000). The second reaction happens very rapidly when compared to the first reaction, which then makes the first reaction the rate-determining step. The third reaction is primarily there for fuel-rich flames and can otherwise be neglected for most cases.

2.1.2.2 Prompt or Fenimore Mechanism

Prompt NO_x is formed by reaction of atmospheric nitrogen with hydrocarbon radicals in fuel-rich flames (Hill and Douglas Smoot, 2000). In general this mechanism works by having nitrogen react with hydrocarbon radicals to form amines and cyano compounds. The amines and cyano compounds then undergo a series of intermediate reactions to form NO (Turns, 2000). The full set of reaction equations can easily be found in the literature and will not be reproduced here in order to be brief in this mechanism's description. Prompt NO_x is of primary concern only for fuel-rich hydrocarbon flames and is only a small portion of the entire NO_x production.

2.1.2.3 N_2O-Intermediate Mechanism

The N_2O mechanism is prevalent in fuel-lean (Equivalence Ratio [Φ] < 0.8), low temperature conditions and follows this three step reaction (Turns, 2000):

1) $O + N_2 + M \Leftrightarrow N_2O + M$
2) $H + N_2O \Leftrightarrow NO + NH$
3) $O + N_2O \Leftrightarrow NO + NO$

In this case, M represents any third body species (e.g,. molecular oxygen or fuel). This reaction set has greater importance when considering lean premixed combustion systems. As will be further explained later, the burner used contains a small amount of premixing with fuel and air, which means this NO_x mechanism plays a less significant role than the previously mentioned pathways.

2.1.2.4 Fuel Bound Nitrogen Mechanism

Fuel NO_x is produced by nitrogen bounded in the fuel reacts to form hydrogen cyanide (HCN) and/or ammonia (NH_3). These molecules are then oxidized to form NO by following the prompt NO_x reaction pathway. Natural gas and its deviants generally have very small, if any, amount of fuel bound nitrogen and has a greater significance for solid fuels such as coal. Hence this mechanism will not be explained further due to its lack of importance in this particular application.

2.1.3 NOx Control Strategies

Now that NO_x formation pathways are understood, the next important topic in this section is how to control and design a burner to perform at operating conditions with a minimal amount of NO_x being produced. Since thermal NO_x is assumed to be the most prevalent in this project it will be the primary focus of the remaining discussion. There are three ways to lower thermal NO_x and they are temperature, time, and oxygen availability (Turns, 2000). The most important parameter out of the three is temperature since it has the most effect on the chemical kinetics. For flames below 1800 °K thermal NO_x is not significant. Therefore, by lowering the flame

temperature one can easily reduce NO_x formation; however, this lower flame temperature can also result in lower system efficiency. The second parameter is time and this involves limiting the time the combustion gases spend at elevated temperatures. Reducing the time spent at peak temperatures limits the amount of chemical reactions that can take place. The third parameter is increased oxygen availability, which can lower NO_x by decreasing the concentration of N_2 available for chemical reactions.

Taking into consideration the three main parameters that effect NOx formation, it is time to discuss control strategies. At this point only physical modifications of hardware both to the burner and downstream systems will be discussed and feedback control will be discussed in a later section. Figure 1 depicts common modifications burners and the supporting systems can undergo in order to lower NOx emissions. As it can be seen there are many technologies available, but only the technologies that will be implemented in this project will be discussed and further information about the remaining technologies can be found in other literature.

Figure 1: NOx Control Technologies. Adapted From (Turns, 2000)

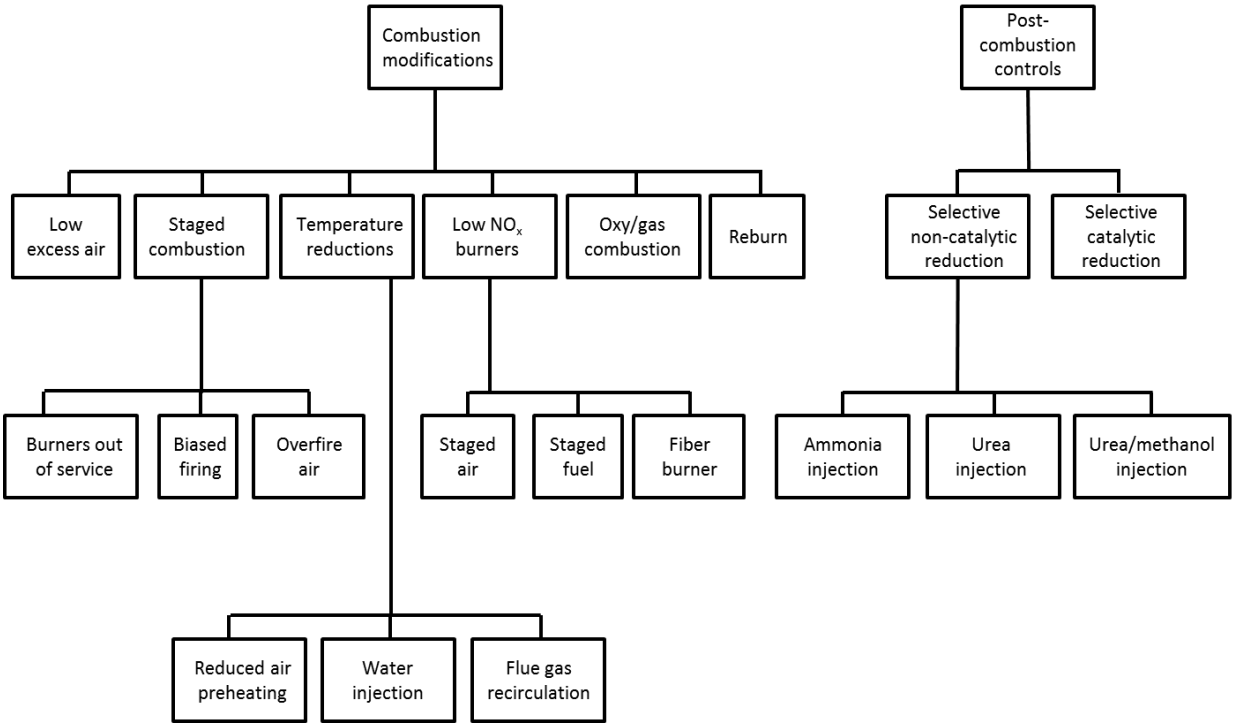

2.1.3.1 Low NO_x Burner

Low NO_x burners, such as the one used in this project, incorporate fuel and/or air staging in the burner design. Typically fuel staging employs a lean-rich combustion design in which the central fuel and air mixture is a lean flame while the outer flame jets are fuel rich. This design feature is the primary technology behind achieving low NO_x levels for the burner being investigated. More details on the exact design of the burner will be given in a later chapter.

2.1.3.2 Low/High Excess Air

The peak emission levels of NOx is reached at leaner than stoichiometric equivalence ratios (Φ~0.9). Operating with low excess air reduces NOx levels; however, this comes at a cost of increasing CO production. Therefore this method has limited use. Operating with high excess air can lower the flame temperature and thus the NOx level; however, this too can have negative side effects. The lower flame temperature will lower the system efficiency as well as potentially make the flame unstable at very lean conditions. The NOx reduction is then a balance between emission levels versus efficiency and stability.

2.1.3.3 Temperature Reduction

There are three common techniques on lowering combustion temperature: lowering preheat, water injection, and flue-gas recirculation (FGR). Lowering preheat will reduce combustion temperatures; however, it comes at the cost of system efficiency. For this project no preheat is added to the system in order to simplify experiments, but the results can be applied for any system operating at a constant preheat level. Water injection adds a heat sink into the system and thus reduces flame temperatures. FGR takes the hot combusted gases and cycles the stream back to the beginning of the burner. The burner in this project is not designed with the latter two technologies in mind. FGR could be a suggestion for future work.

2.2 Natural Gas and Fuel Interchangeability

2.2.1 Natural Gas

Natural gas is a fossil fuel comprised primarily of methane and is considered to be a more environmentally friendly alternative to the burning of oil and coal. Due to decreasing price, improved efficiency, expanded distribution networks, and lower environmental impacts the use of natural gas as a major energy source in the United States has increased significantly in recent years and is projected to continue on this trend. A major concern with this increase in consumption is the role of fluctuating composition on currently installed burners. There is no standard for the composition of natural gas. Every region and extraction technique supplies variations on the chemical makeup of the fuel. The increase demand for fuel flexible burners is on the rise and will continue to be an area of interest due to the heavy demand for natural gas burner systems.

The primary compound of natural gas is methane with small contributions from some higher hydrocarbons (ethane and propane) as well as inert gases (nitrogen and carbon dioxide). Typical percentages of methane are between 75-98 percent, ethane between 0-13 percent, and propane between 0-23 percent (with peak shaving in which propane is added to the pipeline to bolster available energy during high gas demand) (Hack and McDonell, 2008). As a comparison, an online gas chromatograph was used to measure the University of California Irvine Combustion Laboratory's house natural gas and the composition analysis can be found in Table 2. As it can be seen in the table the facility's natural gas supply is approximately 98 percent methane. Due to this high concentration it is reasonable to assume the line is 100 percent methane for the purpose of easing analysis and calculations with minimal loss in accuracy.

Table 2: UCI Combustion Laboratory in House Natural Gas Composition

n	Constituent		Mole Fraction y(i) %
1	Methane	CH_4	97.8783
2	Ethane	C_2H_4	1.3875
3	Propane	C_3H_8	0.3117
4	Iso-butane	C_4H_{10}	0.0476
5	n-butane	C_4H_{10}	0.0521
6	Neo-pentane	C_5H_{12}	0.0000
7	Iso-pentane	C_5H_{12}	0.0139
8	n-pentane	C_5H_{12}	0.0000
9	Hexane	C_6H_{14}	0.0021
10	Heptane	C_7H_{16}	0.0019
11	Octane	C_8H_{18}	0.0000
12	Nonane	C_9H_{20}	0.0000
13	Decane	$C_{10}H_{22}$	0.0000
14	Carbon Dioxide	CO_2	0.0000
15	Nitrogen	N_2	0.3049
		Total (%)	100.0000

In 2011 natural gas comprised 26 percent of the United States' fuel energy usage and the Energy Information Administration projects that natural gas will obtain 28 percent of this usage by 2040 (EIA, 2013). There are several reasons for this increase which rely on production, economic, and regulation efforts. On the production side a new extraction technique to collect previously difficult gas locked in shale formations has become now technologically and economically viable. Natural gas derived from shale gas extraction accounted for 34 percent of total natural gas production in the United States in 2011 and is projected to rise to 50 percent by 2040 (EIA, 2013). A major challenge with shale gas is that the composition can vary drastically from region to region and requires a large amount of fuel conditioning/cleaning to reach normal and/or acceptable natural gas compositions for injection into the pipeline. This can impact the ultimate price of the gas. If the gas is used on-site (which is the case for local power generation to support the operations), the variability in composition can preclude low emissions combustion systems.

With most states adopting Renewable Portfolio Standards (RPS), which generally favor the use of renewable fuels and natural gas, the demand for natural gas burning systems has increased drastically with special emphasis in the electrical generation sector (EIA, 2013). The combination of increased production and increased demand has made the natural gas market a very economically viable energy source. Therefore it is apparent that the number of burners operating on natural gas will increase dramatically and to compensate for discrepancies in fuel composition caused by varying extraction techniques the burners will have to be able to respond to fuel fluctuations. Burner geometric designs can attempt to accommodate all the various possibilities in fuel supplies, but having a system designed for a primary fuel with an intelligent fuel flexible control system implemented might prove a better route in optimizing system performance.

2.2.2 Fuel Interchangeability

2.2.2.1 Parameters and Indices

Fuel interchangeability is most often defined as the ability of one gaseous fuel being a substitute for another gaseous fuel without significantly altering the combustion characteristics and operation (Ferguson et al., 2007). Measuring and defining how well of a substitute one fuel is for another is a difficult task and is still an ongoing debate. There have been various indices proposed throughout the years that attempt to define interchangeability, but each one has their drawbacks. There are many important parameters associated with characterizing a combustion system such as flame speed, autoignition, flashback, blowout, and flame instabilities to list a few. So far there has been no single index that correlates to all of these combustion properties, but a few indices have been used repeatedly despite their shortcomings.

The most widely used index to characterize fuel interchangeability is the Wobbe Index. The Wobbe Index is a measure of heating content in a fuel and is defined by the following equation:

$$\textit{Equation 1}: \qquad Wobbe = \frac{HHV}{\sqrt{SG}}$$

where HHV is the higher heating value and SG is the specific gravity compared to air. The most common unit used in the United States is British thermal units per standard cubic foot (Btu/scf). The gas supply industry relies heavily on this index when determining if a fuel can be safely used in the distribution system. The Natural Gas Council formed the NGC+ Work Group on Interchangeability in 2005 and developed the acceptable range of Wobbe values for natural gas as between 1291 to 1400 Btu/scf with a maximum of 4 percent by volume of inert gases (Ferguson, Richard, and Straub, 2008). The Wobbe Index does well for burner systems that rely on thermal load as the main input, but for systems such as gas turbines the flame temperature is the most important input and Wobbe Index does a poor job at this estimation. Another problem is that the Wobbe Index does not capture the flame speed or combustion chemistry (Lieuwen et al., 2008).

The Schuster Index tries to characterize a fuel by computing the Wobbe number and then divides by the fuel's laminar flame speed. This index received limited use when it was first proposed due to limited amount of reliable flame speeds for various fuels. Recently flame speed calculations have become more available for pure fuels, but flame speeds of multi-component fuels have been difficult to obtain (Ferguson et al., 2008). Ferguson et al. showed that neither Schuster nor Wobbe could accurately predict the dynamic response to a change in fuel and recommends an index (or set of indices) that use the relative difference between a substitute gas and a baseline gas.

2.2.2.2 Effects on Burners

There has been a considerable amount of research done in the study of fuel interchangeability with many interesting results. The most relevant results deal with the presence of higher hydrocarbons in methane to that of emissions and flame stability. Hack et al. and Flores et al. both have shown that the addition of propane to natural gas increases the NO_x level at the same adiabatic flame temperature for two different lean premixed burners (Flores et al., 2008). Reasons for this increase could be due to local differences in flame temperatures and/or

facilitation of additional NO_x formation pathways that are present with higher hydrocarbons. The other important result is flame stability which has been shown to decrease with propane additions of 5 percent by volume or more (Ferguson et al., 2007). Reasons for this decrease in stability include changes in flame temperatures and flame speeds. Other combustion parameters such as flashback, autoignition, and blowout have also been investigated for natural gas fuel interchangeability but will not be discussed here due to lack of relevance with current project (Lieuwen et al., 2008).

2.3 Control and Optimization

In classical control and optimization problems a well-defined equation that accurately portrays the dynamics of the system is required to design various algorithms. However, for combustion systems mathematical descriptions of the plant are very difficult to obtain. For this reason a different approach must be taken for these types of scenarios.

The inputs (or actuators) for this project are fuel split (FS) and excess air (EA). There are many measureable outputs, but the three main parameters of concern are: emissions (NO_x), flame stability (oscillations in flame luminosity), and efficiency (based on thermodynamics and/or air flow). A cost function will be defined that computes a single value based on the three main output parameters. An optimization algorithm will effectively search in this two dimensional FS-EA space to find the optimal operating condition that can balance all three output parameters by finding the minimum value of the cost function. This type of optimization situation is generally termed as a two dimensional constrained problem. The constrained term is derived from the fact that the algorithm must search within the allowable operating boundaries of the burner.

There are many different methods to search in a multidimensional parameter space and selecting an effective optimization search algorithm generally depends on the system it is being used for. For this situation there are a few main features that an optimization algorithm must have in order to be selected. (1) The algorithm must rely solely on cost function data and not a mathematical model of the system. (2) The algorithm will use as minimal amount of data as possible. Recording data for each operating condition can be very time consuming. Therefore, a search algorithm will attempt to find the optimal condition without requiring a full detailed map of the parameter space. (3) The minimum found by the algorithm must be the global minimum of the given topology. Certain algorithms can potentially converge to local minimums which would not be ideal since there is an even better result still located on the map. (4) The algorithm must be able to handle constraints.

For this project many optimization search techniques were researched in the literature, but only a select few have been chosen to be simulated, based on ease of implementation, expected robustness, and speed. The following sections in this chapter give detailed descriptions and explanations of each algorithm along with examples of previous studies.

2.4 Direction-Set Algorithms

2.4.1 Powell's Method

The direction-set method developed by M. J. D. Powell is a derivative-free based algorithm used to search for the minimum (or maximum) of an objective function that has dynamics unable to be expressed mathematically (Powell, 1964). There are two important features to the direction-set method: derivative-free based search, and no mathematical model is required. For complex systems, as such for the case for combustion, an accurate dynamics model is very difficult to create. The classical simulation and modeling approach to controlling a system is not valid in such a scenario, but the direction-set method allows the system to reach its optimal value without prior knowledge. Due to the derivative-free approach the computational complexity is greatly reduced, which is beneficial for systems where obtaining the derivative of the objective function is expensive, unreliable, or impractical to obtain (Rios and Sahinidis, 2012).

2.4.1.1 The Procedure

The direction-set algorithm outlined by Powell can be summarized by the following steps. The algorithm searches in n linearly independent directions $\xi 1, \xi 2, \ldots, \xi n$ starting from an initial estimation of the minimum at a point Po. The initial directions are selected to be co-ordinate directions; or in other terms, the algorithm initially searches by changing one parameter at a time. Each iteration generates a new conjugate direction, ξ, and the new direction set created for the next iteration is $\xi 2, \ldots, \xi n, \xi$. A conjugate direction set (q,v) are said to be conjugate if qAv=0 for a positive definite matrix A. In other words, the vectors q and v are linearly independent. After n iterations all the directions are mutually conjugate, which Powell proves is enough to ensure the algorithm will find the global minimum of a quadratic function, f(x) (Powell, 1964). The exact procedure for each iteration is as follows:

1. For r = 1, 2, …, ***n*** calculate λ_r so that $f(\mathbf{P}_{r-1} + \lambda_r \boldsymbol{\xi}_r)$ is a minimum and define $\mathbf{P}_r = \mathbf{P}_{r-1} + \lambda_r \boldsymbol{\xi}_r$
2. For r = 1, 2, …, ***n***-1 replace $\boldsymbol{\xi}_r$ by $\boldsymbol{\xi}_{r+1}$
3. Replace $\boldsymbol{\xi}_n$ by $\boldsymbol{\xi} = (\mathbf{P}_n - \mathbf{P}_o)$
4. Choose λ so that $f(\mathbf{P}_n + \lambda\boldsymbol{\xi})$ is a minimum and replace $\mathbf{P}_o = \mathbf{P}_n + \lambda\boldsymbol{\xi}$

Figure 2: First Iteration of Powell's Direction-Set Algorithm for Two Parameters (n=2)

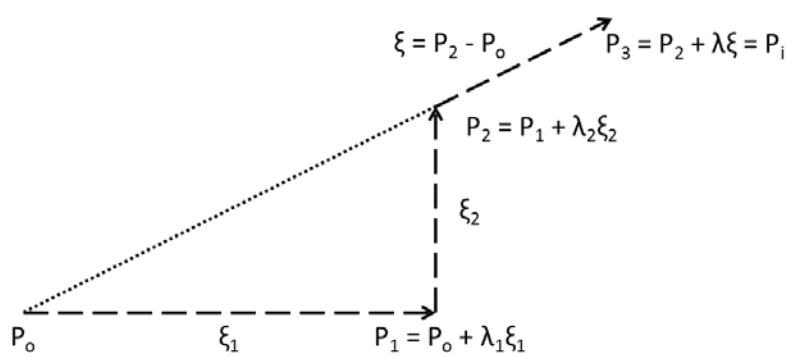

Figure 2 is an illustration of the first iteration of Powell's direction-set algorithm for a system with two adjustable variables (n=2). The second iteration would have the direction set list of ξ_2 and ξ, starting at the point $\mathbf{P}_1$. Problems can arise when the λ term equals to zero since the remaining directions will not span the full parameter space. This issue can create nearly dependent directions and can be a serious problem for functions with five or more variables (Powell, 1964). Since this project is only concerned with two adjustable variables, an adaptation of Powell's recommendation is as follows:

- If $\lambda = 0$, reset the direction set to the initial directions
- Else, continue updating directions as normal

2.4.1.2 Search for an extremum along a line

A hidden aspect of the algorithm that has been overlooked until now is how to evaluate the λ term that minimizes the objective function, $f(\mathbf{x})$. Powell provides a recommended technique on how to compute the minimum along a direction search line, but he warns that no search is perfect and is subject to different issues depending on the particular problem. In Powell's method five inputs must be provided:

1) A point on the line, $\mathbf{p}$
2) The direction of the line, ξ
3) An upper bound to the length of step along the line, $\mathbf{m}$
4) An order of magnitude of the length of step along the line, $\mathbf{q}$, assumed to be less than $\mathbf{m}$
5) The accuracy to which the minimum is required, $\mathbf{e}$

Three points of the objective function are computed:

1) $f(\mathbf{p} + a\xi)$, where initially $a = 0$. Also known as f_a
2) $f(\mathbf{p} + b\xi)$, where initially $b = \mathbf{q}$. Also known as f_b
3) $f(\mathbf{p} + c\xi)$, where initially $c = -\mathbf{q}$ or $c = 2\mathbf{q}$ depending on whether $f(\mathbf{p} + a\xi)$ is less than or greater than $f(\mathbf{p} + b\xi)$. Also known as f_c

A turning value, d, is evaluated using the following formula in order to predict the possible minimum at point f(p + dξ):

$$Equation\ 2: d = \frac{1}{2} * \frac{(b^2 - c^2)f_a + (c^2 - a^2)f_b + (a^2 - b^2)f_c}{(b - c)f_a + (c - a)f_b + (a - b)f_c}$$

And it is a potential minimum if

$$Equation\ 3: \frac{(b - c)f_a + (c - a)f_b + (a - b)f_c}{(a - b)(b - c)(c - a)} < 0$$

It is important here to discuss the possible scenarios that could occur when calculating the turning value, d. If d is a maximum (above equation is greater than 0) or if d is greater than $\mathbf{m}$,

then the maximum allowed step is computed in the direction of decreasing f. The function f_a, f_b, or f_c is discarded based on which one is furthest from f_d. Otherwise, two more sub-cases can arise. The value of d is compared with a, b, and c by taking the absolute value of the difference between each function value ($abs(f_i-f_d)$). These differences are then compared to the allowable error established by the controller, **e**. If one of the error values is within the allowable error then that value of d is chosen to be the minimum. Else, f_d is calculated to replace the function value (f_a, f_b, or f_c) that is greatest and the cycle continues.

It should be noted here that this method to search along a line was not used. Instead a simple hill-climbing algorithm was incorporated due to its easier code implementation and faster convergence to the minimum. The hill-climbing algorithm moves in the desired direction a specified step length. It computes the objective function at this point and compares this value to the previous point. For the case of minimization, if the current point is lower, then the next step length is computed. If the current point is greater, then the direction is flipped by 180 degrees and the search continues in this new direction. When the algorithm has experienced three flips in direction the hill-climbing algorithm is completed.

2.4.1.3 Convergence

Powell has provided a detailed proof explaining how the direction-set method using conjugate directions converge to the global minimum value of a quadratic function (Powell, 1964). In practice there are actually cases where convergence might be an issue. For a simple example, the system might not be truly quadratic or unimodal. Selecting an initially poor point in such a scenario could have the algorithm converging to a local extremum and not the global extremum. Or the algorithm could get struck along a direction and never be able to escape to a new area in the parameter space. One potential solution to this problem is to add an amount of randomness in the calculations within each iteration as implemented by St. John (St. John, 1994). However, it must be said that this random variable addition does not have any mathematical proof behind it allowing it to be definitive in proclaiming the extremum found is a local or global value. It can only provide potential solutions to some of the pitfalls encountered for special function cases when using Powell's method.

2.4.2 Combustion Applications

There have been at least three major combustion projects completed in the literature that have used slight variations of Powell's direction-set method to reach optimal operating conditions. Each researcher is associated with the University of California, Irvine Combustion Laboratory and has built on top of each other's work over the years. The very first optimization research was done by St. John and he investigated the performance of the direction-set method verses a genetic algorithm method (St. John, 1994).

St. John's particular burner application was for an industrial, swirl-stabilized, natural gas-fired burner where the swirl intensity (S') and excess air (EA) of the system were the two primary forms of control. The optimization algorithm was required to minimize the NO_x emissions while maintaining high combustion efficiency (η_c). A performance index, J, was established that would equally weight (w) the two parameters, [NO_x] and η_c, by the following formula:

$$Equation\ 4: J = w_1 f([NO_x]) + w_2 f(\eta_c)$$

The function describing [NO_x] is comprised of two piecewise equations that are supposed to penalize [NO_x] readings that are above allowable limits and heavily reward [NO_x] readings that are below allowable limits. The performance index can vary between zero to one, with one being the highest optimal condition and zero being the worst. It is here that the first difference is seen since St. John decides to maximize his objective function rather than minimize. The reasoning behind using a performance index styled objective function was to give a reader, who has no detailed knowledge of how J is defined, a very intuitive sense on which conditions are better than others.

The basic procedure that St. John uses for his direction-set algorithm is as follows:

1. Initialize position, X_o = [S' EA], and direction, α_o = R*360°, where R is a random number between 0 and 1
2. Find X_1 by maximizing J along the direction α_o
3. Next direction is defined by $\alpha_1 = \alpha_o + 90°$
4. Find X_2 by maximizing J along the direction α_1
5. Next direction is defined by $\alpha_2 = X_2 - X_o$
6. Find X_3 by maximizing J along the direction α_2
7. Repeat steps (2)-(6) using $X_o = X_3$ and $\alpha_o = \alpha_o + R*45°$

A visual representation of St. John's direction-set algorithm can be found in Figure 3. The major differences between Powell's method and St. John's are in the procedure of defining direction sets and finding extremum along a line. St. John initializes the first direction by a random selection and not the co-ordinate direction. The second direction is always 90 degrees from the first direction and does not change in this relationship. The third direction is the same for both methods in that the algorithm searches in the direction of greatest change. Finally the updated initial direction is again subjected to a random variable selection. The way St. John has defined the direction sets does not guarantee that the alphas are conjugate directions. This then means that St. John's method has no guarantee of convergence in a finite amount of iterations.

The second distinction to be made is in the extremum search along the search direction. St. John relies on a simple hill-climbing algorithm to find the maximum along a search line. Starting at a given position X the settings are incremented along the direction α until J no longer increases. If J decreases the direction is reversed and the search continues. An optimal point is defined when J has been found to decrease three times. Looking ahead to the topology of the cost function selected, the hill climbing algorithm was chosen due to the unimodal topology (one extremum) of J and the limited computational complexity of the algorithm. The unimodal topology ensures the algorithm will converge to a single global point and not a local extremum.

Figure 3: First Iteration of Powell's Direction-Set Algorithm for Two Parameters (n=2)

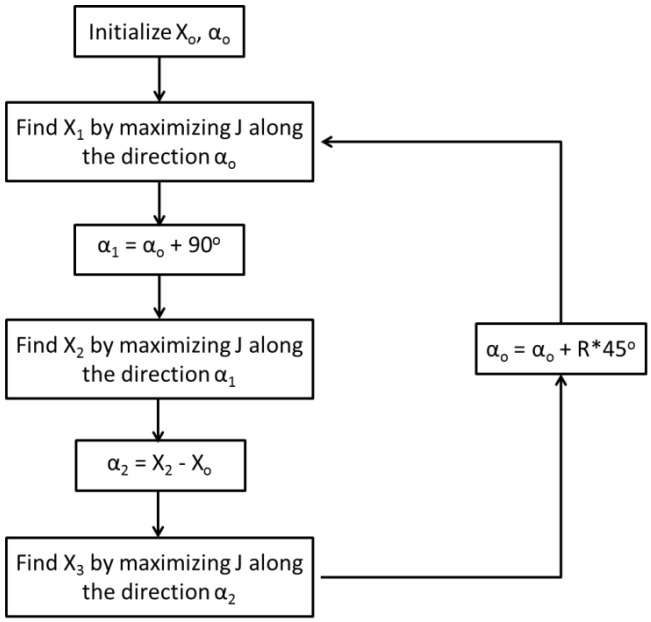

Ultimately St. John proved that this direction-set algorithm could in fact find the optimal operating conditions for the selected burner with two inputs and two outputs in a reasonable convergence time. This success led further research to be done by Demayo and Miyasato (Demayo, 2001; Miyasato, 2005). Building on top of St. John's recommendations, Demayo incorporated a stability sensor as well as more outputs to be controlled for the generic burner St. John used and for the boiler burner used in this current project. The performance index J was defined in a similar fashion, granted it attempted to incorporate [CO] and reaction stability into the formula as well. The basic procedure of the direction-set algorithm defined by Demayo is very similar to St. John with some minor variations. Both algorithms defined by the two researchers do not produce guaranteed conjugate direction sets while Powell's method does. Therefore, only Powell's direction-set algorithm will be used to compare with the other search algorithms to see if there are indeed any major differences in their performance. The remaining researcher, Miyasato, did not add any significant developments to the direction-set algorithms already outlined here by St. John and Demayo, but did show the algorithm worked well for a natural gas-fired gas turbine combustor in normal, part load, and hardware failure scenarios.

2.5 Downhill Simplex Algorithm

2.5.1 Nelder and Mead

The downhill simplex method was first popularized by Nelder and Mead in 1965 and is a derivative-free based optimization algorithm (Nelder and Mead, 1965). The more important trait of this method is it does not require a mathematical model to describe the dynamics of the system. The downhill simplex method is computationally and mathematically very simple to implement and converges to an extremum in a finite number of iterations. The general concept relies on an "amoeba" or "simplex" that moves in the operating space while expanding or

contracting its size based on the topology of the map. According to Press et al. the downhill simplex is not very efficient in terms of the number of function evaluations, but it is a good method to implement when a code is required quickly for the less computationally intensive problems (Press et al., 2007).

2.5.1.1 The Procedure

The following procedure is a summary of the information found in the journal paper by Nelder and Mead (Nelder and Mead, 1965). In a two-dimensional operating space a "simplex" or "amoeba" with 3 vertices (P_1, P_2, P_3) is initialized either at random or by a good first guess. The function values at each point are evaluated and the points are ranked based on a high-to-low scale of their function values (H, M, L). The goal of this method is to minimize the function values of the vertices or in other words minimize the difference between the high (H) and low (L) of the vertices. The amoeba can now undergo four possible operations: reflection, expansion, single contraction, and/or double contraction.

Before any of the operations can occur the centroid ($\bar{P}$) of the simplex must first be calculated. The following equation is based on the x and y coordinates of the three vertices (H, M, L):

$$Equation\ 5 : \bar{P} = \frac{H + M + L}{3}$$

Reflection is the first operation to occur and it happens every iteration. The reflection point H_1 is calculated by the following equation:

$$Equation\ 6 : H_1 = (1 + \alpha) * \bar{P} - \alpha * H$$

Where α is a positive constant and is called the reflection coefficient. Note that H1 is on the line joining H and $\bar{P}$. The function value f(H1) is computed and is compared to f(L). If f(H1) is less than f(L) then the next operation is expansion. The expansion point H2 is computed based on the following equation:

$$Equation\ 7 :\ H_2 = \gamma * H_1 + (1 - \gamma) * \bar{P}$$

Where γ is the expansion coefficient and is greater than unity. The function value $f(H_2)$ is computed and compared to $f(H_1)$. If $f(H_2)$ is less than $f(H_1)$ then replace H with H_2; else replace H with H_1. Test for convergence by the following equation:

$$Equation\ 8 : abs\big(f(H) - f(L)\big) \leq tol$$

If the above inequality is true then exit the algorithm, else repeat steps with the new vertices. Let's go back a few steps to the comparison between $f(H_1)$ and $f(L)$. If $f(H_1)$ is greater than $f(L)$, but less than $f(M)$ then replace H with H_1. If $f(H_1)$ is greater than $f(M)$ then the next operation is a single contraction. The contraction point H_3 is computed by the following equation:

$$Equation\ 9 : H_3 = \beta * H + (1 - \beta) * \bar{P}$$

Where β is the contraction coefficient and lies between 0 and 1. The function value $f(H_3)$ is computed and compared to $f(H)$. If $f(H_3)$ is less than $f(H)$ then replace H with H_3; else continue onto the final possible operation, double contraction. In double contraction the middle ranked point M is contracted to a new point M_2 and is calculated based on the equation:

$$Equation\ 10 : M_2 = \frac{M + L}{2}$$

The new function value $f(M_2)$ is computed. The convergence criteria are checked as per the normal routine. The reflection, expansion, single and double contraction operations can be found in visual format in Figure 4. The preceding steps can be summarized in a flow chart found in Figure 5.

Figure 4: Starting Simplex With Pperations Overlapped

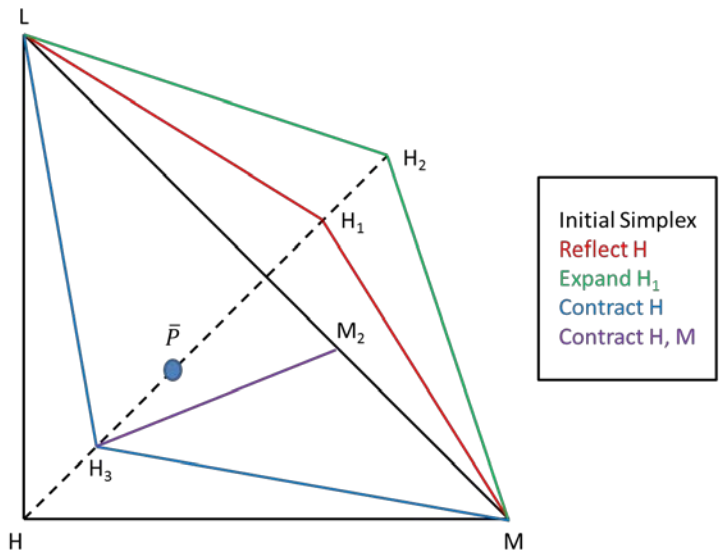

Figure 5: Downhill Simplex Flowchart Modified (Jackson and Agrawal, 1999)

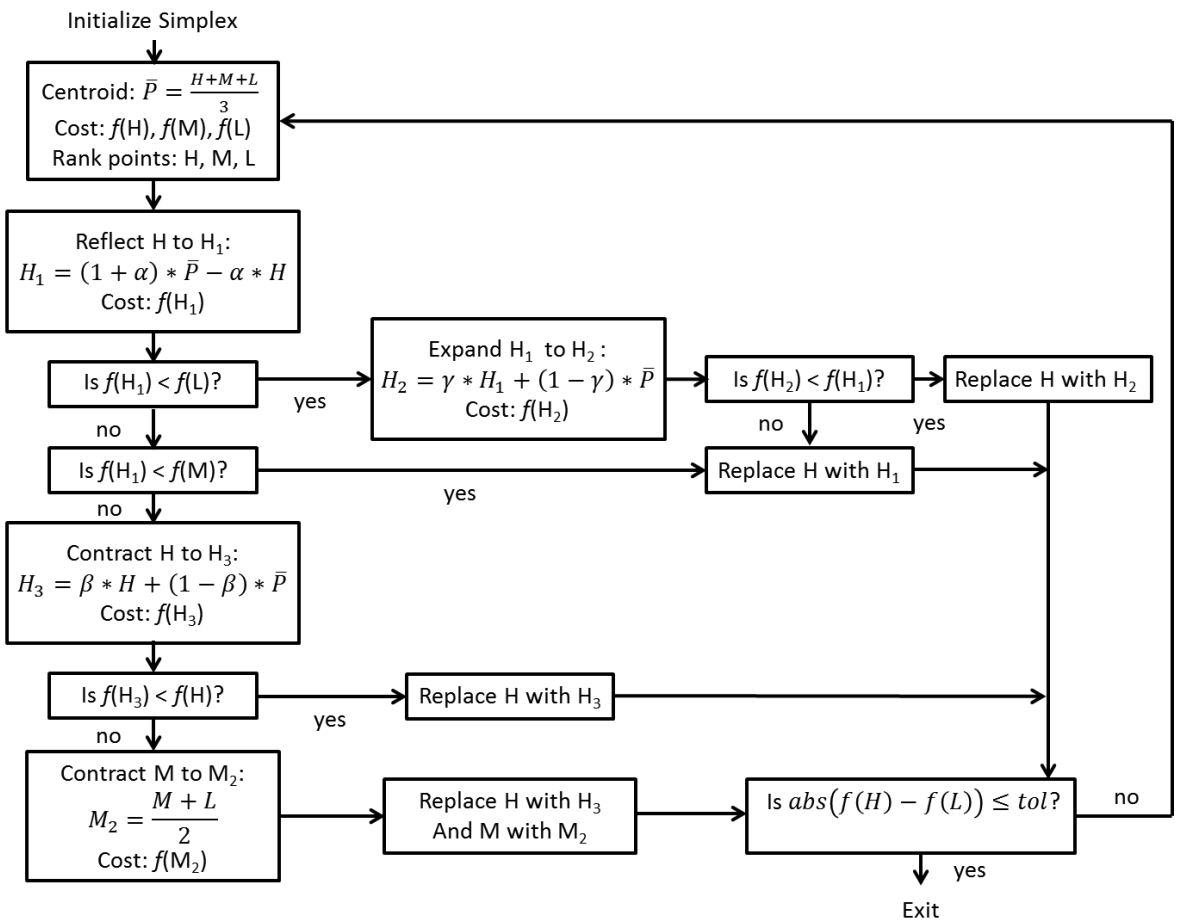

2.5.1.2 Number of Function Computations

A small section should be spent on discussion of number of times a function calculation must be called per iteration of the downhill simplex. Initially all three points (H, M, L) must have their function value computed (either using collected data or polynomial approximation). For the remaining steps only the new H points or M_2 point need to be computed for their function value. When initializing for the next iteration the new H and M values have already been collected from the previous iteration. Therefore after the initial iteration every subsequent iteration can add 2 to 3 more function calls (depending on expansion or contraction route). This type of clever programming can significantly reduce the number of times data points must be collected, thus lowering the overall time required to reach optimal conditions.

2.5.2 Combustion Applications

There have been three major studies done in the literature that have involved using downhill simplex algorithms to optimize combustion system performance. The first project was done by Padmanabhan et al. and it developed actuation techniques to control volumetric heat release and pressure fluctuations for a laboratory-scaled combustor (Padmanabhan, Bowman, and Powell, 1995). According to Padmanabhan the control strategy choice whittled down to two main algorithms: direction-set and downhill simplex. The direction-set algorithm was

eliminated due to its lack of flexibility with functions with multiple extremum. The downhill simplex algorithm was chosen due to its simplicity and ability to handle multiple extremum. The actual algorithm used in the experiment followed Nelder and Mead's algorithm closely and only varied in its overall convergence criteria. The amoeba would be initialized at a point and allowed to converge to an optimal point. Once the first starting point reached an optimal point, a new starting location was selected and the process restarted. After two more restarts, the final optimal values and their locations are compared to each other. If the four points varied significantly in their values and location then the whole process would begin again, else the program would conclude that it reached the optimal point. This resetting feature of the amoeba allowed the algorithm to adapt quickly and effectively to changing environments. In the paper there are three main parameters of the control strategy that require special attention and tuning: amoeba size, amoeba convergence tolerance, and initial starting points. The paper concludes with remarks on algorithm time and number of iterations. For long measurement times the function values proved to be highly repeatable and reliable; however, figuring out the best mix of measurement time and the number of iterations to evaluate is a necessary tradeoff problem that needs to be addressed in future works.

The second project in this discussion is from Jackson and Agrawal in which they studied the effects from downhill simplex optimization on a residential furnace (Jackson and Agrawal, 1999). The objective was to vary the geometry and equivalence ratio to minimize the NO_x and maximize the heat transfer to the water. The algorithm followed Nelder and Mead's method identically and did not have the overall convergence criteria as done in Padmanabhan. Several tests were conducted and the number of iterations of the algorithm required to reach the optimal solution varied based on several parameters: starting location, convergence tolerance, and amoeba size. In their concluding remarks, the authors reiterate the importance on finding a faster and more efficient way to extract the required data in order to decrease the time to converge to an optimal point.

The third project was conducted by Davis et al. at the University of California, Irvine Combustion Laboratory (Davis and Samuelsen, 1996; Davis, 1995). Davis developed a hybrid control algorithm that incorporated properties of a hill-climbing technique with the geometric design of the downhill simplex method. The theory behind this hybrid model selection was to avoid the potential of the simplex contracting on a local minimum and not a global minimum. The control algorithm performed well, but less than perfect (Davis and Samuelsen, 1996). There was also the conclusion that the traditional downhill simplex algorithm was better at dealing with noise in the sensor data than the hybrid model. Essentially the conclusion made was the hybrid method was no better or worse than the traditional method and so this hybrid technique will not be pursued in this research.

2.6 Current Project

The current project is based on the work done by St. John and Demayo, but with a few key differences. No study has investigated what happens to the direction-set algorithm when the fuel is subject to change. Many studies have investigated what happens when there is a hardware malfunction, but fuel composition changes pose quite different dynamics that could

disrupt the algorithm. This current study also attempts to compare the efficiency, efficacy, and robust nature of Powell's direction-set algorithm verse the downhill simplex method. The two algorithms have only been compared on a theoretical stand point in the literature and never with the same combustion system. The results gathered from simulations will ultimately determine if indeed one algorithm is superior to the other or if it makes no difference.

CHAPTER 3:
Experimental Apparatus

3.1 Burner Geometry

3.1.1 Burner

A commercially available Coen Quantum Low NO_x (QLN) burner scaled to 400,000 British thermal units (Btu/hr) was used in this study. A top down and side view of the burner geometry can be found in Figure 6. The burner is 6.5 inches in diameter and 14.5 inches in total length. The combustor is comprised of three main fuel injection circuits (Core, Radial, Outer) and one central location for air mixing. This burner and test facility were previously used by D. Brouwer and T. Demayo and are described in great detail in their respective theses (Brouwer, 1996; Demayo, 2001).

Figure 6:Scaled Quantum Low NO_x Burner (Adapted From (Demayo, 2001))

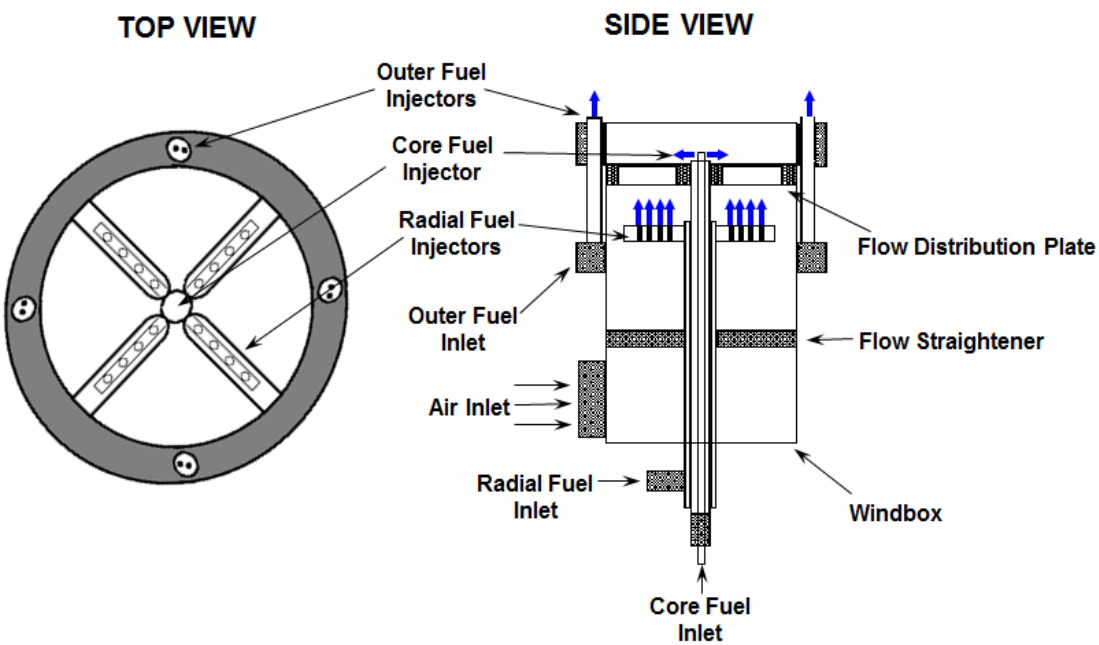

3.1.2 Distribution Plate and Throat Area

The distribution plate has four slots directed radially outward from a center hole meant for the Core injector. The slots have a width of 0.5 inches and a length of 1.5 inches. The Radial injector tubes sit directly below these openings. These dimensions produce an approximate velocity of 80 feet per second (ft/sec) for the reactants passing through the slots at an operating condition of 25 percent excess air (Brouwer, 1996). The sudden expansion from the windbox to the primary reaction zone creates two features. The first feature is increased mixing between the air and Radial fuel. The second feature is it creates recirculation zones in the throat section that helps

stabilize the flame. Based on the geometric optimization work done by D. Brouwer, the throat depth was chosen to be held fixed at 1.125 inches.

3.1.3 Windbox

The windbox contains a 4.0 inch outside diameter pipe extrusion which acts as the air entry point. The air enters horizontally and then turns vertically into a honeycomb flow straightener to uniformly distribute the flow before exiting through the slots in the distribution plate. Air is only allowed to mix with the Radial fuel in the short distance between the Radial tubes and the flame side of the distribution plate. The air flow rate varies between 68 to 82 standard cubic feet per minute (scfm) depending on the fuel selected and the amount of excess air chosen for operation. The air is controlled by a sonic orifice coupled to a pressure regulator.

3.1.4 Core Fuel Injector

The Core injector consists of a 0.25 inch diameter tube capped at the top and has four 0.05 inch diameter holes equally spaced around the circumference. The injection holes are placed 0.125 inches above the distribution plate and aligned with the four slots seen in the top view of Figure 6. The flow is constrained to 25 percent of the total fuel flow and primarily acts as a pilot flame to the Radial injectors. This circuit is a non-premixed system.

3.1.5 Radial Fuel Injectors

The Radial injectors are located beneath the distribution plate and have the capability to move along the length of the burner. The injector tube has four spokes that branch from the center of the burner and are aligned with the four slots of the distribution plate. Each spoke consists of four equally spaced 0.12 inch diameter holes placed facing upward in the normal direction of the distribution plate. For this study the Radial tube has been placed flush with the distribution plate, which offers very minimal mixing with the incoming air. The remaining 75 percent of the total fuel flow of the system is split between the Radial and Outer injectors, which is a parameter being investigated known as fuel split (FS) and will be discussed in a later section.

3.1.6 Outer Fuel Injectors

The Outer injector is comprised of four 0.5 inch diameter tubes placed on the upper ring of the burner. Each tube has two holes slightly angled toward the center of the burner and are angled tangentially to the inner circle. The tubes sit 0.25 inches from the top plate. The Outer injector is a non-premixed system and due to recirculation the injectors have some flue gas combustion properties that help in lowering emissions.

3.2 Test Facility

3.2.1 Test Stand

The entire boiler enclosure sits on top of a heavy-duty transverse system and is located between two optical tables that can be used for mounting various optical equipment systems. Figure 7 shows a schematic of the test stand in relation to the furnace enclosure. In this study, a fiber optic probe had a mounting mechanism that was located on the left hand side (as viewed from the picture in Figure 7) of the burner on the optical bench.

Figure 7: (Top) Schematic of Test Stand (Adapted From (amuelsen and Miyasato, 2000)) and (Bottom) Furnace Enclosure

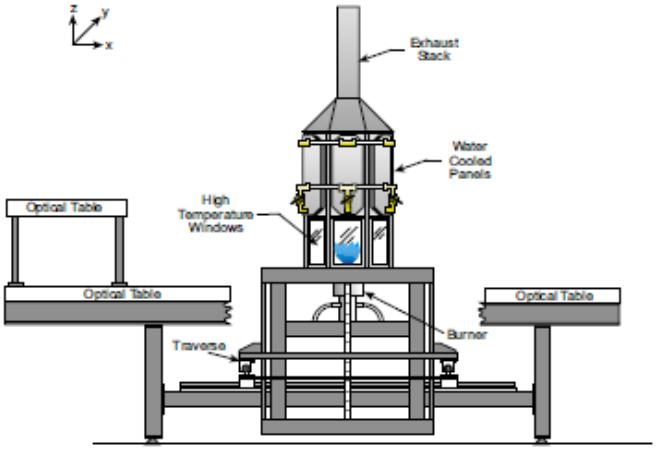

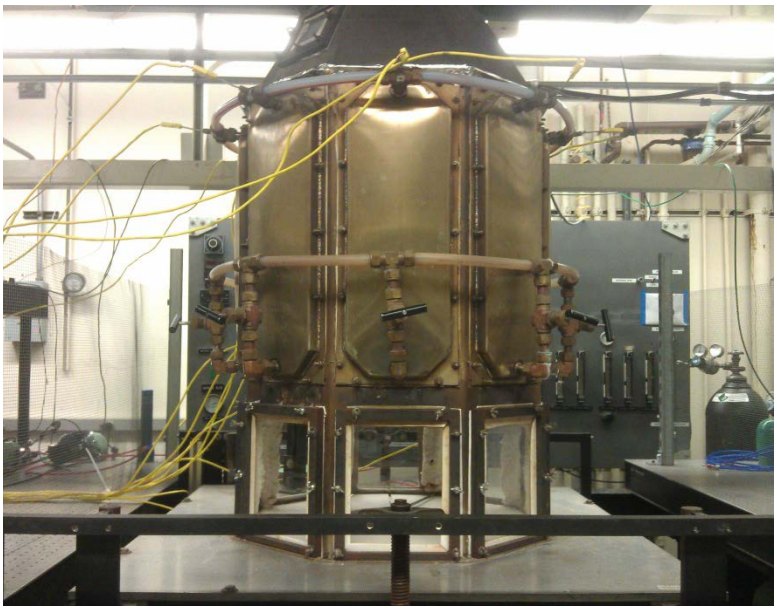

3.2.2 Furnace Enclosure

The furnace has 8 flat sides and is 2 feet in width and 3 feet in height (excluding exhaust stack length). A picture of the furnace can be seen in Figure 7. Inside the furnace the walls near the optical windows are insulated with high temperature insulation lining. The base around the burner is an extra-high temperature calcium silicate insulation that comes in ½ inch thick 12 inch by 12inch sheets. This insulated layer limits the heat loss from the burner to the aluminum plate supporting the entire furnace. There are three main parts to the furnace: optical windows, water cooling panels, and exhaust stack.

The optical windows have dimensions of 7.5 inch by 9.5 inch width/height and hold high temperature flat plates of a material known as VYCOR. The VYCOR plates are held in by 0.75

inch thick cold rolled steel frames that have dimensions of 9 inches x 10.5 inches width/height. The frames hold the VYCOR windows in place with a thin layer of high temperature ceramic paper sealing the two pieces to the furnace. The windows are located on the bottom portion of the furnace. The flat windows allow for easier optical access for laser systems or in this case a fiber optic probe.

Above the optical windows are the cooling panels. Water enters from the bottom tubes and exits through the top ring of tubing. The placement of the cooling panels is away from the main flame which is not very conducive for optimal heat transfer. The primary heat for this section is from the hot products after the combustion. This design feature will be later referenced to when explaining the poor boiler efficiency results.

The exhaust stack has a conical to cylindrical design that has two unique purposes. The first purpose is it helps propel the exhaust products into the overhanging hood. The second purpose is to facilitate mixing of the exhaust products to create uniform mixtures for the emission sampling measurements.

3.2.3 Water Cooling System

There are two main water cooling circuits: boiler water cooling circuit and laser cooling circuit. The boiler water cooling circuit directly cools the furnace while the laser cooling circuit cools the hot return water from the boiler. The system configuration that combines these two circuits can be seen in Figure 8. The water cooling system consists of three main components: water tank, pump, and heat exchanger. Water is stored in the water tank and then is pumped through the heat exchanger at a rate of approximate 1.2 pounds per second (lb/s). The heat exchanger transfers energy from the laboratory's laser cooling water loop with the boiler water cooling loop. During tests the hot water in the boiler loop maintains a temperature of approximately 100 degrees Fahrenheit. The purpose of the water cooling system is to minimize structural damage to the furnace and simulate the dynamics of a commercial boiler unit.

Figure 8: Water Cooling Configuration

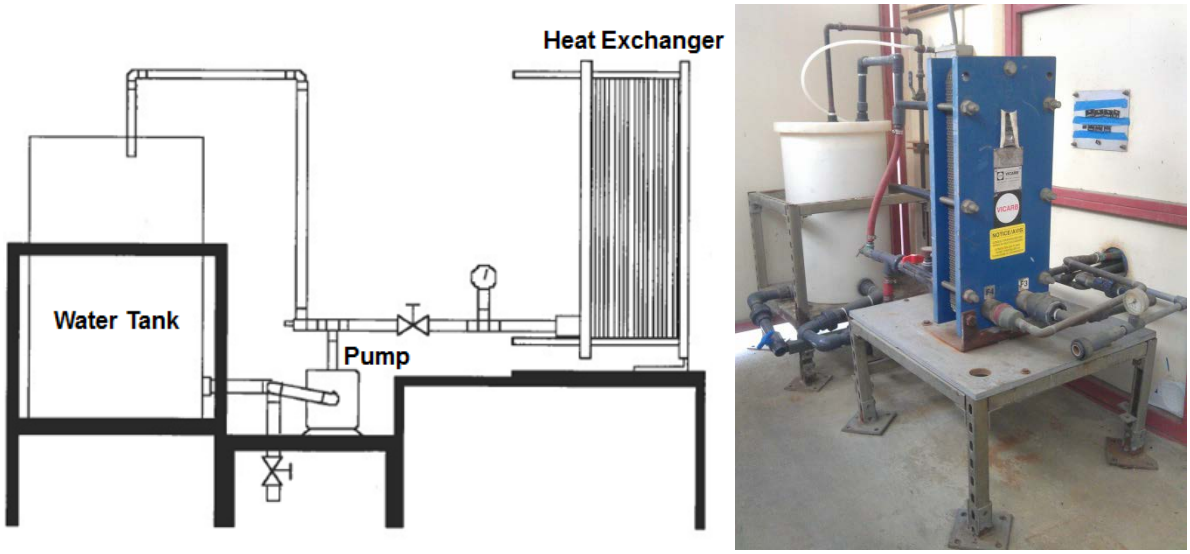

3.2.4 Flow Control System

There are two main components to the flow control system: physical lines and data/electrical lines. The overall schematic of the system can be seen in Figure 9. The physical lines are presented in black solid lines while the data/electrical lines are presented in blue dashed lines. The blue boxes represent various hardware components such as sonic orifices, sensors, and computer. In the initial stages of this research mass flow controllers (MFCs) were originally used. These devices worked well when controlling just natural gas, but when propane was required to be added to the line the acquired MFCs and their series configuration were ill suited for the task. Two MFCs were configured in a fuel mixing stage, combined into a single line and then separated into the Core, Radial, and Outer circuits using three more MFCs. This series configuration of MFCs could not produce stable/repeatable pressure drops across the MFC units which ultimately led to uncontrollable flow splits. Thus a new flow control strategy was required to be designed.

In order to stay within a reasonable budget the solution of buying six additional MFCs was abandoned due to the extravagant cost of each device. Eventually sonic orifices were chosen as the flow control system due to their ease of installation, control, and steady and repeatable flow characteristics. The major drawback to the use of sonic orifices is their lack of computer control capabilities. A pressure regulator is upstream of the orifice and is manipulated by a human operator. This can be seen as an added safety measure when testing unverified control algorithm codes. Furthermore, the sonic orifices can be regulated by digitally controlled pressure regulators coupled with pressure transducers or ultimately replaced for the more compact and computer friendly MFCs if a fully autonomous control demonstration is desired. From an optimization algorithm point of view, whether the system is computer controlled or requires some form of human interaction makes no difference to the optimization algorithm since all it is concerned with are the data gathered and not how it is gathered. Therefore, active control can still be reasonably demonstrated in either case. The convergence time to the optimal solution will be somewhat longer in the sonic orifice scenario than it would in a MFC computer controlled scenario; however, the number of iterations taken by the algorithm will still be the same.

Figure 9: Flow Control Schematic

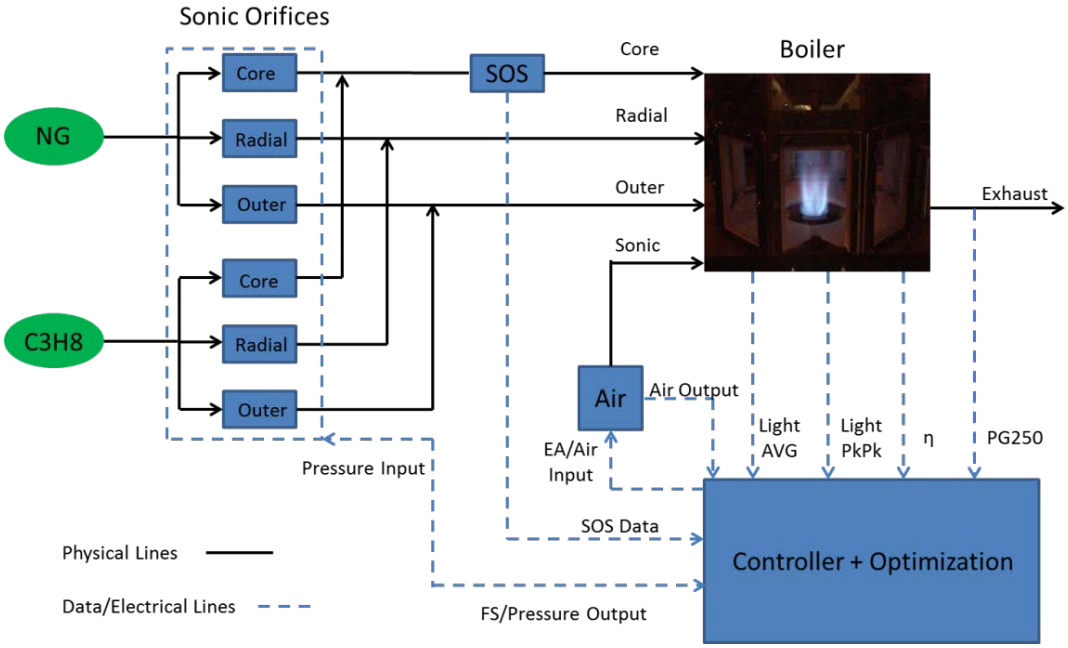

A picture of the sonic orifice control panel can be seen in Figure 10. The bottom three regulators and pressure gauges are for the natural gas line while the above three regulators and gauges are for the propane line. The natural gas supply line enters through the bottom Swagelok cross at 120 pounds per square inch (psi). Propane is added to the system by a cylinder at 110 psi. The regulator circuits are situated to be the Core, Radial, and Outer (C,R,O) circuit from left to right (as seen in the picture). The sonic orifices are steel Male-Male National Pipe Thread (NPT) ¼ inch fittings and are threaded directly into the exit of their respective regulator. Using a constant firing rate (400,000 Btu/hr) and adjusting the fuel flow rate based on the higher heating value of the fuel blend, the various orifices were sized accordingly. The orifice sizes selected for the natural gas supply are 0.03 inch, 0.04 inch, and 0.04 inch (C,R,O) while the propane orifices are 0.0 inch, 0.016 inch, and 0.016 inch (C,R,O). The remaining physical line is the air line which is controlled by a sonic orifice (size 0.4 inch) and pressure regulator with a pipeline pressure of 140 psi.

Figure 10: Sonic Orifice Control Panel

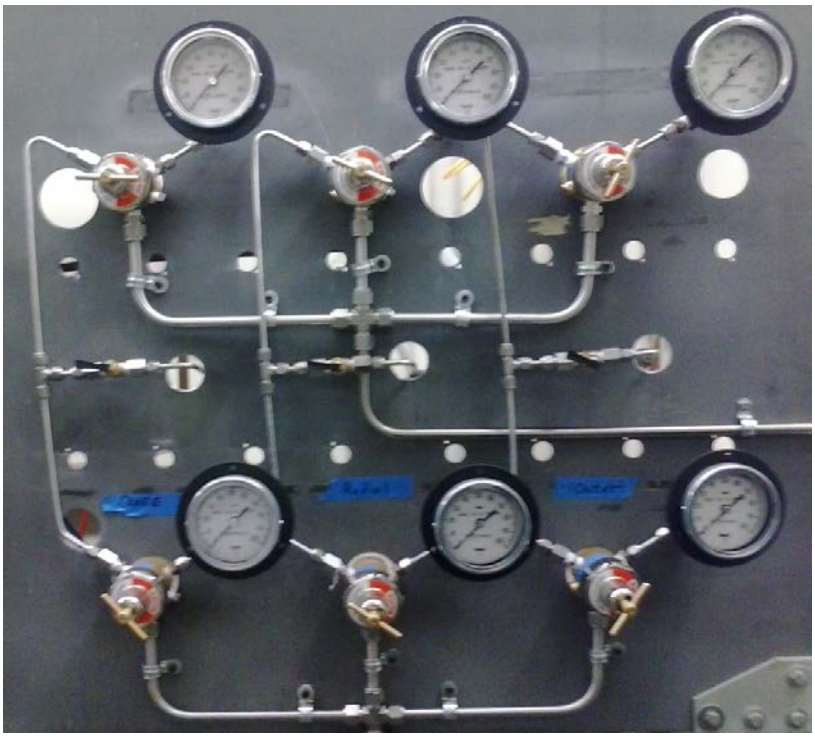

The remaining components of the system diagram are the data/electrical lines. These components are essentially all the sensors and data acquisition hardware. The sensors will be discussed in more detail in the next section; however, one point that will be made is about the speed of sound (SOS) sensor. The SOS is placed on the Core fuel line after the gas mixing has occurred from the sonic orifice panel. The SOS was placed on this line in particular because the Core fuel flow rate (and the mixture blend as well) was held constant and consistent throughout each test. Therefore, the signals were very steady and repeatable for each test. The data acquisition hardware consisted of National Instruments FieldPoint modules and ran LabVIEW version 2009 on the supporting computer. The FieldPoint modules operated at a frequendy between 1-10 Hertz (Hz). A separate National Instruments PCI-6024E module that has a sample rate of 1,000 Hz was used to measure the fast dynamics of the flame luminosity associated with the fiber optic probe measurement.

3.3 Sensors

The main sensor information required to complete this project can be divided into four categories: fuel identification and properties, flame stability, emissions, and efficiency. Sensors were chosen based on accuracy, cost, and ease of implementation. There are many sophisticated devices that detect the composition of a gas; however, many of those devices are expensive and only practical in laboratory environments. Using an ultrasonic sensor originally designed to measure distances away from objects, the sensor was repurposed to detect the speed of sound in an unknown gas mixture. From this information the fuel composition and its physical

characteristics can be computed. Flame stability is determined by measuring the oscillations in luminosity of the flame via a fiber optic probe connected to a photomultiplier. If the flame blows out the probe will detect the sudden decrease in luminosity and alert the control program of the situation. The emission analyzer chosen was a Horiba PG250, which is a common and accurate analyzer, used by many institutes. It is capable of measuring the NOx, CO, CO2, and O2 content of the exhaust stream. The efficiency of the system has been defined in two separate ways: boiler efficiency and excess air usage. After several experiments the boiler efficiency proved too unreliable and inaccurate in describing the efficiency of the overall system which led to a new definition of efficiency based on excess air usage.

3.3.1 Fuel Identification and Properties

The most common way to measure fuel composition in a pipeline is to use a gas chromatograph, but these devices are generally expensive, have a large footprint, low sample frequency, and require considerable amount of regular maintenance and calibrations. A novel approach of estimating composition is to measure the speed of sound of the fuel source. Determining the composition of a binary gas is very simple, but natural gas is a multi-constituent fluid that contains flammable substances as well as inert gases. As shown in (Lueptow and Phillips, 1994), the speed of sound of natural gas variants with a large amount of inert gases creates very unreliable results when trying to predict parameters such as Wobbe Index and mole air-fuel ratio. To counter the presence of inert gases in the fuel, two additional sensors have been proposed by (Loubar et al., 2007) with significant success. In Loubar et al. a thermal conductivity sensor and a CO_2 sensor were added to the speed of sound sensor array. From this information a set of nonlinear equations could be solved to accurately estimate the Wobbe Index and mole air-fuel ratio for a wide variety of natural gas mixtures. For this project only two gases will be used: natural gas and propane. As shown in Chapter 2, the laboratory's natural gas line is approximately 98 percent methane. To simplify the complexity of the system this project will make the assumption that the fuel supply consists of only a binary set of gases (methane and propane). The thermal conductivity and CO_2 sensors will not be implemented in this project due to this binary gas assumption; however, if more fuel variations wanted to be studied then these sensor would be required.

The RPS-409A-IS intrinsically safe ultrasonic sensor from Migatron (Figure 11) was chosen to act as a speed of sound measuring device that can then be used to correlate to fuel properties. This sensor is nominally designed to measure the distance from the sensor to a nearby object by emitting and receiving ultrasonic sound waves. For a fixed medium, such as air, the speed at which a sound wave can propagate is known and can easily be modeled. By recording the time delay between emitting a pulse and receiving the reflected signal the distance of an object can be calculated using basic kinematic formulas (distance = speed*time). Now when the object is fixed (in this case a wall at the end of a tube) and the medium is varied, the time between emitting and receiving a pulse will fluctuate. Rearranging the terms from the previous equation, the speed of the sound wave can be measured for an unknown medium. Since every substance has a corresponding speed of sound it is easy to correlate the results to a single or binary mixture of gases. Complications arise when the medium is composed of several substances since multiple solutions can be achieved. For example a blend of 85-15 methane-propane by

volume percent can have the same speed of sound as an 80-10-10 methane-ethane-propane blend. It must be noted here that knowing the exact fuel blend might be irrelevant in finding correlations between fuel interchangeability and burner performance. Alternative parameters such as the carbon to hydrogen (C/H) ratio or the Wobbe number could potentially be used as explained in (Ferguson et al., 2008). Once the speed of sound C of the gas can be estimated it can be correlated to the Wobbe number and C/H ratio by plotting against C^2/T, where T is the absolute temperature in the chamber.

Figure 11: Migatron RPS-409A-IS Intrinsically Safe Ultrasonic Sensor

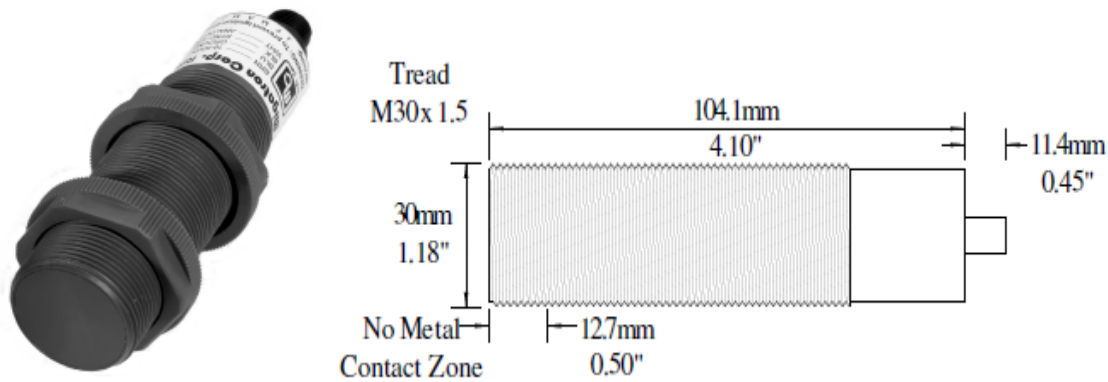

While the measured time varies for a fixed object with a fluctuating medium the output of the Migatron sensor is only the "appeared" distance if the medium was air. In other words, the sensor thinks the object is moving while really it is still stationary and it is the medium that is changing. Therefore, the following equation was derived to relate the various "appeared" distances to the speed of sound of an unknown gas:

$$Equation\ 11:\ C_{gas} = \frac{D}{D_{gas}} * C_{air}$$

where C_{gas} and C_{air} are the speed of sounds in the gas and air, respectively. D_{gas} is the appeared distance of the wall and D is the actual distance of the wall. For example, if methane was the medium the appeared distance D_CH4 would be less than the actual distance D due to methane's lower density (higher speed of sound), as seen in Figure 12. In order for the sensor to work properly it needs a flat reflective surface. For this reason a 3 inch by 3 inch by 14 inch rectangular aluminum tube was constructed, which can be seen as a schematic and actually implemented in Figure 12.

Figure 12: Speed of Sound (SOS) Model and Physical Hardware

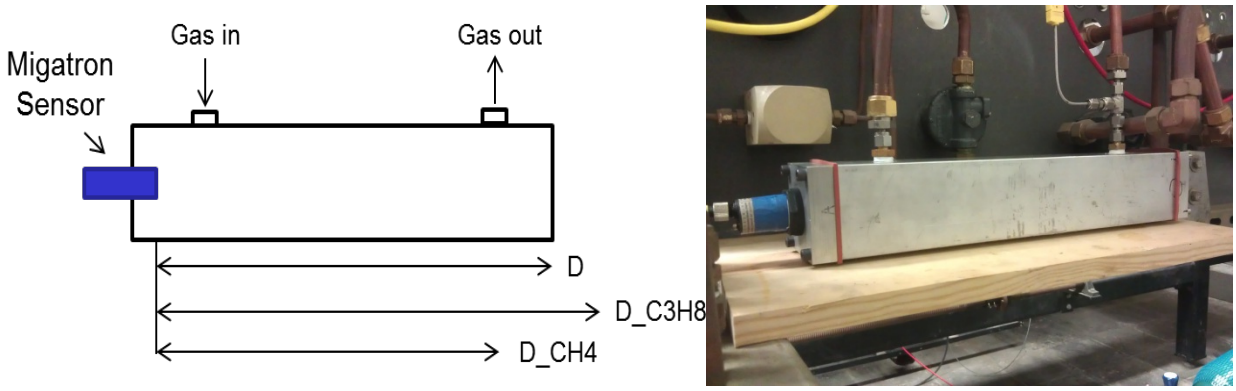

In order to account for fluctuation in the temperature of the working fluid, while relating the speed of sound to the medium properties, the following proportionality was derived using basic ideal gas laws.

$$Equation\ 12: \frac{C_{gas}^2}{T} \propto \frac{\gamma}{MW}$$

Where γ is the specific heat ratio, MW is the molecular weight, and T is the absolute temperature in Kelvin. The above equation states the speed of sound squared divided by the temperature is proportional to a gas's physical properties. This solution can also be extended to relate the speed of sound to the C/H ratio (mole) and Wobbe number. Tests of the Migatron sensor were conducted and relations between the speed of sound and the C/H ratio as well as the Wobbe number are shown in Figure 13.

Figure 13: C/H ratio (left) and Wobbe (right) vs. C2/T

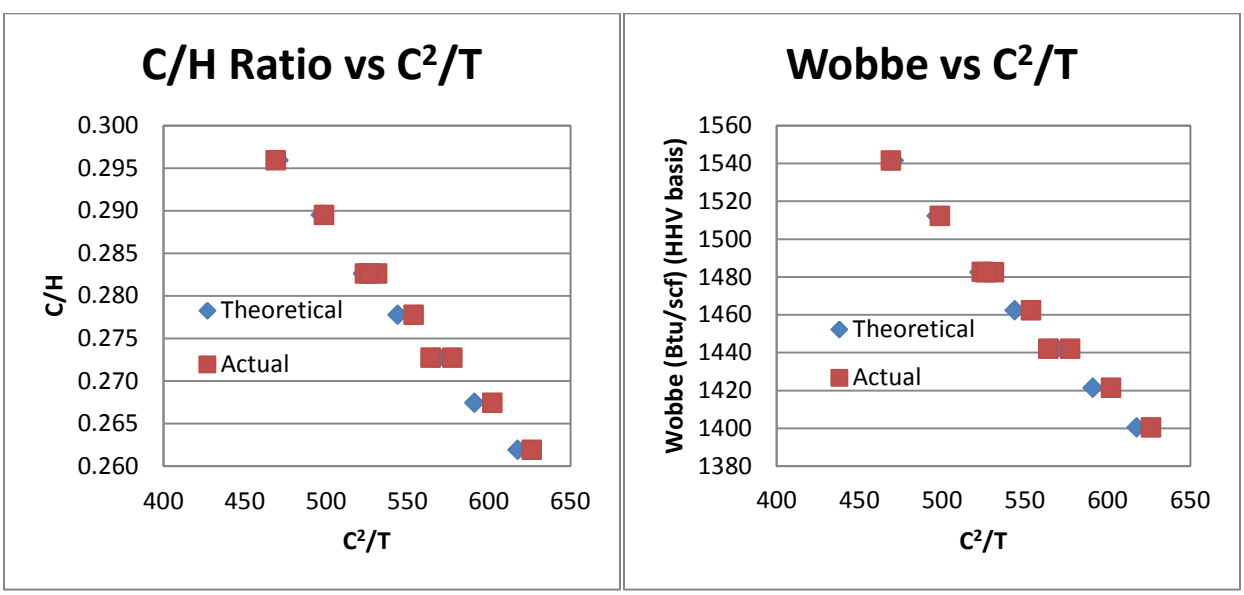

For the mixtures planned to be investigated, the C/H ratio and the Wobbe number are both linearly related to the term C^2/T. Therefore, these correlations will be used later during actual experiments to relate the fuel properties to the emission and stability data. The Migatron sensor has proven to be accurate to within 2 percent of the actual speed of sound and 0.5 percent accurate in determining the Wobbe number and C/H ratio for this range of mixtures.

3.3.2 Flame Stability

Monitoring flame stability is an important parameter when operating in very lean conditions in order to prevent lean blow-off. For this reason a fiber optic probe coupled to a photomultiplier tube was chosen to measure the luminosity of the emitted light from the flame. Figure 14 shows how the fiber optic probe was attached to the test stand. The photomultiplier tube (C1053-51, No. 500091) was connected to a Bertan high voltage supply set to 0.80 and a 15 volt power supply.

Figure 14: Side-wall Mounted Fiber Optic Probe

There was no physical filter attached to the fiber optic probe, which resulted in measuring all emitted light frequencies. In order to negate the potential effects from ambient light the experiments were conducted in complete darkness. Filters that would isolate the OH* or CH* frequency bands, as used in (Scott, King, and Laurendeau, 2002), could have been implemented. A digital filter was used to isolate the signal from noise and was a lowpass inverse Chebyshev of order three with a cutoff frequency of 20 Hz.

There are three main categories the data gathered from the fiber optic probe can be used: flame detection, emission estimator, and flame stability. The simplest method using the luminosity data would be to detect whether a flame is present or not. This is very important when operating in large enclosed vessels with lean flame conditions. If a flame is extinguished, but the fuel is not immediately shut off the combustion chamber will be filling with hot and easily combustible material. If there was a spark or if the fuel was able to autoignite then there could be a devastating explosion or puff in boiler industry terms. Thus having the ability to detect

when a flame is present becomes an important safety mechanism. These data types will later be referenced to as Light Average (AVG).

An interesting aspect of luminosity data are its ability to correlate with NO_x emissions (Demayo, 2001). Demayo's research found that there is a linear correlation between NO_x emissions and the light intensity of a natural gas flame. This result suggests a sensor that can measure luminosity can also estimate emissions, which can make an expensive emission analyzer not necessary.

The last important measurement the luminosity data can provide is information on the oscillation characteristics of the flame. The minimum and maximum vertical peaks in the luminosity signal can vary significantly at very unstable conditions. By measuring the distance between two peaks one can measure how much the flame is oscillating, which can then be used to quantify stability regions. High oscillating regions would like to be avoided since these are areas of high instability and could damage components. This parameter will later be referenced to as Light PkPk.

3.3.3 Emissions

The emissions measurement system that is being used for this investigation is a Horiba PG250 analyzer (Figure 15a) in line with a refrigerated water dropout system. The analyzer measures NO_x, CO, CO_2 and O_2 using EPA approved methods. A vacuum pump is used to collect the sample gas from the burner exhaust stream via a stainless steel probe, which is inserted inside the exhaust stack. This probe has a 0.5 inch outer diameter, which is designed to take an integrated average measurement of the emissions over the diameter of the sampling plane via five area-weighted sampling holes (Figure 15b). Sampling systems and testing protocols based on California Air Resources Board (CARB) Method 100 are followed. In addition, the PG250 is zeroed and spanned before the start of each test using EPA certified gases.

Figure 15: Horiba PG250 Analyzer (Left) and Emissions Probe (Right)

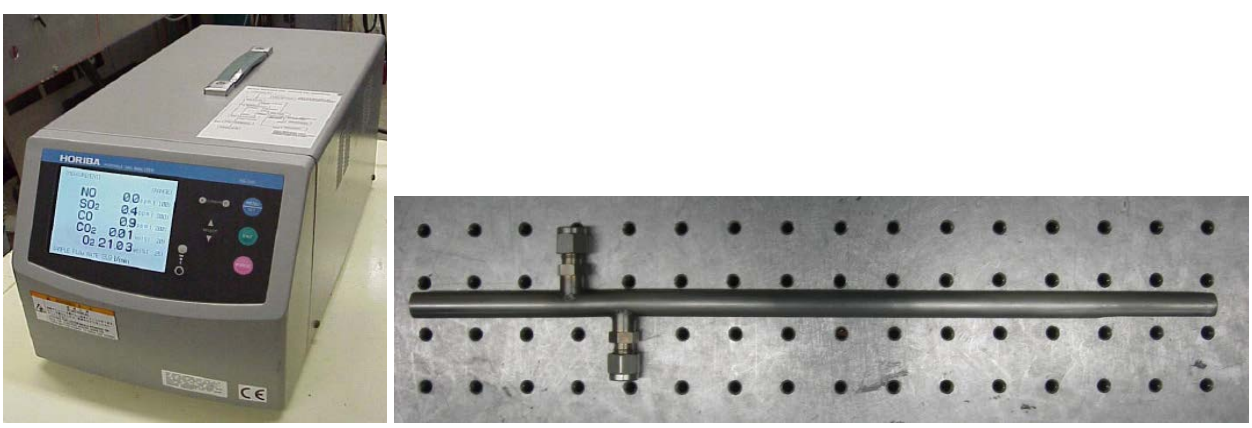

3.3.4 Efficiency

There are two efficiency measurements that are utilized in this work. The first uses the standard definition of boiler efficiency: heat in cooling water divided by the heat input from the fuel. The

heat generation in the cooling water is calculated based on the temperature of the supply and return values of the water circuit. The boiler efficiency equation can be seen below:

$$Equation\ 13: \eta_B = \frac{\dot{m}_w C_w \left(T_{return} - T_{supply}\right)}{\dot{m}_f HHV_f}$$

The mass flow rate (m)of the water was calculated to be 1.12 lb/s and assumed to be constant throughout each test. The assumption of constant and repeatable water flow rate was later to be found incorrect and upon recalibration of the flow rate it was found the flow had changed to 1.3 lb/s. Recall now that the furnace enclosure is designed to have the cooling panels located above where the flame is burning. Therefore the amount of heat transfer from the flame to the walls is not optimal. This results in very poor boiler efficiencies as well as minimal change in values for various flow conditions. For these reasons an alternative efficiency measurement based on the amount of excess air being used is proposed. The laboratory is equipped with a high pressure air line; however, in normal commercial applications there will be a compressor unit that does the same function. The compressor consumes more energy when more air is required. Thus, by basing the efficiency on the amount of compressed air required a more accurate efficiency model is produced. The following equation is adapted from Demayo and instead of using [O_2] concentrations it simply uses EA:

$$Equation\ 14: \eta_{EA} = 1 - \frac{EA}{EA_{max}}$$

CHAPTER 4:
Burner Performance Mapping

4.1 Test Plan

Three fuel composition cases were selected for this study: 100-0 percent, 95-5 percent, and 92.5-7.5 percent by volume natural gas-propane (NG-PG). The maximum standard load is 400,000 Btu/hr, which if using the higher heating value of natural gas equates to 6.59 scfm of fuel flow. Two different tests were conducted for the 95-5 percent NG-PG case: the first test at the same volumetric flow rate as the 100-0% NG-PG case (6.59 scfm) and the second test at the corrected heating load case (6.12 scfm). The first test case simulates a scenario where the speed of sound sensor is not operating and the burner cannot adjust to the correct heating load. This case demonstrates what happens when the burner is unaware of a fuel composition change which is the current design of the burner. The second test case simulates a scenario where the speed of sound sensor is turned on and the burner is able to adjust to the correct heating load. Essentially these two cases show the differences between not using sensor feedback and using sensor feedback. To avoid damaging the boiler unit by overheating the 92.5-7.5 percent NG-PG was only tested at the adjusted heating load flow rate (5.91scfm).

Recall that there are two actuator parameters available for this burner: fuel split and excess air. Fuel split (or FS) is defined as the percent of total fuel flow in the Outer injector minus the percent of total fuel flow in the Radial injector. This can best be summarized in the following equation:

$$Equation\ 15: \boldsymbol{FS} = \%\boldsymbol{Outer} - \%\boldsymbol{Radial}$$

When there is a positive FS it means more fuel is being burned by the Outer injectors while a negative FS means more fuel is being burned by the Radial injectors. The excess air (or EA) is used here to be consistent with boiler industry standards. It is defined using the overall equivalence ratio by the following equation:

$$Equation\ 16: EA = \left(\frac{1}{\phi} - 1\right) * 100$$

Manufacturer specifications call for acceptable operating ranges of 5 to -5 FS and 10 to 30 EA. For each blend a matrix consisting of the operating conditions specified by the manufacturer was created. The matrix consists of FS on the vertical (between 5 and -5, increments of 1) and EA on the horizontal (between 10 and 30, increments of 2). An example can be found in Table 3.

Table 3: Test Plan Matrix

FS\EA	10	12	14	16	18	20	22	24	26	28	30
5											
4											
3											
2											
1											
0											
-1											
-2											
-3											
-4											
-5											

4.2 Experimental Procedure

In order to be consistent between tests, various procedures were put into effect to minimize the error and bias in the data. Each test, regardless of the fuel blend selected for that day, experienced 10 minutes of 100 percent natural gas combustion at an EA of 10 and a FS of 0. This step allowed adequate time for the burner and combustion chamber to heat up to a repeatable equilibrium temperature after a cold start. The next step would be to adjust the fuel composition by manually setting the pressure regulators for the sonic orifices that controlled the natural gas and propane lines. At this point the hydrogen pilot flame would be turned off. The lights in the test cell would also be turned off to mitigate the influence of ambient light on the fiber optic probe sensor readings. Data was collected by first setting the desired FS and then traversing across the range of EAs. At each point in the test matrix data was gathered for two intervals of 10 seconds with 10 seconds of no data collection in between the two sets. Each data set was then averaged to determine the various sensor outputs at each FS/EA condition. The sensor outputs that are of most concern to this project are: NO_x and O_2 emissions, light intensity and oscillations (also known as Light AVG and Light PkPk), and boiler efficiency. In the proceeding chapter, contour plots of the NO_x corrected to 3 percent O_2 and Light PkPk from the various test cases will be presented which constitute the "performance maps" of the burner. The other additional sensor data will be used to draw correlations and help with the analysis of the system.

4.3 Burner Performance Mapping Database

4.3.1 Performance with No Sensor Feedback

In order to establish why fuel composition sensor feedback is important two cases were conducted. Figure 16 shows contour plots of air flow rate verse fuel split on the horizontal and vertical axes, respectively, with NO_x emissions corrected to 3 percent O_2 as the third color coded axis. The left side contour is the 100-0 NG-PG case at full load (6.59 scfm) and air flow rates between 68-82 scfm (equivalent to EAs of 10-30). The right side contour is the 95-5 NG-PG case at the same fuel flow rate (6.59 scfm) and air flow rates. These contours represent a scenario where the burner has no knowledge of the type of fuel being burned and is unable to adjust to the appropriate fuel flow rate to maintain the same heating load. As it can be seen the NO_x

emissions in the 95-5 NG-PG case are considerably worse than the 100-0 NG-PG baseline case. Recall the target NO_x emission acceptable level is 20 ppm. This goal is never reached in the 95-5 NG-PG case when sensor feedback is turned off. Thus with no sensor feedback of fuel composition the burner is never able to reach acceptable operating conditions.

Figure 16: Air SCFM vs NO_x. Left 100-0, Right 95-5 NG-PG. No SOS Control

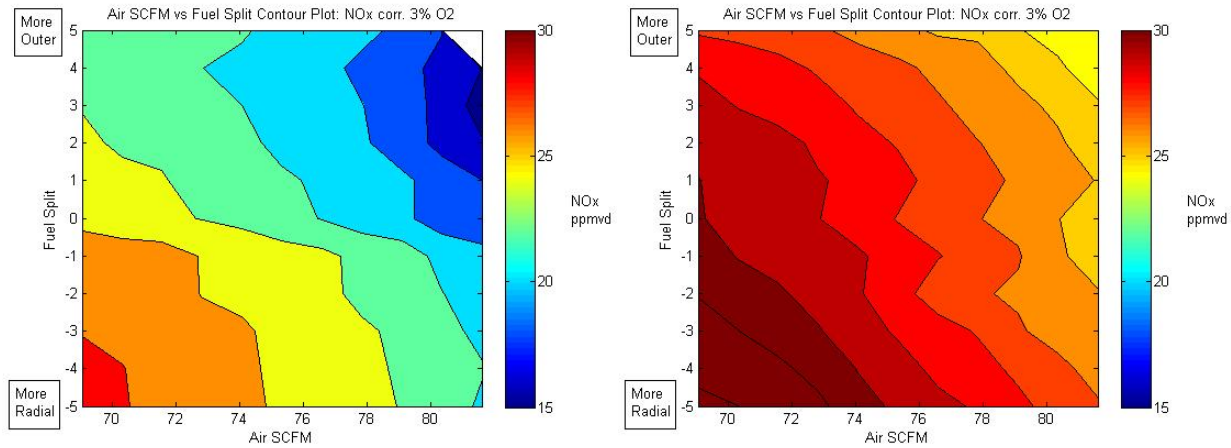

4.3.2 Trends and Correlations with Sensor Feedback

This section is concerned with displaying and analyzing the basic trends found in the data gathered from the three different fuel blend cases that have been corrected to the same heating load. It should be noted that for all the following figures presented in this section the color code system is: blue diamonds are 100-0 NG-PG, red squares are 95-5 NG-PG, and green triangles are 92.5-7.5 NG-PG blends.

Figure 17 is a plot of EA verse NO_x emissions for the various fuel blends. NO_x has been corrected to the industry standard of 3 percent O_2 and is expressed in units of parts per million (ppm) on a dry volume basis (ppmvd). In Figure 17 the NO_x decreases with increasing EA, which coincides with the common knowledge that leaner flames produce less NO_x. As more propane is added the NO_x levels actually increase, but the EA trend remains the same. For the same EA a fuel with a higher propane content will produce more NO_x than one with less or none at all.

Figure 17: EA vs NO_x Corr 3%O2 (Blue: 100-0, Red: 95-5, Green: 92.5-7.5 NG-PG)

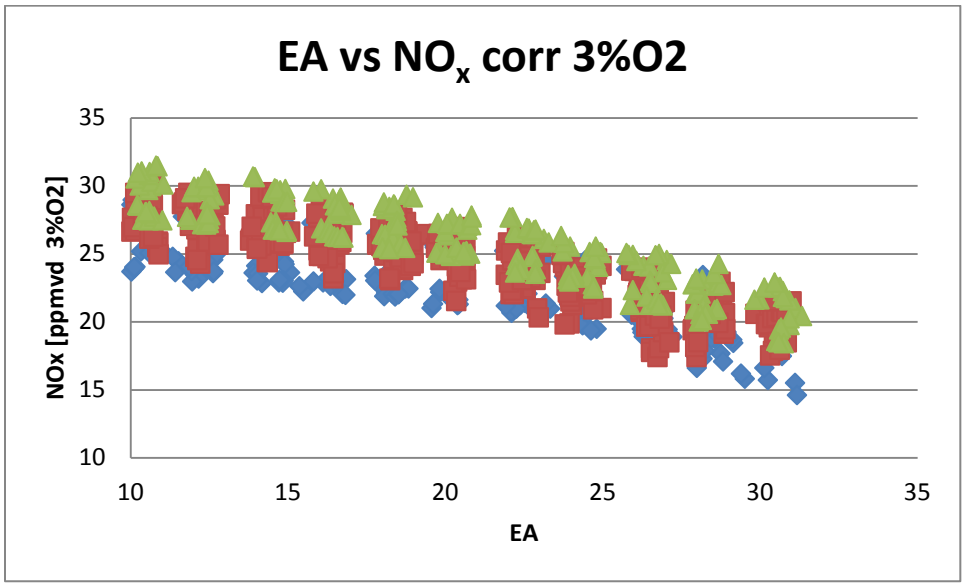

Figure 18 demonstrates what happens when NO_x is plotted against FS. As it can be seen fuel splits of positive values (more fuel to the Outer injectors) produce less NO_x than negative fuel splits (more fuel to the Radial injectors). However, it should be noted there is an optimal FS that produces the least amount of NO_x for each fuel. This occurs in the region of a FS of +3. An explanation for this result can be thought of in the following manner. The EA is calculated based on a total flow rate basis and does not concern itself with a local EA estimation. The primary combustion zone occurs at the Core and Radial injectors which is approximately 60-65 percent of the total fuel flow at any given time. As more fuel is taken away from this primary zone (trend towards positive FS) the local EA increases in the primary zone. As seen from Figure 17 already the NO_x emissions decrease with increasing EA. The extra fuel is now displaced to the Outer injectors which are non-premixed flames. These types of flames produce a large amount of NO_x at low EA conditions. Therefore, as the primary flame becomes leaner and produces less NO_x, the Outer flames are becoming richer and producing more NO_x. The NO_x production rates for both areas are slightly different which results in this minimum point at an FS of +3.

Figure 18: FS vs NO_x Corr 3%O2 (Blue: 100-0, Red: 95-5, Green: 92.5-7.5 NG-PG)

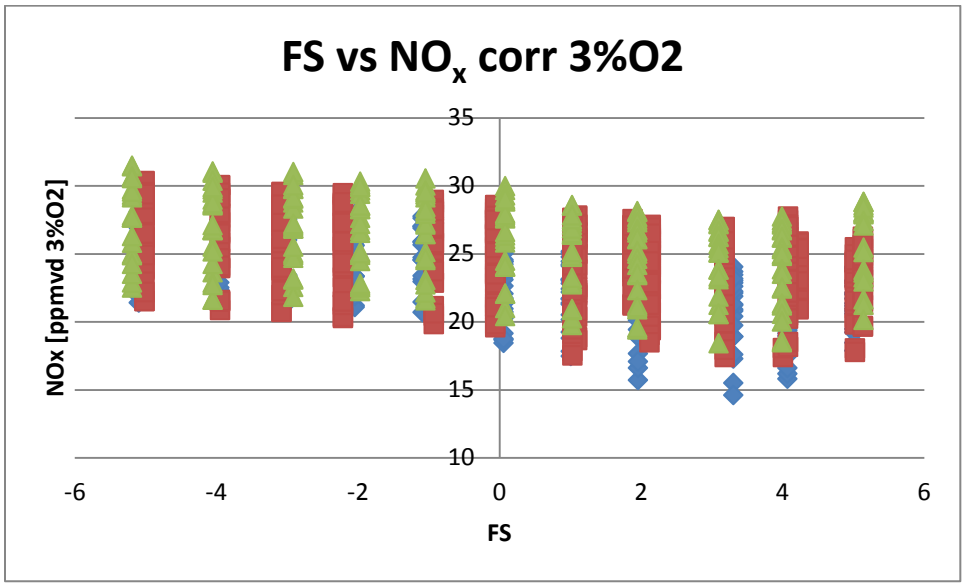

Flame chemiluminescence can be used as a simple way to detect whether a flame is on or not; however, based on previous work in the laboratory and the findings from this research a more useful application of the technology has been identified. Figure 19 shows the light intensity (or Light AVG) readings for various EA conditions. As it can be seen, the light intensity decreases with increasing EA which is very similar to the trend in Figure 17 with NO_x and EA. Due to this similarity Figure 20 was generated to show the correlation between Light AVG and NO_x emissions. A nice linear correlation exists (R^2=0.94) between the two parameters and is fuel blend independent. This result suggests that the light intensity data can be used as a NO_x predictor and could replace or stand in for a continuous emissions monitoring system.

Figure 19: EA vs Light AVG (Blue: 100-0, Red: 95-5, Green: 92.5-7.5 NG-PG)

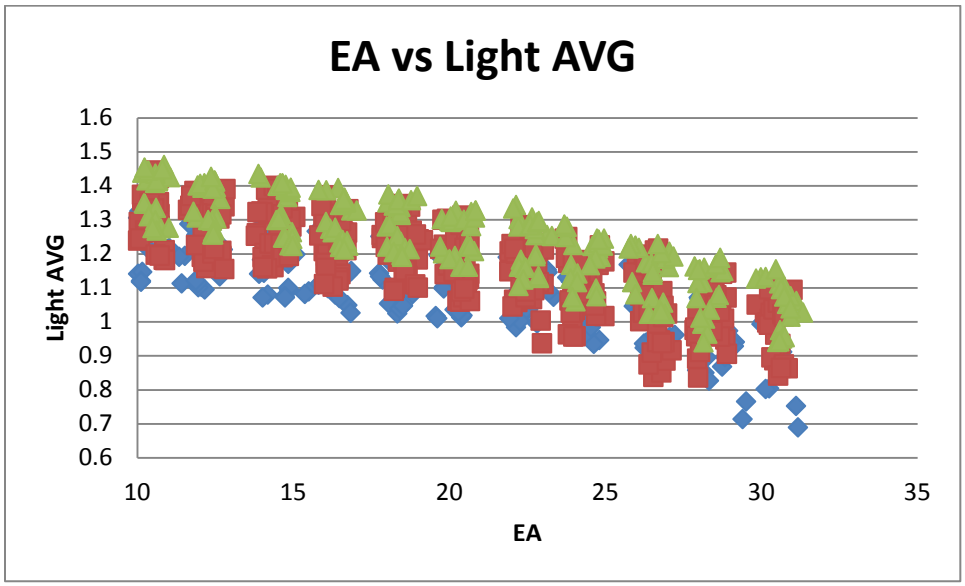

Figure 20: Light AVG vs NOx Corr 3%O2 (All Blends)

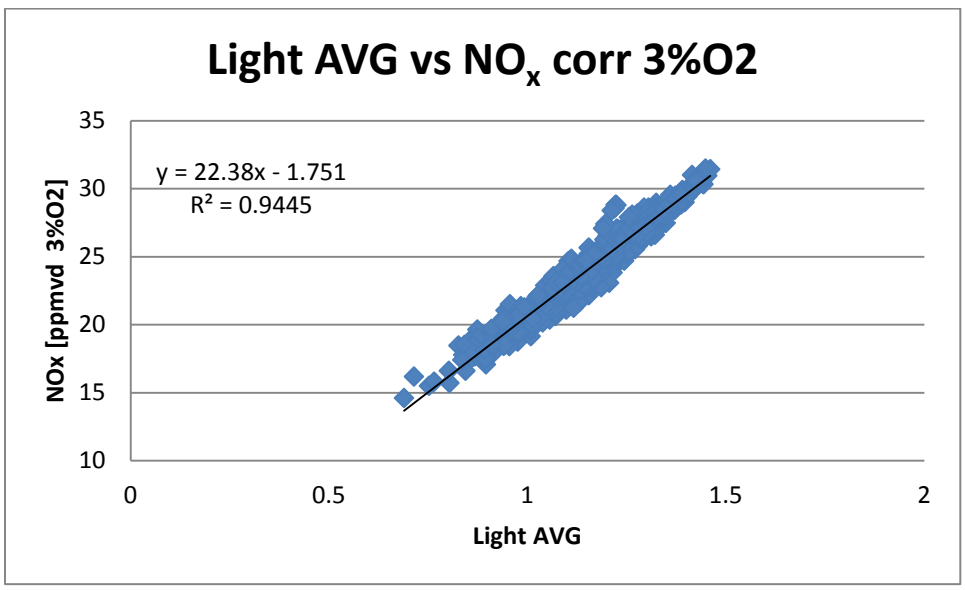

There are some hypotheses for the linearity between light intensity and NO_x. Thermal NO_x is assumed to be the primary contributor to the NO_x emissions due to the high adiabatic flame temperatures (AFT) for the given operating conditions. Figure 21 displays AFT verse NO_x for each fuel blend. It is apparent that the trend is not linear nor is it fuel blend independent. Therefore, there are other factors besides just flame temperature that are producing this linearity with light intensity of the flame. One such factor could be the change in species or radicals in the combustion zone when higher hydrocarbon fuels (such as propane) are added to

the blend. An increase in species that have pathways to produce NO_x could also be luminous reactions. Therefore, theoretically an increase in these species would increase both the NO_x and light intensity.

Figure 21: AFT vs NOx Corr 3%O2 (Blue: 100-0, Red: 95-5, Green: 92.5-7.5 NG-PG)

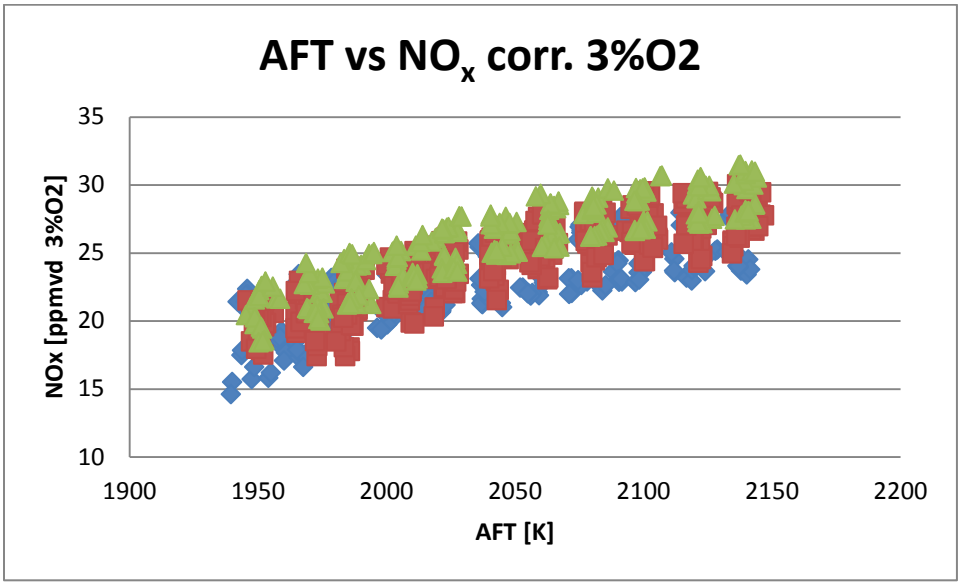

The second set of information the fiber optic probe can offer is the oscillations in the light intensity, also known as Light PkPk (Peak-to-Peak). By measuring the vertical distance between two readings in light intensity a quantifiable method of categorizing the stability of a flame becomes available. Figure 22 displays a plot of EA verse Light PkPk. As EA increases the Light PkPk readings also increase. At a Light PkPk value of approximately 0.3-0.35 the flame becomes noticeably oscillatory and highly unstable. Anything higher, and the flame starts to increase its likelihood of blowoff. Any flame below this oscillation threshold is a sign of a very stable flame and would be a desirable location to operate.

Figure 22: EA vs Light PkPk (Blue: 100-0, Red: 95-5, Green: 92.5-7.5 NG-PG)

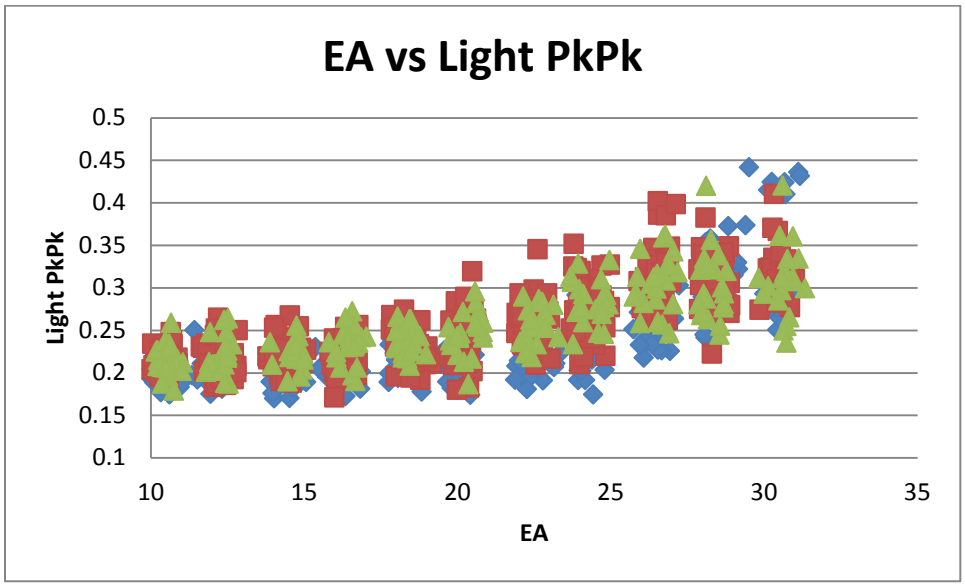

The last trend that will be covered is associated with the boiler efficiency of the system. Figure 23 shows EA verse boiler efficiency for the three fuel blends. Boiler efficiency decreases with increasing EA due to the lower flame temperatures associated with a leaner flame. This plot represents a few hurdles that must be overcome if this efficiency definition is to be used in the optimization algorithms. The first is the limited fluctuation between the highest efficiency and the lowest efficiency for a given fuel blend. There is approximately a 2 point difference in efficiency between these two extremes which indicates that the efficiency of the system, while affected by EA, does not significantly change for various FS-EA conditions. The second hurdle is the efficiency difference between each fuel blend for the same conditions. As more propane is added to the line the efficiency is decreased; however, this decrease might be due to several physical phenomenon and not due to fuel properties. For example, the flame length could fluctuate in size for different fuel flows at which point the distance between the cooling walls and the hottest portion of the flame would also fluctuate causing a disturbance in the heat transfer properties. In order to make these results general and not specific to this burner an efficiency based on the amount of air flowed through the system is a better alternative. In a commercial burner the energy required to pump air into the unit increases with increasing air flow and thus lowers the overall system efficiency.

Figure 23: EA vs Boiler Eff (Blue: 100-0, Red: 95-5, Green: 92.5-7.5 NG-PG)

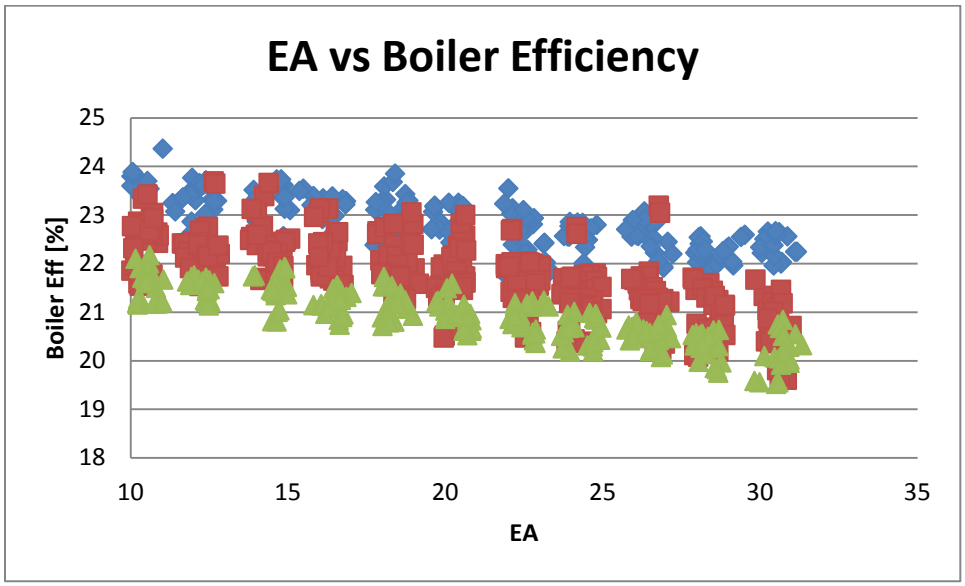

4.3.3 Performance Mapping

Having shown what happens to the performance maps when the fuel composition sensor is turned off, the next set of contours show what happens when the fuel composition sensor is turned on. Figure 24, Figure 25, and Figure 26 show the associated performance maps for the three different fuel blends. Each graph has on the horizontal EA (10 to 30) and on the vertical FS (-5 to 5). The contours on the left hand side display NO_x corrected to 3 percent O_2 while the contours on the right hand side display Light PkPk (aka stability). NO_x is cast between a range of 15-30 ppmvd while Light PkPk is cast by a range of 0.15-0.4. In both scenarios blue represents areas of good performance (low NO_x, high stability) and red represents areas of bad performance (high NO_x, low stability). White, as seen in the upper right hand corner of each graph, shows where the flames experienced blowoff.

Looking at the figures with propane in the line it is apparent that the burner can now meet the NO_x emission requirements for a range of FS/EA conditions. The same trends mentioned in the previous section can still be seen in the following graphs; however, now it is easier to see how NO_x and stability interact at the same conditions for a given fuel blend. Take for example the plots in Figure 24 for the 100-0 NG-PG case. Increasing EA and positive FS result in a low NO_x scenario, but at a cost of low stability. It would seem then that the optimal operating position is higher EA and negative FS to get both the added benefit of low NO_x and high stability; however, take into account that efficiency decreases with increasing EA and this region loses its appeal. The problem only worsens as propane is added to the line as seen in the remaining two figures. The NO_x graphs essentially shift towards the upper right hand corner while the Light PkPk graphs become more sporadic over a wider range of FS-EA conditions.

Figure 24: 100-0 NG-PG Performance Maps

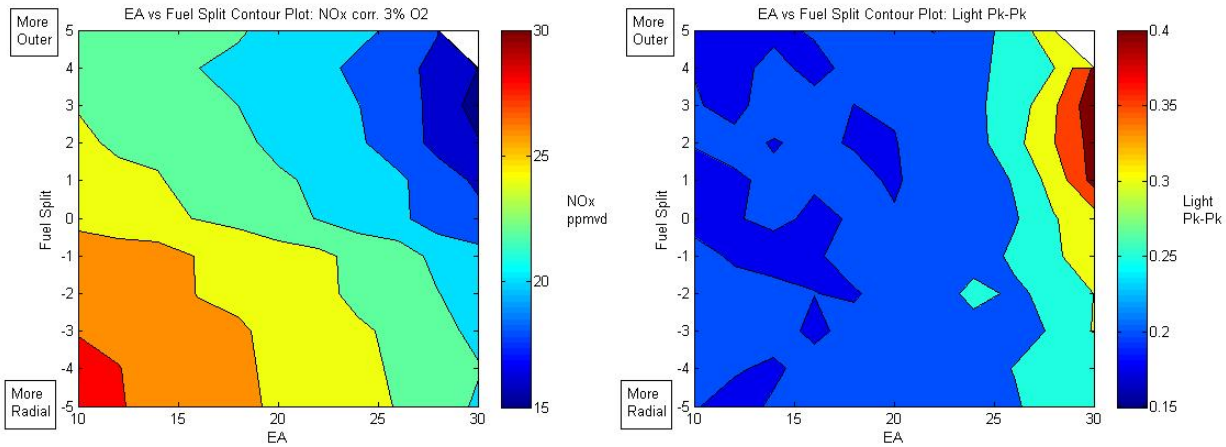

Figure 25: 95-5 NG-PG Performance Maps

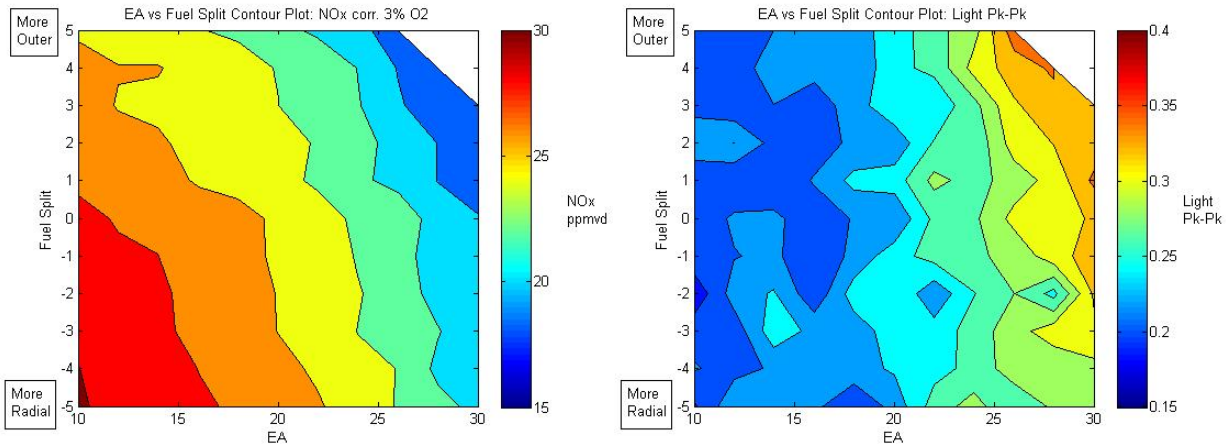

Figure 26: 92.5-7.5 NG-PG Performance Maps

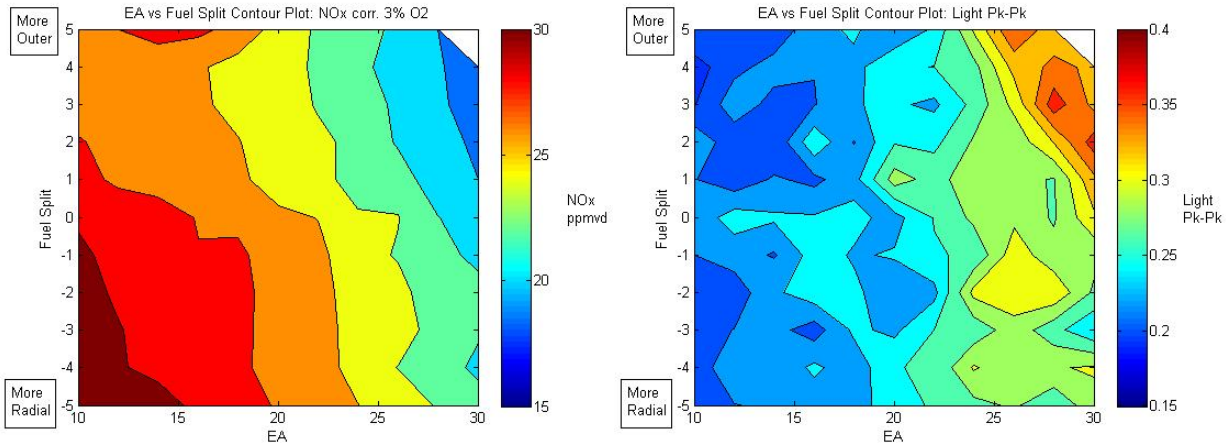

CHAPTER 5:
Closed Loop Control

5.1 Simulations

5.1.1 5th Order Approximations

After collecting data for NO_x and Light PkPk at various FS/EA and fuel cases, 5th order approximations of the results were generated to serve as the foundation for simulation experiments. The MATLAB code can be found in the Appendix section labeled Approx.m. Some of the accuracy of the data collected can be lost for data with seemingly random bits of noise with large order approximations, but for the purposes of this project the 5th order approximations gave smooth topologies and proved to be very valuable in the simulation process. Interpolation between experimental data points could have been used alternatively, but the plots proved to be very jagged. The approximation plots give the search algorithms the most ideal scenario to operate in and attempt to see if there are any fundamental differences in the algorithms before adding too much variation in the cost function topology from subtle physical disturbances. The 5th order approximations were generated by the following set of equations:

$$m = \#data\ points$$

$$Equation\ 17 : A = [EA\ EA^2\ EA^3\ EA^4\ EA^5\ FS\ FS^2\ FS^3\ FS^4\ FS^5] \qquad (m\ x\ 10)$$

$$Equation\ 18 : c = NO_x\ or\ LPkPk\ data\ @\ FS - EA\ conditions \qquad (m\ x\ 1)$$

$$Equation\ 19 : t = (A^T A)^{-1} A^T c \qquad (10\ x\ 1)$$

The t variable generated the unique coefficient terms used to estimate the NO_x and LPkPk values for each fuel case:

$$Equation\ 20 : A_i = \left[EA_i\ EA_i^2\ EA_i^3\ EA_i^4\ EA_i^5\ FS_i\ FS_i^2\ FS_i^3\ FS_i^4\ FS_i^5\right]$$

$$Equation\ 21 : NO_{x@FS_i,EA_i} = A_i t_{NO_x}$$

$$Equation\ 22 : LPkPk_{@FS_i,EA_i} = A_i t_{LPkPk}$$

5.1.2 Types of Simulations

There are four main types of simulated cases that each optimization search algorithm was tested on and they are referred to as follows: no composition fluctuations (NF), with composition fluctuations (WF), simulated noise no composition fluctuations (SNNF), and simulated noise with composition fluctuations (SNWF). A well-defined cost function based on the NO_x, LPkPk, and efficiency data for each fuel case was the foundation for each simulation scenario. The NF case initiates the search algorithm at a predetermined or random FS/EA condition for a single fuel composition and is allowed to search for the optimal operating condition. The WF case initiates the search algorithm at a predetermined or random FS/EA condition in one fuel type and is allowed to optimize. The optimal operating condition found in the first fuel type serves as the initial point for the next fuel type. This scenario simulates what happens when the burner has been operating at optimal conditions for a single fuel, but then undergoes a fuel change and

is allowed to search for the new optimum. The remaining two main cases, SNNF and SNWF, are the same scenarios as their NF and WF counterparts but with random noise in the data. These tests will determine how well the search algorithms can perform with noisy data signals which are ultimately a measure of the robustness of the algorithms. The simulated noise was generated based on the average signal noise found in the performance mapping data.

5.2 Cost Function

A cost function (F) is used in optimization algorithms to quantifiably compare one point verse another. Generally cost functions are designed in a way that the optimal condition is at the function's minimum (minimize cost of system). The goal is to weigh the parameters deemed important by the function designer through a set of specified equations. In this particular case the three parameters that are of importance are: NO_x (emissions), Light PkPk (stability), and EA (efficiency). In equation format the cost function can be constructed as:

$$Equation\ 23 F = w * f(NO_x) + w * f(LPkPk) + w * f(EA)$$

$$w = \frac{1}{3}\ (weighting\ coefficient)$$

The sub-functions for each parameter are as follows:

$$Equation\ 24 : f(NO_x) = \left(\frac{NO_x}{NO_{xlim}}\right)^2 + \frac{\exp\left(\frac{NO_x}{NO_{xlim}}\right)}{\exp(1)} - 1$$

$$Equation\ 25 : f(LPkPk) = \frac{LPkPk}{LPkPk_{lim}}$$

$$Equation\ 26 : f(EA) = sqrt\left(\frac{EA}{EA_{lim}}\right)$$

$$NO_{xlim} = 20\ ppmvd\ corr.\ 3\%O_2\ (regulation\ standard)$$

$$LPkPk_{lim} = 0.3\ (low\ LPkPk = stable, high\ LPkPk = unstable)$$
$$EA_{lim} = 30\ (manufacturer\ specifications)$$

There are no predetermined equations that are required to be used when defining a cost function; however, there are general guidelines that can make computing optimization algorithms easier. The main feature of a cost function is it should be continuous in order to allow smooth topology of the cost function contour for multiple inputs. Functions can contain piecewise continuous equations for a given parameter, but that increases the amount of logic required for the algorithm to compute.

The above sub-functions rely on a ratio of the current parameter reading divided by that parameter's allowable maximum limit. This was used as a way to measure how close a parameter is to reaching its allowable limit. In other words, it answers the question "how close is the parameter to being not acceptable"? By design each sub-function when the parameter ratio equals to unity so does the value of the sub-function. A ratio below unity will have a cost of less than unity while a ratio above unity will have a cost above unity. In this way it is easy to

determine which of the parameters is being met and which are not. Figure 27 plots the sub-functions with the parameter ratios plotted on the horizontal axis and the function values on the vertical axis. Note the curvatures and slopes for each line.

Figure 27: Cost Function: Sub-Functions

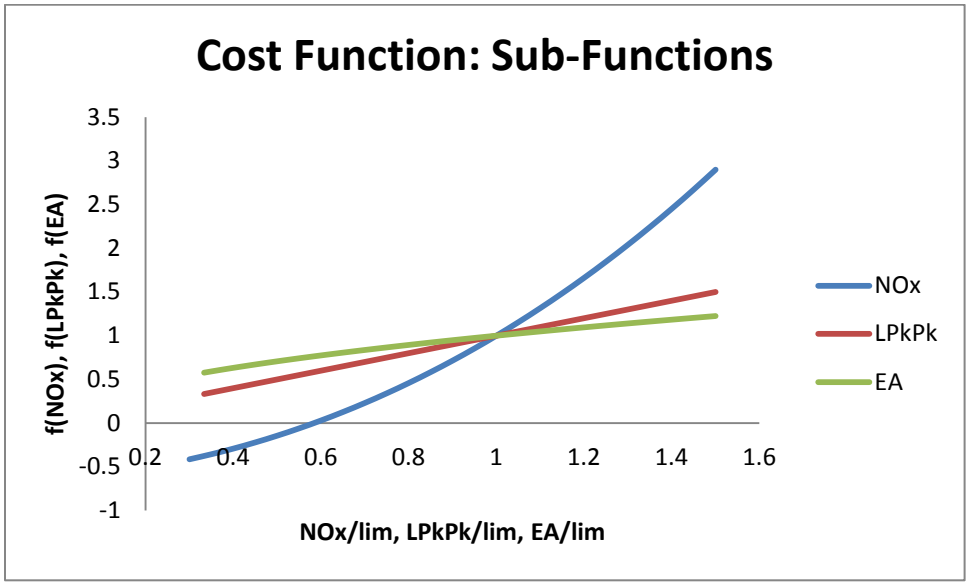

The NO_x sub-function has two main parts: the square term and the exponential term (includes the minus 1). The reasoning behind this choice is in the rewards and penalties wanting to enact. When the NO_x is below 20ppmvd the cost function will greatly reward the point; however, if the NO_x is above the limit then it will greatly penalize the point. The exponential function is one of the fastest smooth rising functions. For this reason when the NO_x ratio is above the unity threshold the cost sub-function increases drastically which quickly penalizes any slight deviations above unity. The square term was to further the intensity/magnitude of the exponential term. The sensitivity to the reward/penalty system can be adjusted by multiplying a constant in front of the exponential term. In this way it increases or decreases the severity of the reward/penalty system. The Light PkPk term is dictated only by the parameter ratio. The sensitivity for this parameter can be increased by increasing the exponent term (ex: to a square or cube exponent).Raising the Light PkPk term to the first power was determined to be adequate through repeated tests using the experimental data gathered. The EA term was selected to be a square-root in order to minimize the effect of this parameter. The efficiency of the system was determined to be less valuable to maintain compared to the emissions and stability of the flame. For this reason the efficiency cost sub-function was desired to have a small impact on the overall cost function for medium and large fluctuations in EA. The EA term is a measure of efficiency and a high efficiency means the parameter ratio is low which is desirable. To lower the sensitivity of the cost function to the efficiency term, the exponent was selected to be a fraction. In this way large changes in EA result in small changes in the cost function.

5.3 5th Order Approximation

Using the data collected in the previous section a 5th order approximation of the NO_x and Light PkPk graphs were generated. Figure 28, Figure 29, and Figure 30 show the approximations of both parameters (NO_x on left and Light PkPk on right) for the three fuel blends. The NO_x approximation contours resemble to that of the experimental data quite satisfactorily across the entire FS/EA map; however, the conditions where each fuel blend has experienced blowoff has not been accounted for in the approximation maps. The approximation maps are meant to be models of the system to best predict how the search algorithms might respond under real conditions, but these approximations do have errors. For example, the approximation Light PkPk contours are clearly smoother than the actual Light PkPk contours. Many of the sporadic peaks that are characteristic of the actual data are lost in the approximation. This creates errors when trying to model blowoff. Since blowoff is most commonly preceded by high oscillations in flame luminosity the ability of the search algorithm to accurately predict blowoff becomes unreliable in this simulated environment. The results generated by the search algorithms should only serve as guides as to predicting the performance under real conditions and what the optimal operating conditions might be.

Figure 28: 100-0 NG-PG Approximation Maps

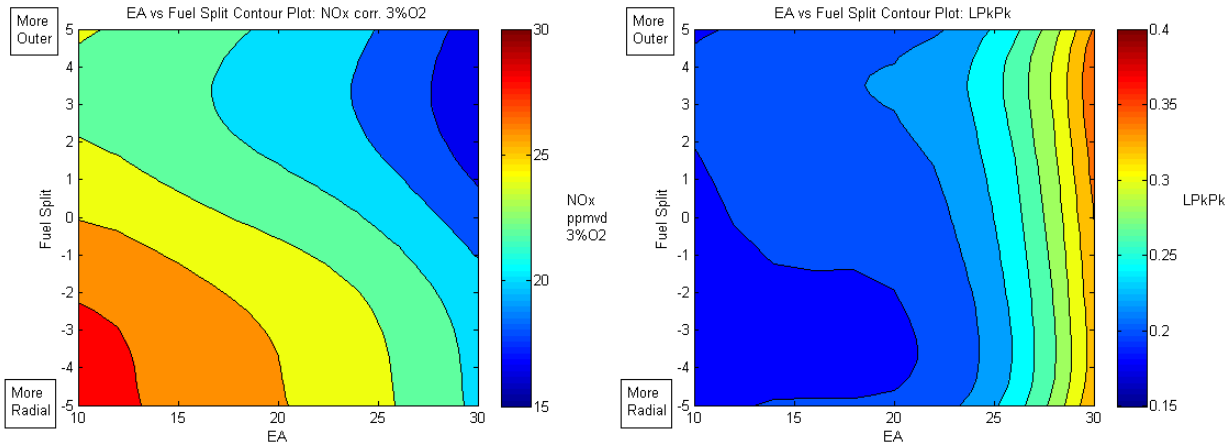

Figure 29: 95-5 NG-PG Approximation Maps

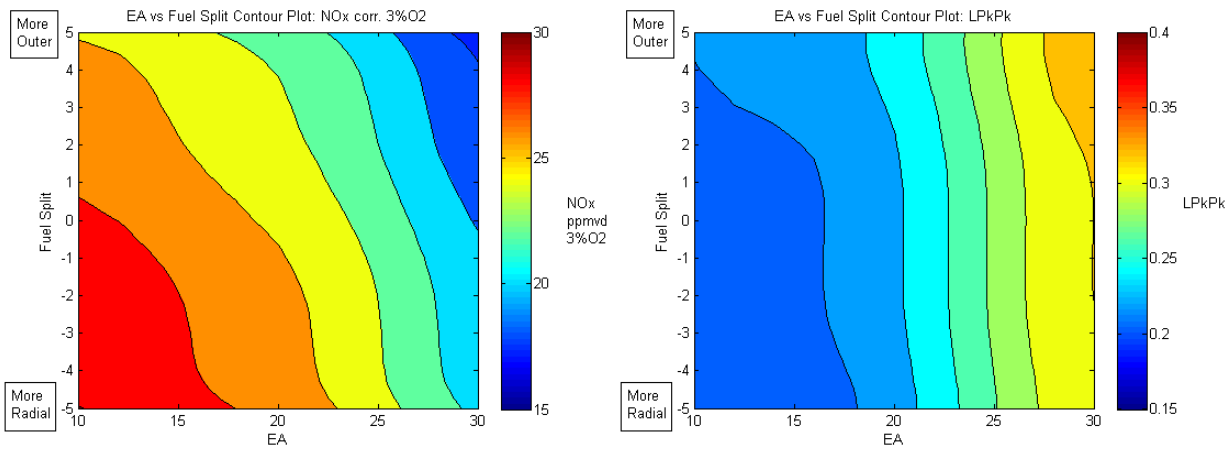

Figure 30: 92.5-7.5 NG-PG Approximation Maps

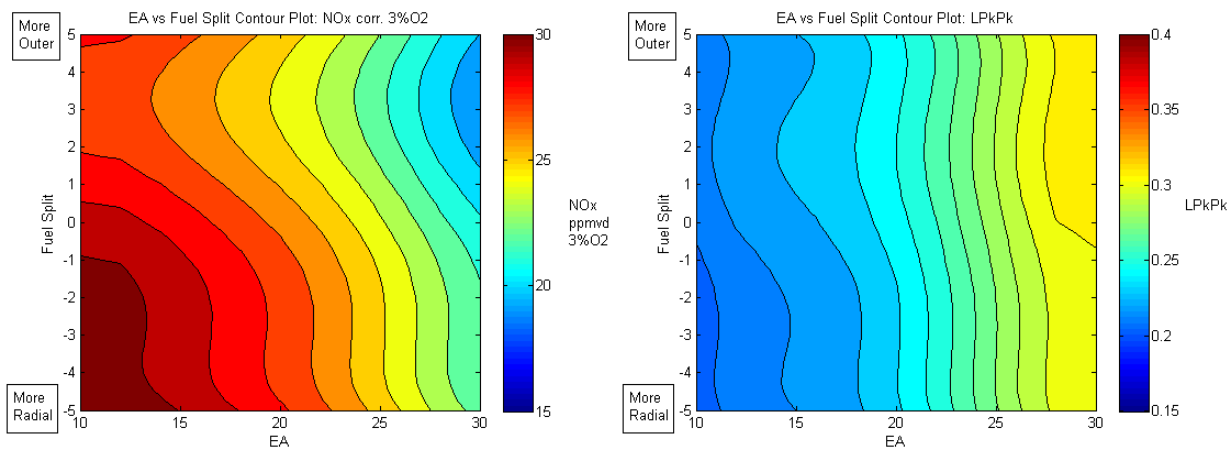

5.4 Cost Function Maps

Now that the 5th order approximation maps have been generated for the three fuel blends it is now possible to define the corresponding cost function maps. Figure 31, Figure 32, and Figure 33 are the cost function maps for the three fuel blends. These contours were generated using the 5th order approximation results developed in the previous section and the cost function equation defined in Chapter 5. Using the colorbar legend for the graphs, areas of dark blue are high performance locations (desirable, low cost) and areas of red are low performance locations (undesirable, high cost). Each contour has a single peak of high performance which is essential for the search algorithms to work reliably. However, it should be noted for the 92.5-7.5 NG-PG case (Figure 33) there is a distinct ridge along an EA of 12 that separates two regions of lower function values. This region could trap a search algorithm into never converging to the true global minimum.

Figure 31: 100-0 NG-PG Cost Function Map

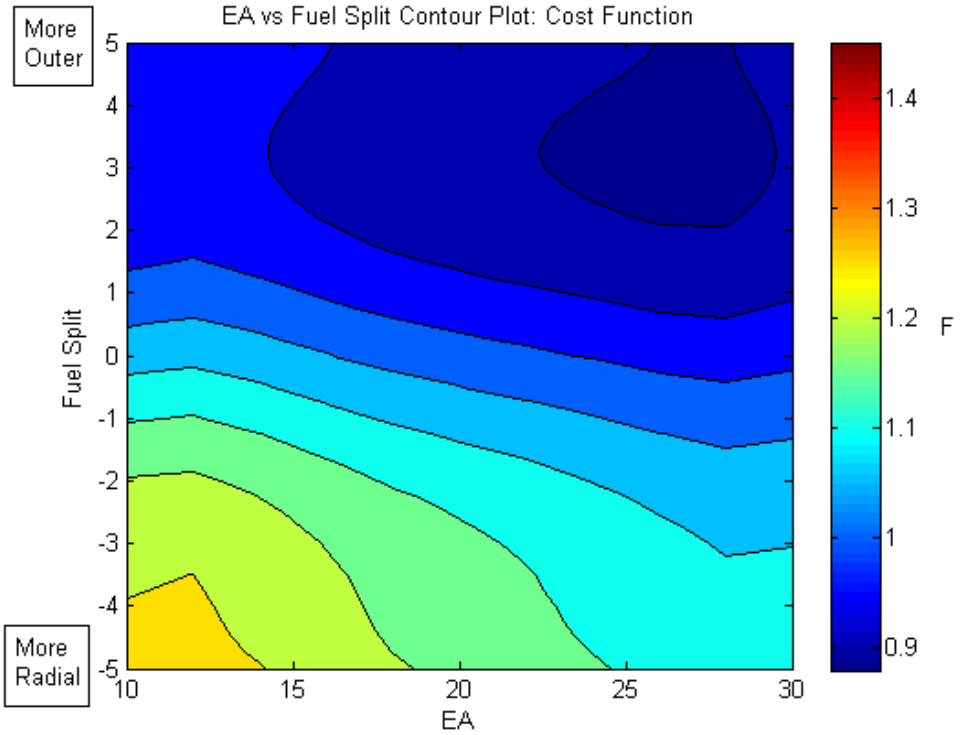

Figure 32: 95-5 NG-PG Cost Function Map

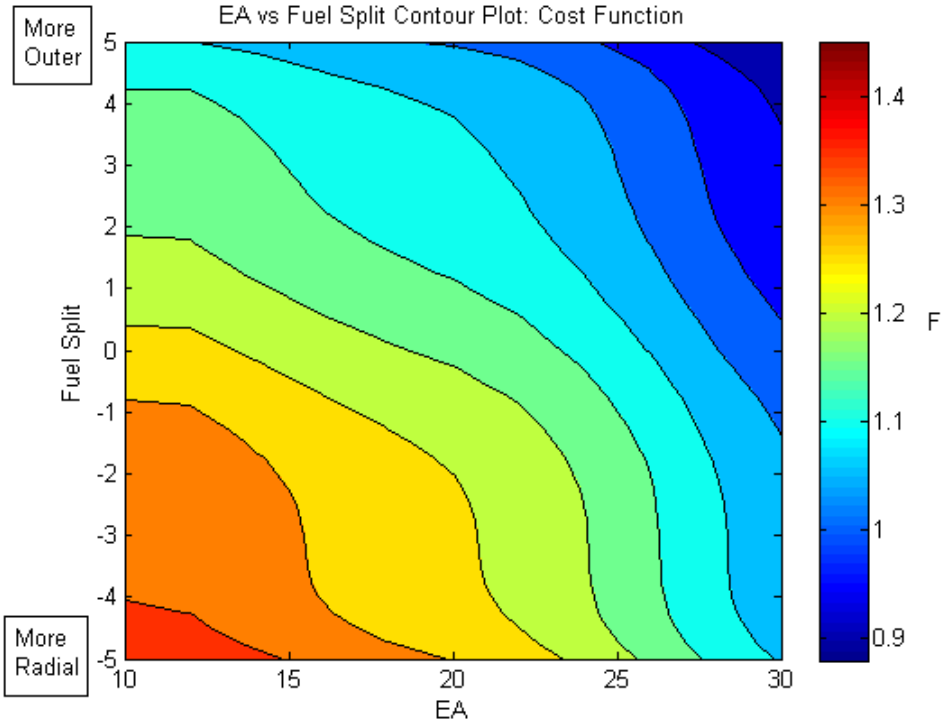

Figure 33: 92.5-7.5 NG-PG Cost Function Map

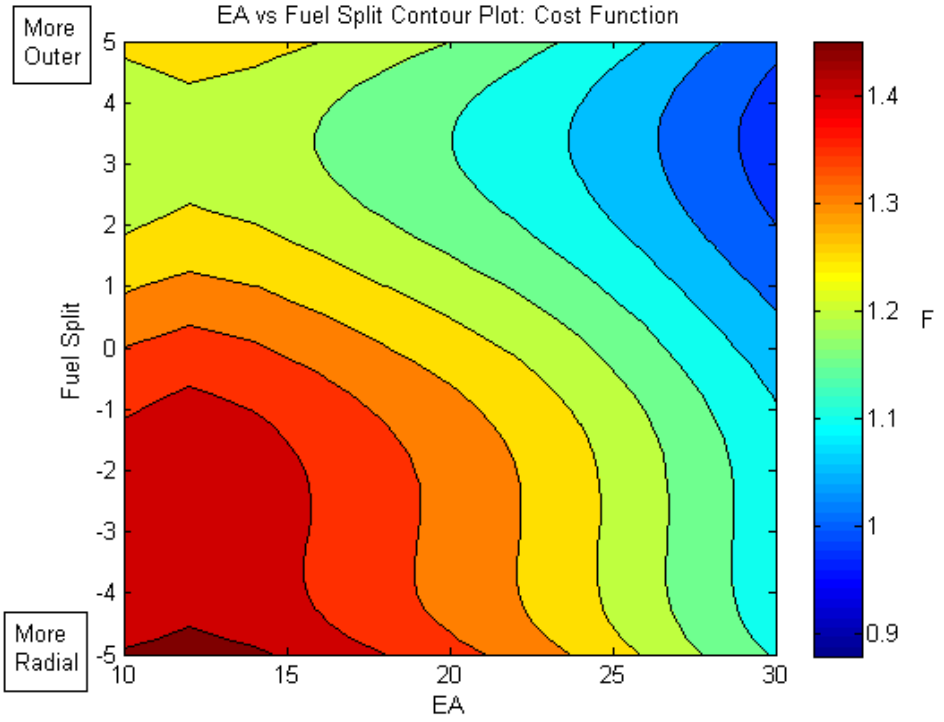

5.5 Simulation Results

5.5.1 No Fluctuations (NF)

5.5.1.1 PDS NF Results

The following results are for Powell's Direction-Set (PDS) method as outlined in Chapter 2 and using a hill-climbing subroutine to find the minimum along a direction-set line. The MATLAB code can be found in the Appendix section. The step sizes in the FS/EA directions are set at 0.5 and 1 respectively. The tolerance for convergence has been set at 0.0005.

The first sets of graphs (Figure 34, Figure 35, and Figure 36) depict the PDS algorithm for a set FS/EA condition at -2/14 for the three fuel blends. For each fuel blend there are three associated graphs: cost function (middle top), NO_x (bottom left) and Light PkPk (bottom right). The pink lines/stars represent the first full iteration of the PDS algorithm. The light blue line/stars are the remaining iterations and the final optimal value. It took 76 function computations for the PDS algorithm to converge on the global minimum for the 100-0 NG-PG case and 50 function computations for the remaining two fuel cases to converge. Recall that function computations represent when the algorithm would actively measure data if this were a real test. Therefore, the more function computations an algorithm must take the longer it will take for the algorithm to converge. For example, if it took a minute to move to the next set point and measure data then the first case would take 76 minutes to converge. If regulation emission measurements occur every 15 minutes then this long time scale could be problematic for the goal of lowering emissions.

Figure 34: PDS NF Results: 100-0 NG-PG, FS/EA of -2/14

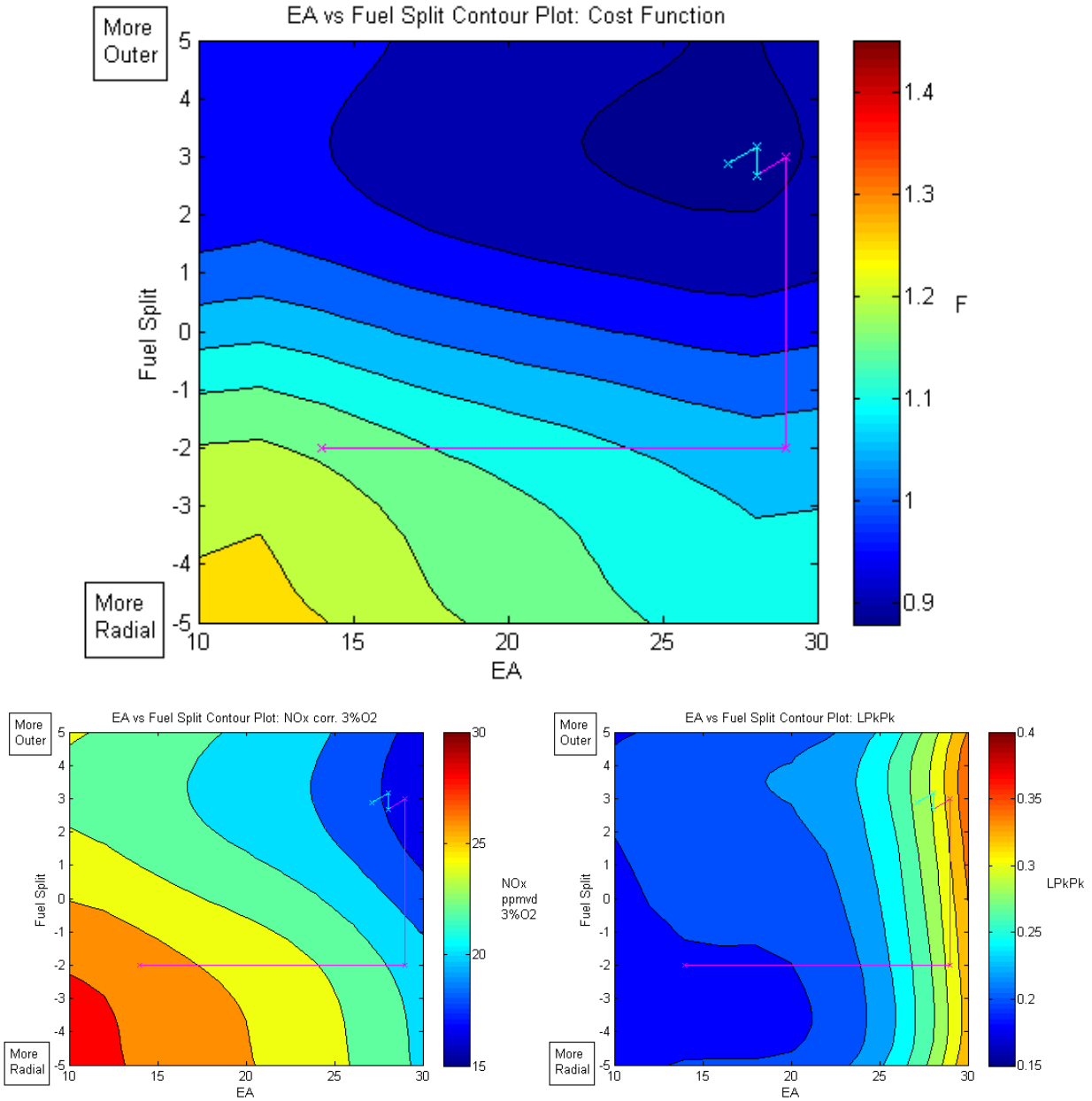

Figure 35: PDS NF Results: 95-5 NG-PG, FS/EA of -2/14

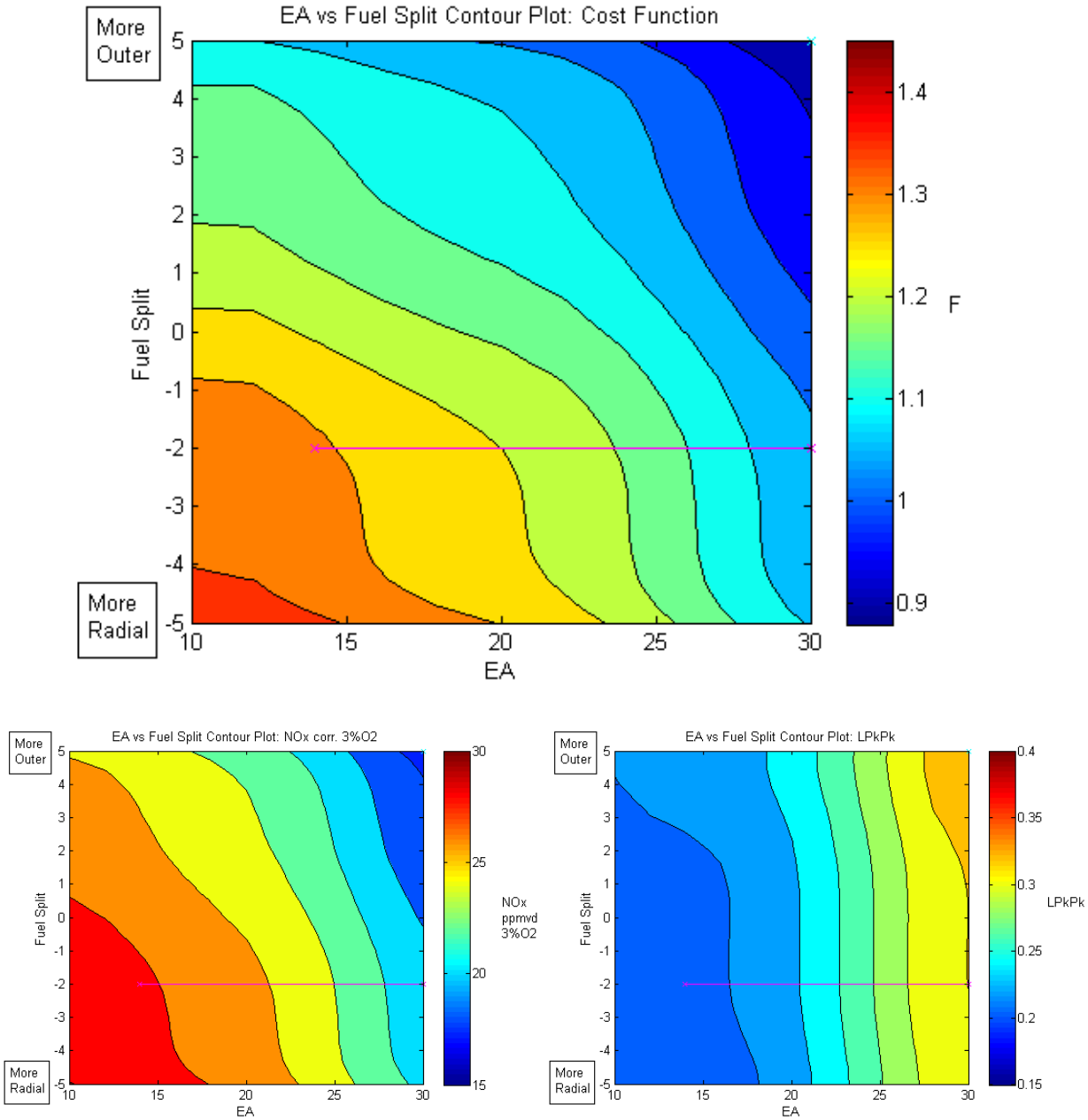

Figure 36: PDS NF Results: 92.5-7.5 NG-PG, FS/EA of -2/14

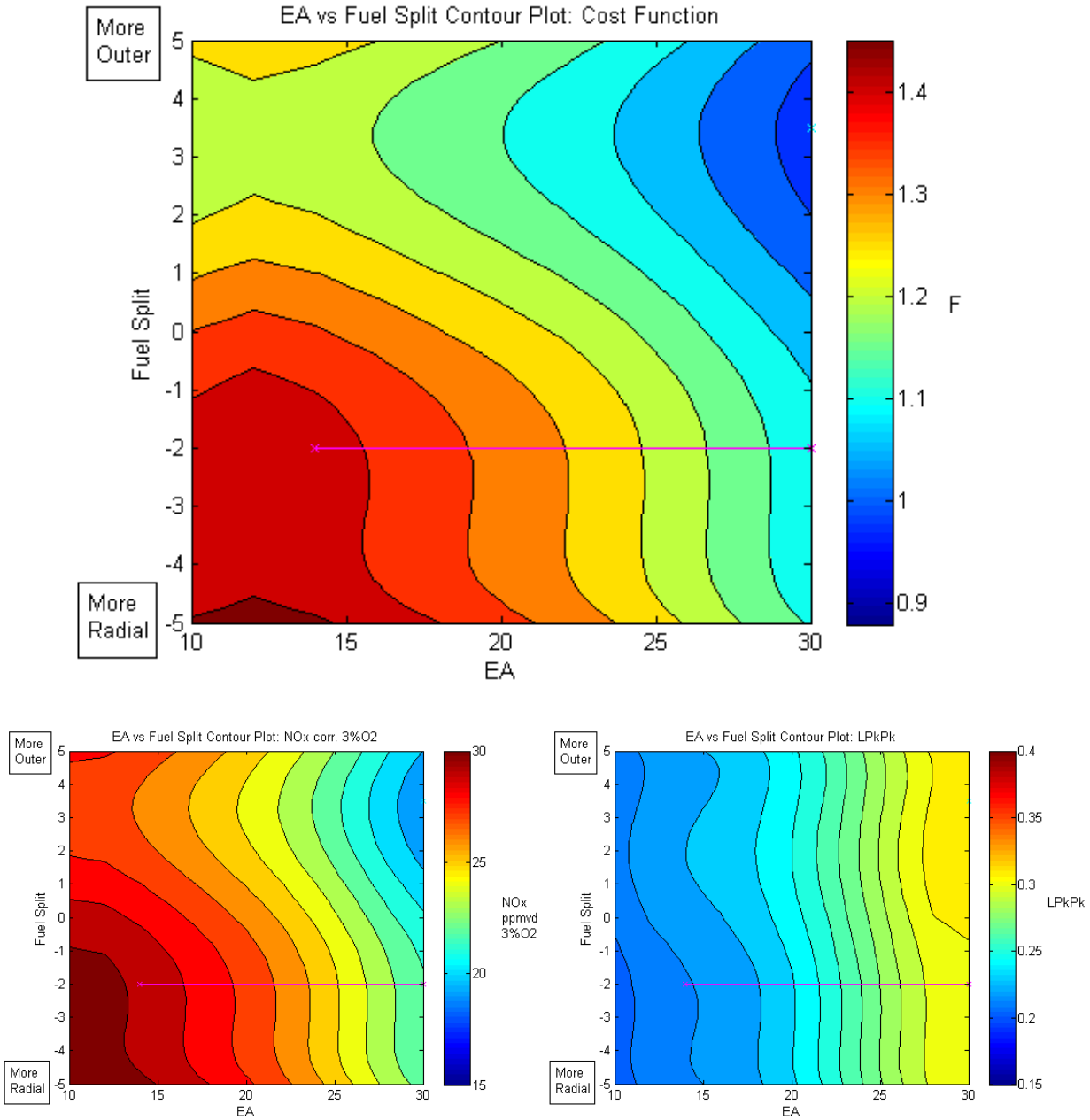

Now that a single FS/EA condition for all three blends has been examined it is time to examine the entire FS/EA map. The PDS algorithm was fed 441 initial positions that ranged in FS from -5 to 5 in increments of 0.5 and in EA from 10 to 30 in increments of 1. Table 4 summarizes the results for this approach. The parameter N is the number of function computations taken from the initial point to the final optimal value. FS Final and EA Final are the FS/EA final optimal operating conditions. F is the final function value at the optimal FS/EA condition. %F_global is a parameter that measures the percent error between the final converged F and the global F for the given fuel case. NO_x is the converged optimal NO_x value in ppmvd corrected to 3 percent O_2. The %NO_x Fail parameter is the percentage of how many initial conditions (441 total) did not converge to an acceptable NO_x value (that is, values above 20 ppmvd).

Table 4: PDS NF Results

NG	N	FS Final	EA Final	F	%F_global	NOx	%NOx Fail	
100	50.72	3.06	26.42	0.89	0.68	18.43	6.58	average
	44.00	3.00	27.06	0.89	0.09	18.37	-	median
95	39.09	5.00	29.05	0.92	1.02	17.63	4.76	average
	39.00	5.00	30.00	0.91	0.00	17.23	-	median
92.5	36.66	1.83	28.10	1.03	5.84	20.69	31.07	average
	37.00	3.50	30.00	0.98	0.00	19.22	-	median

From these results it shows that on average the PDS algorithm takes 35 to 50 function computations to converge to the global minimum for these cost function maps. The PDS algorithm fails to converge to acceptable levels of NO_x for approximately 5 percent of the FS/EA map for the 100 and 95 NG cases; however, it has a more difficult time with the 92.5 NG case and fails on 31 percent of the initial conditions. This large failure rate for the 92.5 NG case is due to the divide in low value regions as discussed earlier. Most of the failures occur for initial conditions on the left side of the ridge (the side opposite of the global minimum). It can then be concluded that initial conditions should be selected carefully. Initial conditions that are far away from the global minimum could potentially experience larger number of function computations and less reliable convergence results.

5.5.1.2 DHS NF Results

This section is concerned with displaying the results found for the Downhill Simplex (DHS) algorithm as outlined in Chapter 2. The MATLAB code can be found in the Appendix section. The tolerance for convergence has been set at 0.0005. Five parameters must be established for the DHS algorithm: the size of the initial simplex (positions of two vertices), reflection coefficient (alpha), expansion coefficient (gamma), and contraction coefficient (beta). After selecting an initial point the two remaining vertices are selected by completing the corners of a 90 degree triangle. Using the initial point as the base, point two is selected by going in the EA direction either to the right or left of the initial point depending on boundary restraints. The third point is selected by going in the FS direction either up or down of the initial point depending on boundary constraints. These two parameters are labeled as EAs and FSs, respectively. The remaining three coefficients have already been described in Chapter 2. All five

parameters start from an initial first guess of the correct values. From several iterations of tweaking these five parameters and comparing the results an optimal set of values can be determined. After several iterations the parameter selection was found to be: EAs = 4, FSs = 2.5, alpha = 1.5, beta = 0.4, and gamma = 1.65.

Using these gains Figure 37, Figure 38, and Figure 39 were generated for a steady FS/EA of -2/14. The initial simplex is shown by black X's. The pink line/stars show the route take by the centroid of the simplex to the convergence point. As done previously for the PDS NF contours there are three graphs per figure: cost function (top middle), NO_x (left bottom), and Light PkPk (right bottom).

Figure 37: DHS NF Results: 100-0 NG-PG, FS/EA of -2/14

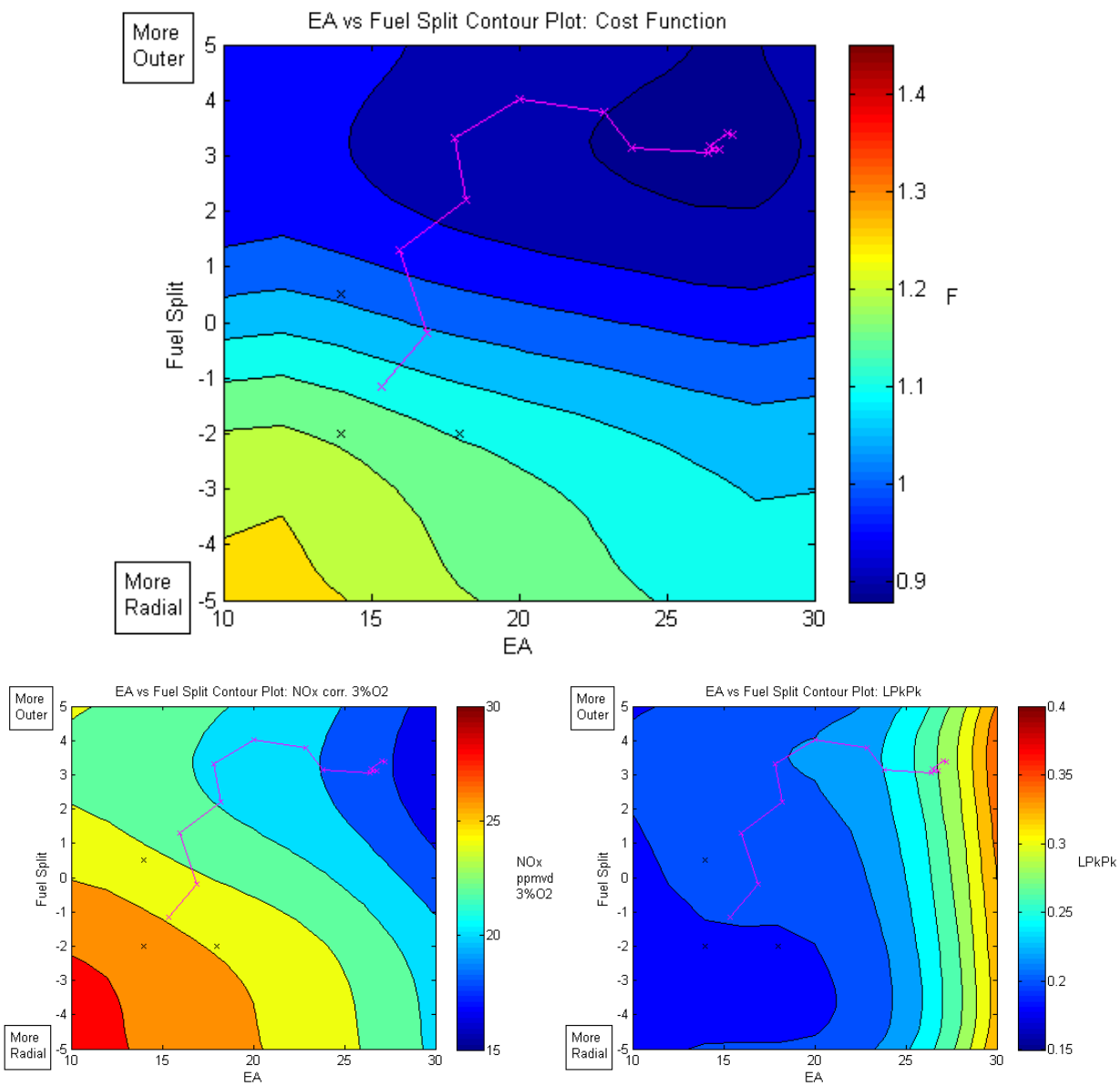

Figure 38: DHS NF Results: 95-5 NG-PG, FS/EA of -2/14

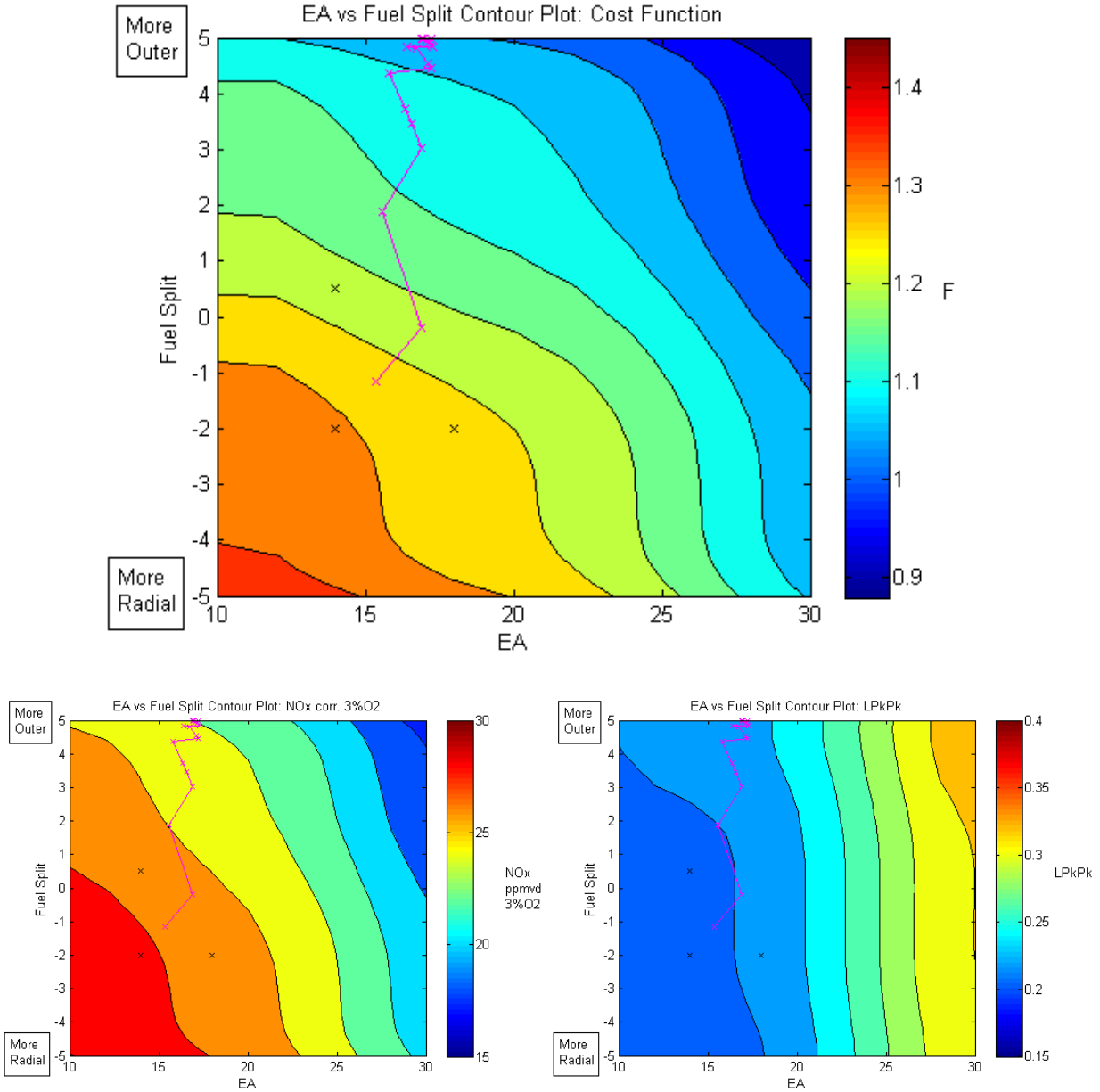

Figure 39: DHS NF Results: 92.5-7.5 NG-PG, FS/EA of -2/14

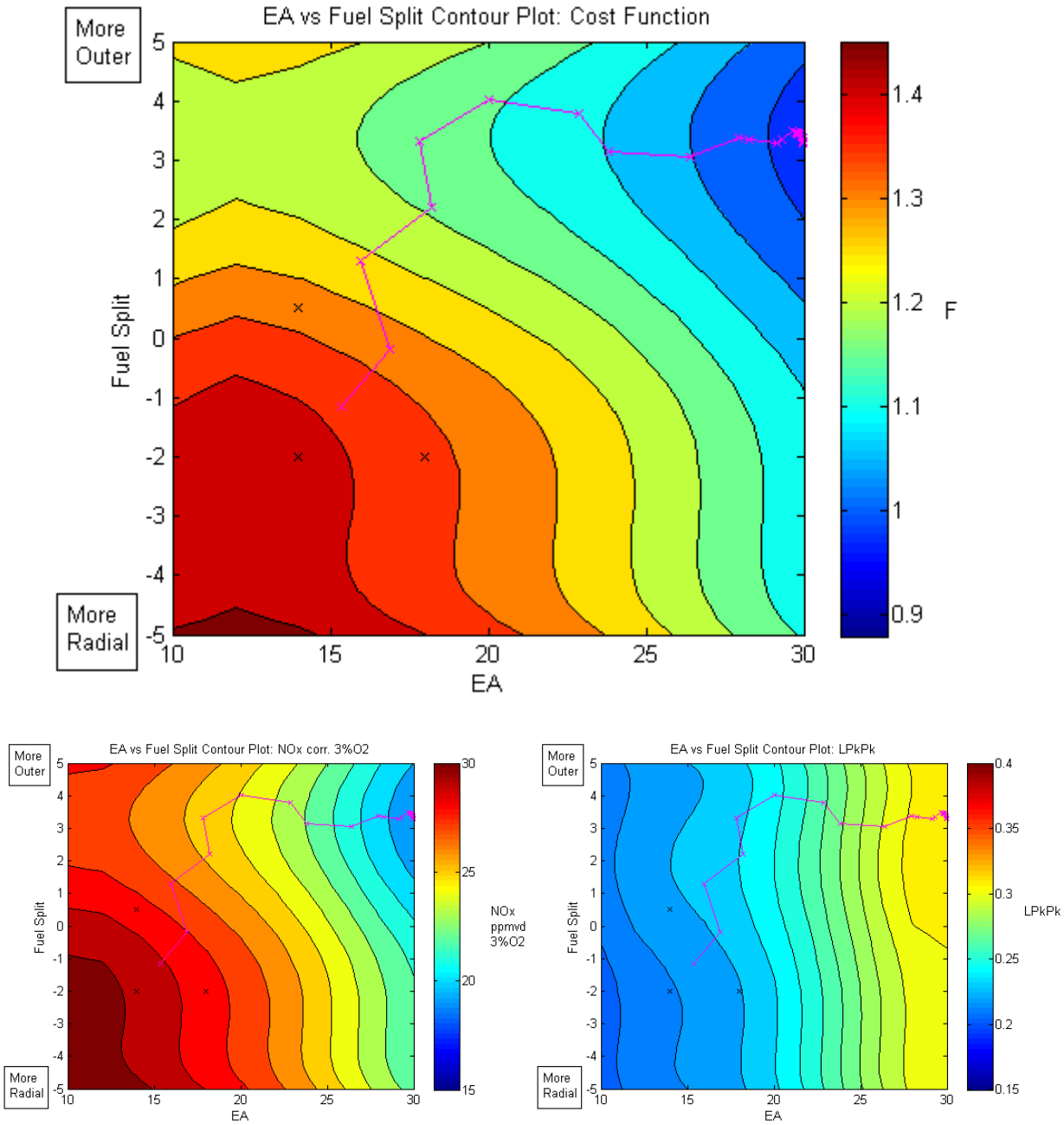

Continuing from a single FS/EA point the rest of the FS/EA map was allowed to undergo the DHS algorithm and the results are summarized in Table 5. The headings/parameters in Table 5 are the same as for Table 4 already presented for PDS NF results. The number of function computations is on average 18 to 40 computations which is reasonable for a 15 minute emission regulation time scale. However, this limited number of computations produces a higher percentage of final convergence cases failing to meet the NO_x requirement.

Table 5: DHS NF Results

NG	N	FS Final	EA Final	F	%F_global	NOx	%NOx Fail	
100	18.93	3.20	25.83	0.89	0.72	18.85	10.88	average
	18.00	3.19	26.91	0.89	0.10	18.45		median
95	38.40	4.55	27.95	0.95	4.38	18.61	19.73	average
	39.00	4.98	29.67	0.92	1.08	17.53		median
92.5	34.58	2.54	28.32	1.02	4.21	20.33	22.22	average
	34.00	3.37	29.97	0.98	0.10	19.23		median

tol	0.0005	alpha	1.5
EAs	4	beta	0.4
FSs	2.5	gamma	1.65

5.5.1.3 PDS vs. DHS NF Results

The following conclusions are based off of the results from Table 4 and Table 5. The DHS algorithm does extremely well in function computations for the 100 NG case, but both algorithms reach the same value of N for the remaining two fuel cases. Both algorithms reached relatively the same final FS/EA, F, and NO_x values on an average calculation. However, the PDS algorithm performed much better in finding operating conditions that meet the NO_x requirements (92.5 NG case excluded). The NF results suggest that PDS has a slight advantage over DHS, but differences are small.

5.5.2 With Fluctuations (WF)

5.5.2.1 PDS WF Results

Recall the WF simulations are meant to simulate what happens when the search algorithms are allowed to converge to an optimal value for one fuel blend and then are switched to a new fuel blend. The final FS/EA conditions (median values) in Table 4 serve as the initial conditions for each scenario in this section. Table 6 summarizes the results for the three cases. The first block assumes that the 100 NG case was first allowed to converge to its optimal operating condition (FS/EA = 3/27) and then experiences either a 95 NG or 92.5 NG fluctuation. The second and third blocks in the table are the cases for the 95 and 92.5 NG cases respectively. As it can be seen the number of function computations (N) has decreased from the average NF scenario by approximately 20 to 30 percent. However, the number of function computations still puts the convergence time at a little over 30 minutes using a one minute sample time estimation. It should be noted that the PDS algorithm is able to still find the global minimum even for fluctuating fuel conditions.

Table 6: PDS WF Results

NG	N	FS Initial	EA Initial	FS Final	EA Final	F	%F_global	NOx
100	-	-	-	-	-	-	-	-
95	27	3	27	5	30	0.91	0.00	17.23
92.5	28	3	27	4	30	0.98	0.00	19.22
100	35	5	30	3	27	0.89	0.09	18.41
95	-	-	-	-	-	-	-	-
92.5	28	5	30	3.5	30	0.98	0.00	19.22
100	33	3.5	30	3	27	0.89	0.09	18.41
95	23	3.5	30	5	30	0.91	0.00	17.23
92.5	-	-	-	-	-	-	-	-

5.5.2.2 DHS WF Results

For the WF simulations the same tolerance, simplex size, and coefficients as established in the DHS NF section were used. The median values for the final FS/EA points for each fuel blend from Table 5 were used for the initial points for these simulations. Table 7 summarizes the results for the three subcases (100 NG steady, 95 NG steady, and 92.5 NG steady). Except for the 100 NG steady block the number of function computations has decreased significantly compared to the average values from Table 5. The other important conclusion to make is the DHS algorithm is able to find the same previously found optimal FS/EA condition for each fuel regardless of which switching scenario is running.

Table 7: DHS WF Results

NG	N	FS Initial	EA Initial	FS Final	EA Final	F	%F_global	NOx
100	-	-	-	-	-	-	-	-
95	41	3.00	27.00	4.99	29.63	0.91	0.60	17.40
92.5	34	3.00	27.00	3.63	30.00	0.98	0.06	19.23
100	7	5.00	29.50	3.08	28.03	0.89	0.04	17.79
95	-	-	-	-	-	-	-	-
92.5	22	5.00	29.50	3.11	29.87	0.98	0.34	19.27
100	10	3.00	30.00	3.71	27.05	0.89	0.04	18.39
95	35	3.00	30.00	4.99	29.84	0.91	0.31	17.31
92.5	-	-	-	-	-	-	-	-

tol	0.0005	alpha	1.5
EAs	4	beta	0.4
FSs	2.5	gamma	1.65

5.5.2.3 PDS vs. DHS WF Results

The following conclusions are based on the results from Table 6 and Table 7. Both the PDS and DHS algorithms performed well in WF simulation scenarios; however, the DHS algorithm found the optimal conditions with fewer function computations. The overall error from the global minimum is significantly lower than the wide map searches for both algorithms.

5.5.3 Simulated Noise with No Fluctuations (SNNF)

5.5.3.1 PDS SNNF Results

This section is responsible for demonstrating what happens to the search algorithms when small fluctuations occur in the sensor readings. These random fluctuations occurred for the three parameters in the cost function equation: NO_x, Light PkPk, and EA. The 5th order approximation was used to generate the baseline NO_x and Light PkPk values. From there the NO_x was allowed to vary ±0.2, Light PkPk was allowed to vary ±0.02, and EA was allowed to vary ±0.2. These values were calculated to be the average sensor reading fluctuations as found in the experimental data. Two key parameters were also altered to adjust to sensor noise. The step sizes in the FS/EA directions were changed to 0.5/1.5. The tolerance was decreased to 0.005. Both of these parameters were adjusted in order to lower the amount of unnecessary function computations.

For comparison with the NF simulations Figure 40, Figure 41, and Figure 42 were generated at the same FS/EA condition as before (-2/14) for the three fuel blends. Clearly more directions are followed in the simulated noise case than the no noise case and no run of the same initial condition is the same due to the random fluctuations in sensor readings. To show this 441 runs were conducted for each fuel blend at the same initial FS/EA condition (-2/14) and the results can be found in Table 8.

Table 8: PDS SNNF for FS/EA of -2/14

NG	N	FS Final	EA Final	F	%F_global	NOx	%NOx Fail	
100	133.00	3.50	24.60	0.90	2.10	19.46	34.69	average
	105.00	3.51	25.70	0.90	1.60	19.23	-	median
95	120.63	4.22	28.63	0.95	4.89	18.50	11.11	average
	101.00	4.70	29.50	0.93	2.94	17.85	-	median
92.5	136.14	3.14	29.02	1.01	3.36	19.94	14.97	average
	118.00	3.40	29.89	0.99	1.54	19.45	-	median

Figure 40: PDS SNNF Results: 100-0 NG-PG, FS/EA of -2/14

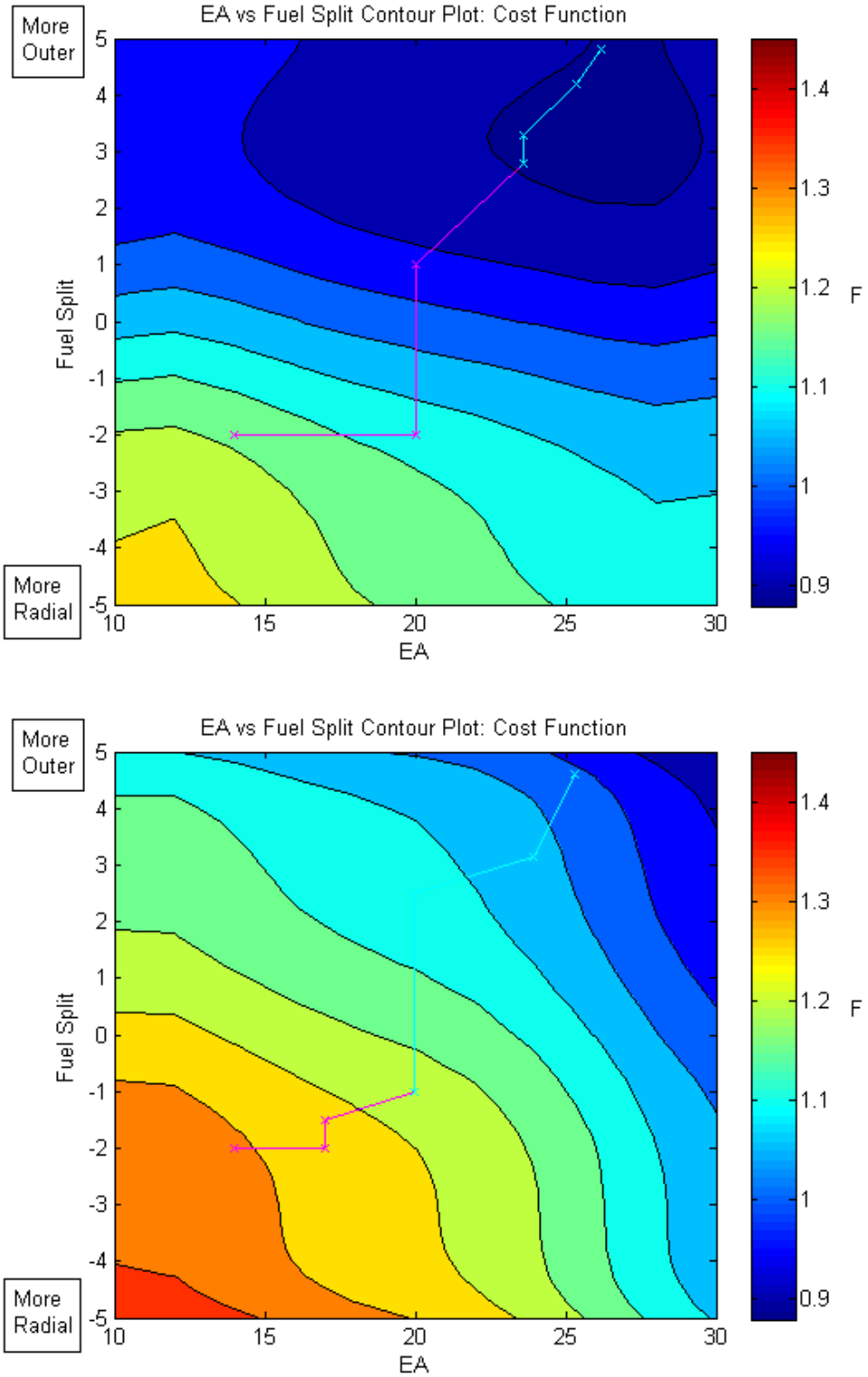

Figure 42: PDS SNNF Results: 92.5-7.5 NG-PG, FS/EA of -2/14

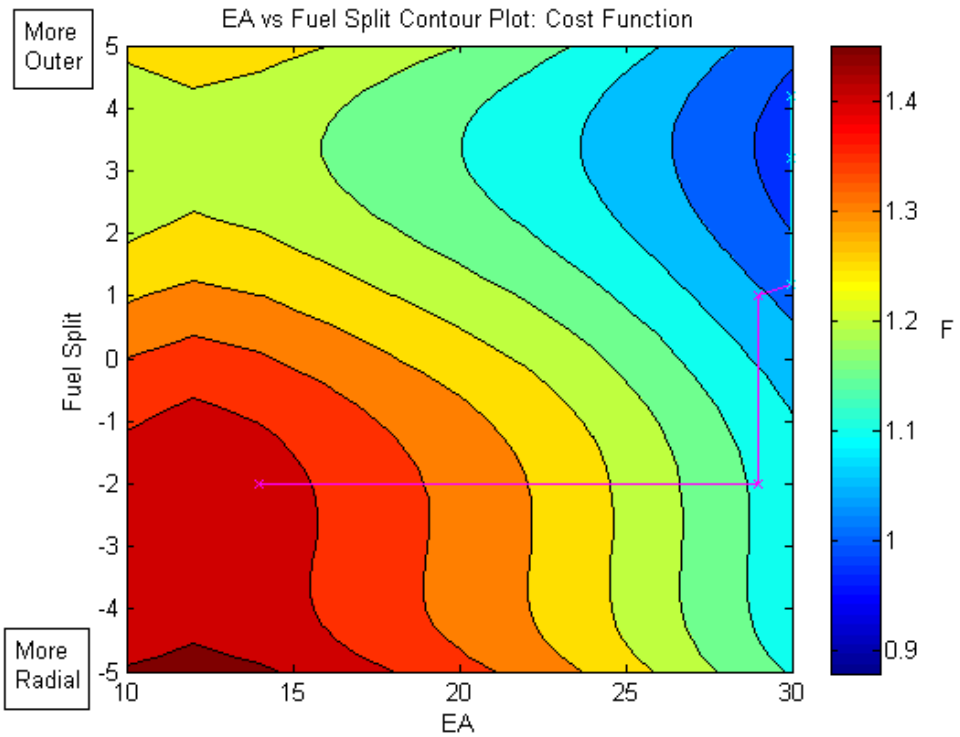

Referring to the data found in Table 8 there are some interesting results to be seen. The first is the number of function computations (N) has increased dramatically; approximately 2.5 to 3 times more than the NF counterpart. This increase can be sourced to the increased number of times the hill-climbing subroutine is called. This subroutine is a costly way to search along a line. The other interesting result is the percentage of runs that did not meet acceptable NO_x levels. The NO_x fail rate percentage was 35 percent, 11 percent, and 15 percent for the 100, 95, and 92.5 NG cases respectively. The 11 and 15 percentages, while not ideal, are more acceptable than the 35 percent for the 100 NG case. This means that approximately one in three runs of the PDS algorithm will not converge to an acceptable optimal value.

The next table of results was generated over the entire FS/EA map as done previously for the NF scenario. The only thing done differently was to run this entire map search process three times for each blend in order to account for the random nature of the simulated noise scenario. Table 9 shows the performance characteristics of the PDS with simulated noise. As seen with Table 8 the average number of function computations (N) has increased drastically (approximately 2 to 2.5 times greater). The NO_x Fail percentage has stayed about the same for each fuel blend.

Table 9: PDS SNNF Results

NG	N	FS Final	EA Final	F	%F_global	NOx	%NOx Fail	
100	122.62	3.32	25.39	0.90	2.47	19.21	27.74	average
	94.00	3.45	26.41	0.90	1.63	18.90	-	median
95	106.09	4.36	28.94	0.94	3.85	18.17	9.22	average
	88.67	4.95	29.50	0.92	2.05	17.65	-	median
92.5	123.54	3.01	28.89	1.01	3.55	20.00	15.19	average
	100.67	3.43	29.50	0.99	1.68	19.53	-	median

5.5.3.2 DHS SNNF Results

The same fluctuations in NO_x, Light PkPk, and EA as expressed in the previous SNNF section for the PDS algorithm occur in this section as well. The tolerance for convergence has been relaxed to 0.005 in order to reach faster convergence times. Initially the same simplex size and coefficients as established in the previous two sections for the DHS algorithm were used in this set of simulations; however, as it will be shown shortly adjustments had to be made in the simplex size to decrease the amount of error and NO_x Fail percentage in the results.

Three example runs of the DHS SNNF simulations were recorded for the three different fuel blends and presented in the following three figures (Figure 43, Figure 44, and Figure 45). These simulations were conducted at the same FS/EA of -2/14 as done in the previous example contours. Visually the paths taken by the DHS algorithm in the SNNF cases resemble very closely to the paths taken in the NF cases. For this reason 441 runs for each fuel blend were computed at the FS/EA of -2/14 and the results are presented in Table 10.

Figure 43: DHS SNNF Results: 100-0 NG-PG, FS/EA of -2/14

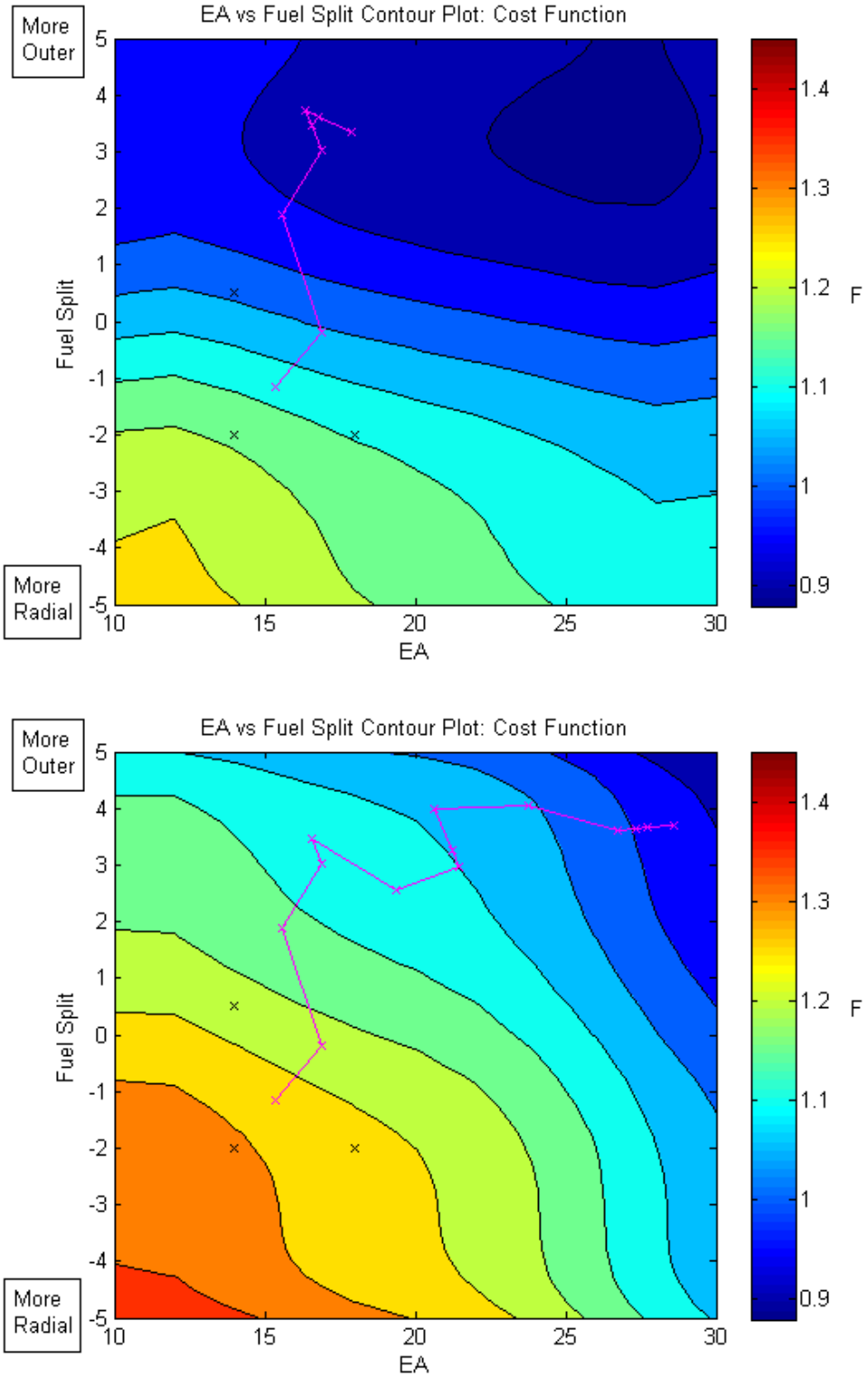

Figure 45: DHS SNNF Results: 92.5-7.5 NG-PG, FS/EA of -2/14

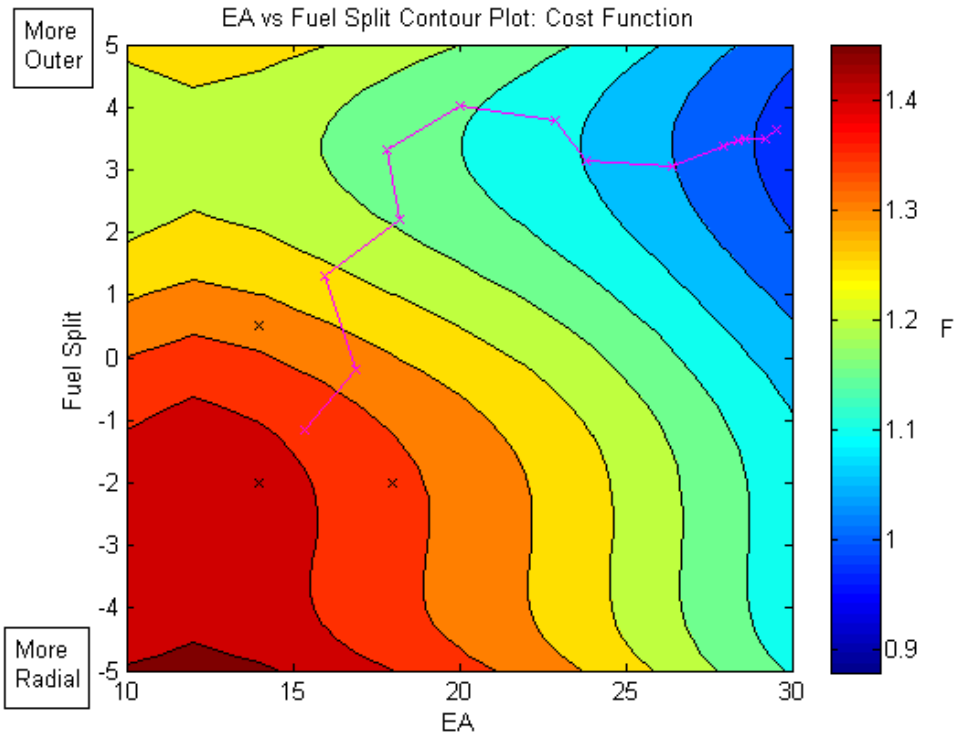

Table 10: DHS SNNF for FS/EA of -2/14

NG	N	FS Final	EA Final	F	%F_global	NOx	%NOx Fail	
100	17.07	2.76	17.89	0.93	5.12	21.97	94.10	average
	14.00	2.91	17.94	0.92	3.90	21.87	-	median
95	20.78	3.64	18.74	1.09	19.89	23.94	88.66	average
	18.00	4.17	17.85	1.10	20.87	24.57	-	median
92.5	22.64	3.17	23.93	1.09	11.24	22.60	58.96	average
	20.00	3.27	26.12	1.07	9.33	21.84	-	median

tol	0.005	alpha	1.5
EAs	4	beta	0.4
FSs	2.5	gamma	1.65

As it can be seen in the above table the failure rate of finding an acceptable operating condition in terms of NOx has spiked significantly. At first the coefficients (alpha, beta, and gamma) were adjusted to see if these values would give different results, but these attempts did not significantly improve the situation. Therefore the initial simplex size was expanded in order to mitigate the effects of converging too quickly in an initially high cost region. As a comparison

Table 11 and Table 12 were generated for the entire FS/EA map with the simplex size being the only difference. By increasing the simplex size the NOx Fail percentage has decreased by almost half in value while the number of function computations has stayed approximately the same. This means that while the simplex is initially larger it is still able to converge to a final answer in the same amount of iterations. Another important result is in the final FS/EA location of the larger simplex case. Comparing these final locations in Table 12 with the final locations found in Table 5 it is seen that they are almost identical. This confirms the DHS algorithm can still perform in a noisy environment albeit with some error.

Table 11: DHS SNNF Results Version 1

NG	N	FS Final	EA Final	F	%F_global	NOx	%NOx Fail	
100	15.43	2.90	22.06	0.91	3.47	20.51	58.88	average
	12.67	3.06	22.80	0.90	1.88	20.54	-	median
95	20.91	3.07	24.61	1.02	12.70	21.17	51.55	average
	19.00	4.27	28.39	1.01	11.09	20.28	-	median
92.5	20.26	2.03	26.02	1.07	9.69	21.86	54.12	average
	18.00	3.04	29.15	1.02	3.85	20.22	-	median

tol	0.005	alpha	1.5
EAs	4	beta	0.4
FSs	2.5	gamma	1.65

Table 12: DHS SNNF Results Version 2

NG	N	FS Final	EA Final	F	%F_global	NOx	%NOx Fail	
100	15.97	3.05	24.55	0.90	2.16	19.60	35.45	average
	13.33	3.14	25.41	0.89	1.31	19.41	-	median
95	23.78	3.30	27.77	0.98	7.72	19.47	26.30	average
	22.67	4.25	29.15	0.96	5.39	18.72	-	median
92.5	22.54	2.23	28.56	1.02	5.12	20.50	35.30	average
	20.33	3.08	29.41	0.99	1.77	19.75	-	median

tol	0.005	alpha	1.5
EAs	7	beta	0.4
FSs	3	gamma	1.65

5.5.3.3 PDS vs. DHS SNNF Results

The conclusions made here are from the results found in Table 9 and Table 12. There are two key differences between the PDS and DHS algorithms: number of function computations and the NO_x Fail percentage. The PDS algorithm takes on the order of 90 to 120 function computations, but has on average less than 25 percent failure rate in terms of NO_x. The DHS

algorithm takes on the order of 20 function computations, but at a much higher NO_x failure rate (~25 to 35 percent). Note here that the DHS algorithm also experienced some difficulty in transferring from the NF to SNNF case. The simplex size had to be corrected in order to reduce failures. The PDS algorithm for the most part was ready to go with only a minor change in the step size in the EA direction. Therefore, the PDS algorithm seems to be more flexible in dealing with alterations in sensor noise measurements.

5.5.4 Simulated Noise With Fluctuations (SNWF)

5.5.4.1 PDS SNWF Results

The final sets of simulations involve simulated noise while transitioning from an optimal position in one fuel blend to the next optimal position for another fuel blend. The same sensor noise fluctuations occur in this simulation as the previous section and the final median FS/EA positions from Table 9 are used for the initial conditions in this section. Table 13 is a summary of the results for the three different steady fuel transition cases. For each transition case, the fuel blends being transitioned to are able to converge to the previously obtained optimal EA/FS conditions as found in the SNNF scenario. Except for the 100NG case in the 92.5 steady block, the number of function computations has decreased by almost a factor of 2. This shows the closer an initial point is to the final optimal value the shorter time it will take the PDS algorithm to converge.

Table 13: PDS SNWF Results

NG	N	FS Initial	EA Initial	FS Final	EA Final	F	%F_global	NOx
100	-	-	-	-	-	-	-	-
95	50.33	3.50	26.00	4.95	29.33	0.93	2.61	17.78
92.5	42.00	3.50	26.00	3.56	29.33	0.99	2.46	19.58
100	83.33	5.00	29.50	3.81	28.29	0.90	1.06	17.81
95	-	-	-	-	-	-	-	-
92.5	59.33	5.00	29.50	3.45	29.17	1.01	2.80	19.79
100	146.67	3.50	29.50	2.79	28.48	0.89	1.49	17.60
95	53.00	3.50	29.50	5.00	29.33	0.91	1.24	17.43
92.5	-	-	-	-	-	-	-	-

5.5.4.2 DHS SNWF Results

This section follows the same conditions as outlined in the previous SNWF section for the PDS algorithm. The simplex size and coefficients have remained the same. The median final FS/EA results from Table 12 are used here as the initial conditions for the different cases. Table 14 summarizes the results for these sets of simulations. The number of function computations has decreased but not by a significant amount. The main result here is that the DHS algorithm is able to adapt to fluctuating fuel environments and find the optimal FS/EA conditions as previously found in the SNNF scenario.

Table 14: DHS SNWF Results

NG	N	FS Initial	EA Initial	FS Final	EA Final	F	%F_global	NOx
100	-	-	-	-	-	-	-	-
95	19.67	3.00	26.00	3.71	28.81	0.95	5.01	18.83
92.5	22.33	3.00	26.00	2.59	29.42	0.98	1.73	19.59
100	12.33	4.50	29.00	3.02	26.72	0.88	1.10	18.63
95	-	-	-	-	-	-	-	-
92.5	15.67	4.50	29.00	3.48	29.02	1.00	2.11	19.96
100	17.00	3.00	29.50	3.28	26.16	0.88	1.17	18.88
95	24.00	3.00	29.50	4.06	29.85	0.94	3.24	17.96
92.5	-	-	-	-	-	-	-	-

tol	0.005	alpha	1.5
EAs	7	beta	0.4
FSs	3	gamma	1.65

5.5.4.3 PDS vs. DHS SNWF Results

The clear winner for this simulation scenario is the DHS algorithm. It was able to converge to an acceptable optimal condition in half the number of function computations than the PDS algorithm. The NO_x failure rate behavior essentially matched the cases without noise, with PDS failing about 25 percent of the time and DHS ~30 percent. What this result suggests is the DHS algorithm could be best used in scenarios where the burner is already operating at the optimal FS/EA condition but then is subject to some type of change (that is, fuel blend fluctuation). Both algorithms are able to find the optimal operating condition, but what is the deciding factor between the two is the time it takes to converge.

CHAPTER 6:
Validation of Fuel Interchange Parameters

The current project developed extensive data associated with fuel compositional impacts on emissions. Under a separate Energy Commission project (Contract CEC 500-08-034), predictive tools for assessing the impact of fuel composition on burner performance were developed and validated under limited conditions. With data obtained for the present effort, it was of interest to see if the tools developed under Contract 500-08-034 could successfully predict the emissions performance of the present burner system as a function of fuel composition.

6.1 Computational fluid dynamics (CFD)

The Computational Fluid Dynamics (CFD)/Chemical Reactor Network (CRN) methodology for predicting how fuel composition impacts emissions requires information about the overall flowfield in order to divide the system into discrete reactors. To guide the division, photographs of the flame or detailed measurements can be used. But generally speaking, this type of information is usually not available. As a result, this information is derived from a CFD simulation. This would be the general approach as applied to any particular burner. All that is required is sufficient information about the geometry of the system that it can sufficiently represented by a mesh of discrete elements.

In the present case, a three dimenstional CFD simulation was conducted using a commercial solver, ANSYS. Figure 46 (a) shows the geometry of simulation domain. To reduce computational cost, only a quarter of the burner is considered. The two planes of symmetry were set as periodic boundary. Tetrahedral mesh was applied for the model, as it is shown in Figure 46 (b).

Figure 46 Geometry and Meshes of the CFD simulation.

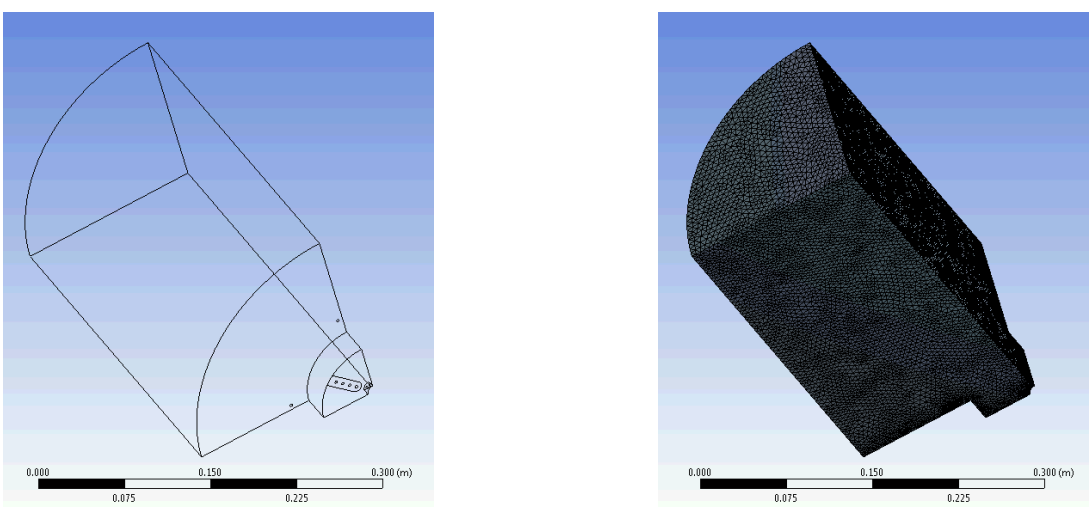

(a) (b)

Two cases with identical EA and FS were selected as a representative scenario for the CFD modeling. Table 15 summarizes the input conditions. The NG case represents the condition with pure methane, whereas the PG case includes 7.5 percent propane. The goal is to see if the CFD/CRN methodology correctly predicts how the additional of propane impacts the NO_x emissions levels. For both cases, the k-e model with standard wall function was used as turbulence model. As for turbulence-chemistry interaction, the eddy dissipation model and probability density function (PDF) method were compared.

Table 15 Summary of the Simulated Conditions

	CH_4 [%]	C_3H_8 [%]	EA	Fuel split
NG case	100	0	21.92	5.01
PG case	92.5	7.5	20.60	5.14

Figure 47 Comparison of Simulated Results of NG Case Using 1) Eddy-Dissipation Model and 2) PDF Model

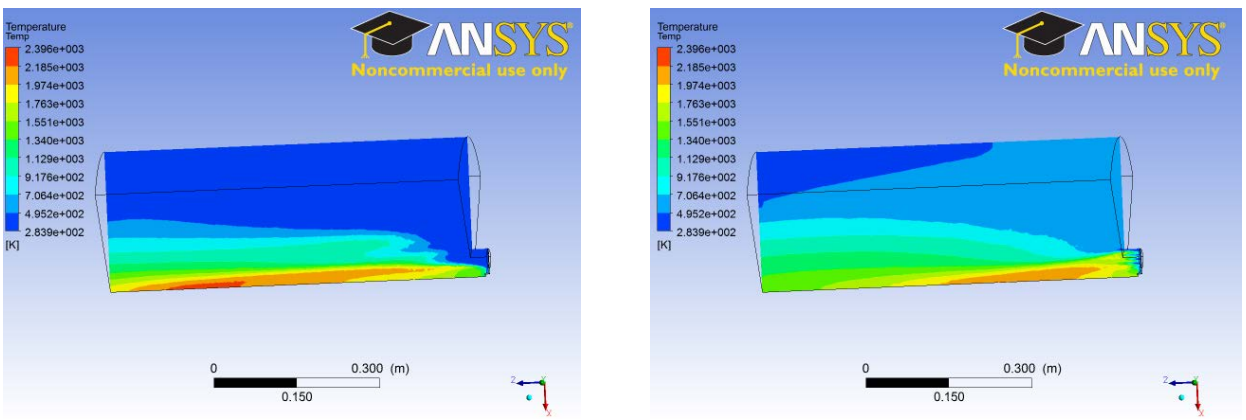

Eddy-Dissipation (b) PDF

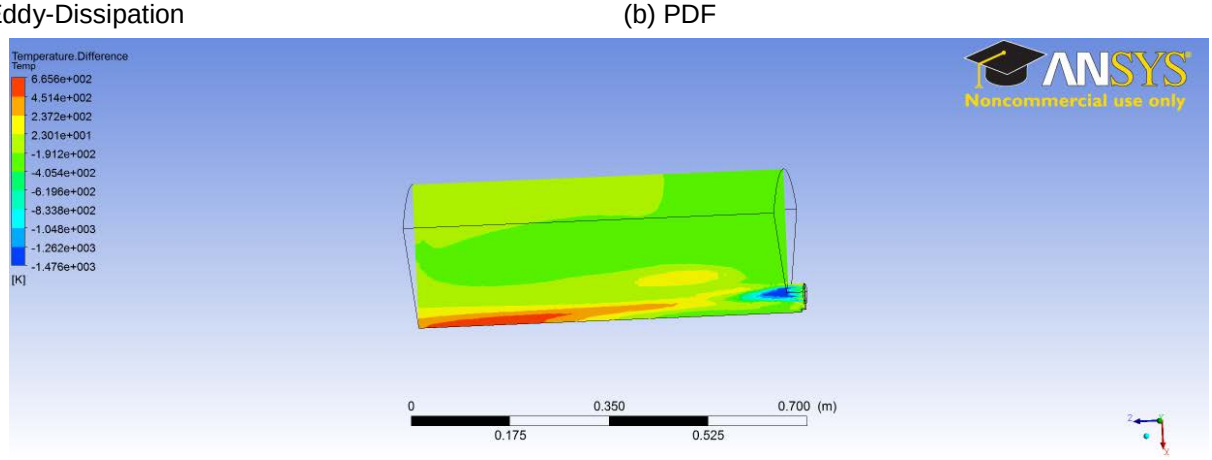

(c) Temperature difference between Eddy-Dissipation and PDF results

Figure 47 presents the comparison of temperature distribution simulated using Eddy-Dissipation and PDF models. The high temperature region is shorter with the PDF model, which is more consistent with the observed flame. Therefore, the PDF model is used for estimating the reaction spatial distribution.

Figure 48 shows a comparison between temperature distributions of NG and PG cases using the PDF model. Figure 48c present results for the difference in temperature at each position for the two fuels. It can be seen that the temperature in the outer flame in PG case is greater than that for the NG case. The temperature difference is around 200 degrees Kelvin (°K), which is large enough to impact the NO_x formation rate. Even without the decomposition of the flowfield into a collection of smaller reactors, this result qualitatively explains the reason why NO_x emission of PG cases is larger than that of NG cases.

Figure 48 Comparison of temperature distribution in PG and NG flames

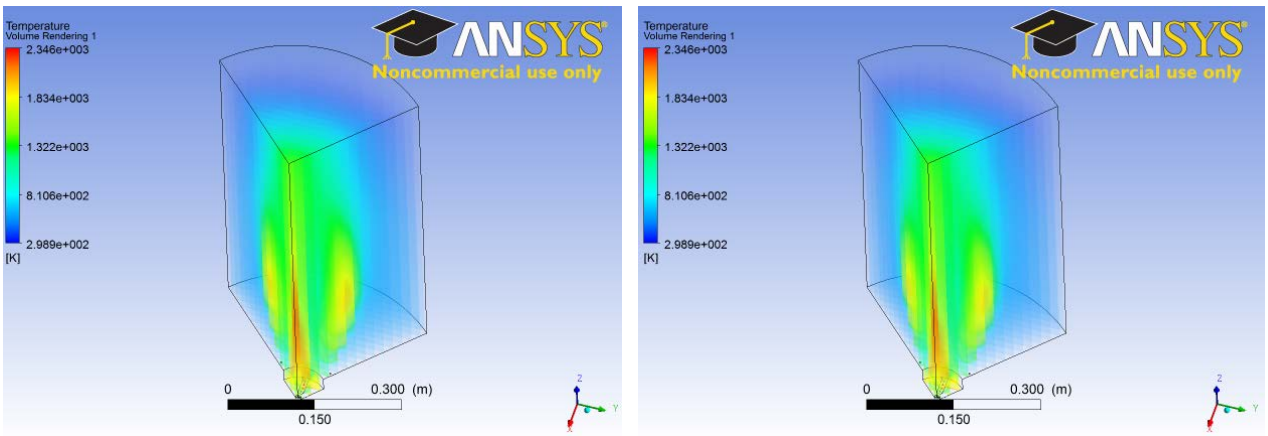

(a) PG (b) NG

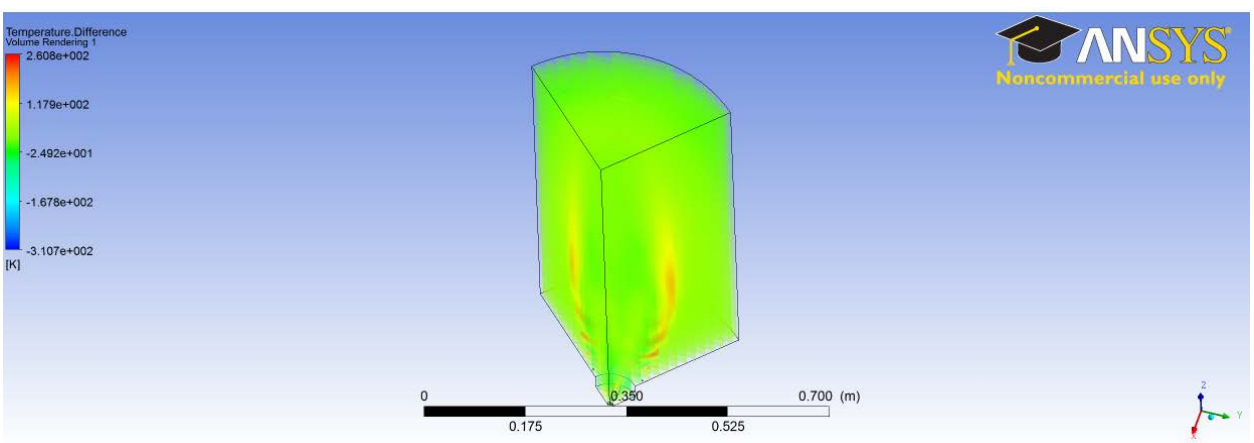

(c) Difference between PG and NG (PG-NG)

6.2 Chemical reactor network (CRN)

The CFD model provides the flow patterns in the combustion chamber. However, to predict NO_x formation, the simplified reaction kinetics used in the CFD is insufficient. By decomposing the overall flowfield into smaller individual chemical reactors, highly detailed reaction kinetics can be used to investigate the nature of NO_x formation. More comprehensive kinetic models are thus introduced without losing the detailed thermal and fluid dynamic information. The input parameters of CRN were determined according to the flow characteristic obtained from CFD simulation. Although the prediction of NO_x was essentially decoupled from the CFD simulation of the combustion environment, no significant effect on the simulation performance occurs because minor species like NO_x only have a small effect on the main combustion process. As a result, the influence of the minor species ignored in the CFD kinetics on on the overall temperature and flow field is negligible. (Faravelli et al., 2001)

6.2.1 Ideal reactor

The advantage of CRN modeling is achieved by using ideal reactors to represent the regions with identical flow patterns and reaction properties. Detailed reaction kinetics can thus be applied with reduced spatial resolution and hence acceptable computational cost. In the current burner, two types of ideal reactors are used: perfect stirred reactor (PSR) and plug flow reactor (PFR). The PSR model assumes reactants are perfectly mixed. It is usually applied for highly turbulent region where a zero dimension simulation can be carried out. The PFR model, on the other hand, is considered for the case where a prevalent streamline is present in the cells of the reactor. Figure 49 (a) shows a typical distribution modeled as a PSR reactor. The velocity vectors are widely spread in all the directions and magnitudes. However, Figure 49 (b) presents a narrow concentration of the velocities. It indicates the presence of a prevalent flow direction which can be described by a PFR reactor. Input parameters for these reactors mainly include residence time and flow rate, which can be determined by post-processing the CFD results.

Figure 49 criteria of ideal reactor selection: (a) polar and sagittal angles of the velocity vectors belonging to a psr reactor. (b) polar and sagittal angles of the velocity vectors belonging to a pfr reactor.(faravelli et al., 2001).

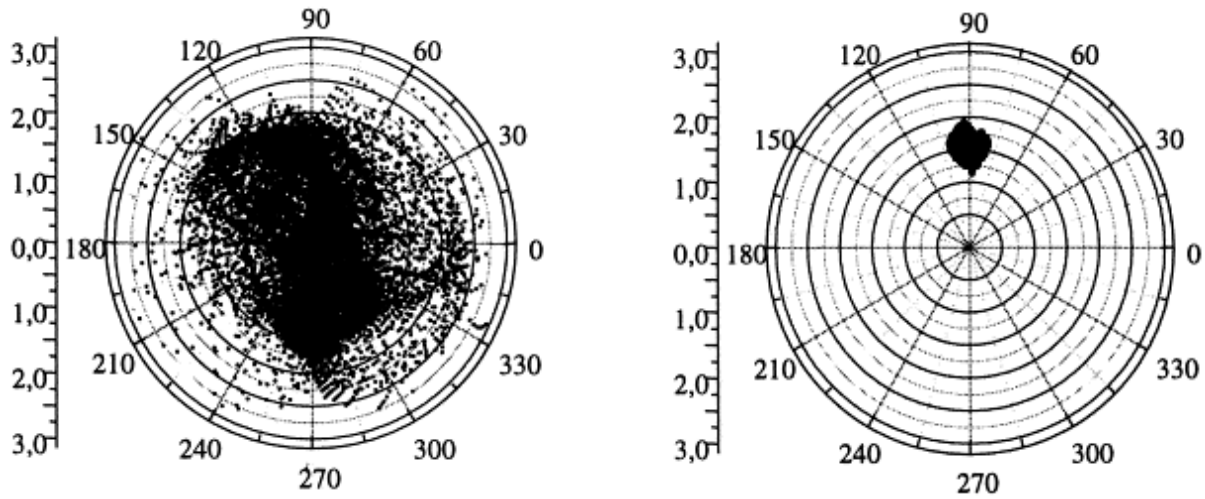

(a) (b)

6.2.2 Construction of CRN model

Figure 50 shows the pathlines passing through reaction region. It can be seen that the flow directions are nearly parallel both in outer and central flames. According to the selection criteria of reactor, these two reaction region can be approximated using PFR. However, the cross jet at the bottom of the flame creates a recirculation zone where flow directions are widely scattered. Therefore, this region can be simulated using a PSR.

Figure 50. Overview of pathlines passing through reaction region, colored by residence time (s)

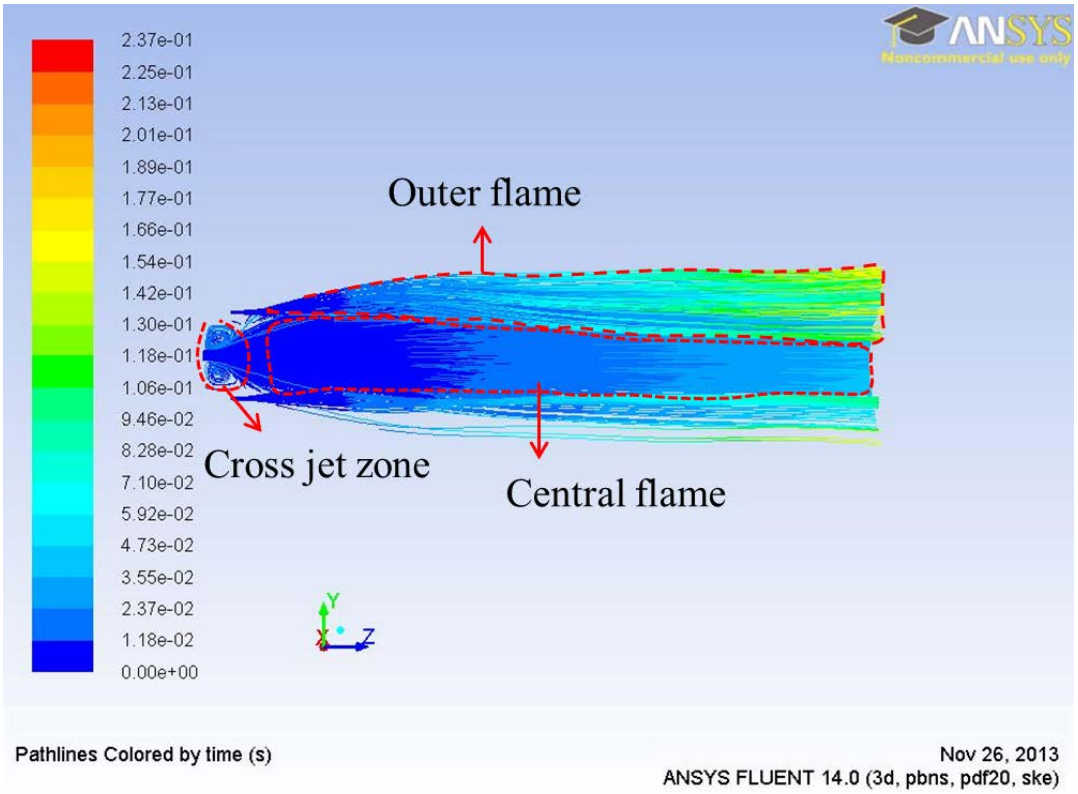

Figure 51 presents an overview of the CRN model constructed using Chemkin 10112. The outer and central flames are both simulated using PFR models (C3 and C5). A PSR model (C1_R1) is applied for the cross jet zone, where the core fuel flow and part of the radial mixture are premixed. The remainder of radial mixture flows into the central flame. Meanwhile, the perpendicular momentum from core fuel injector forces part of the radial mixture diverge from the central stream and feed into the outer flame. The splitting ratio of radial mixture flow and exhaust gas from the cross jet zone are both determined according to CFD. Two gas mixers (C2 and C3), were used for preparation of inflow for the PFRs. The third gas mixer (C6) simulates the post-flame region, gathering exhaust gas from the two reaction regions.

Figure 51 Overview of the CRN Model for Diffusive Flame

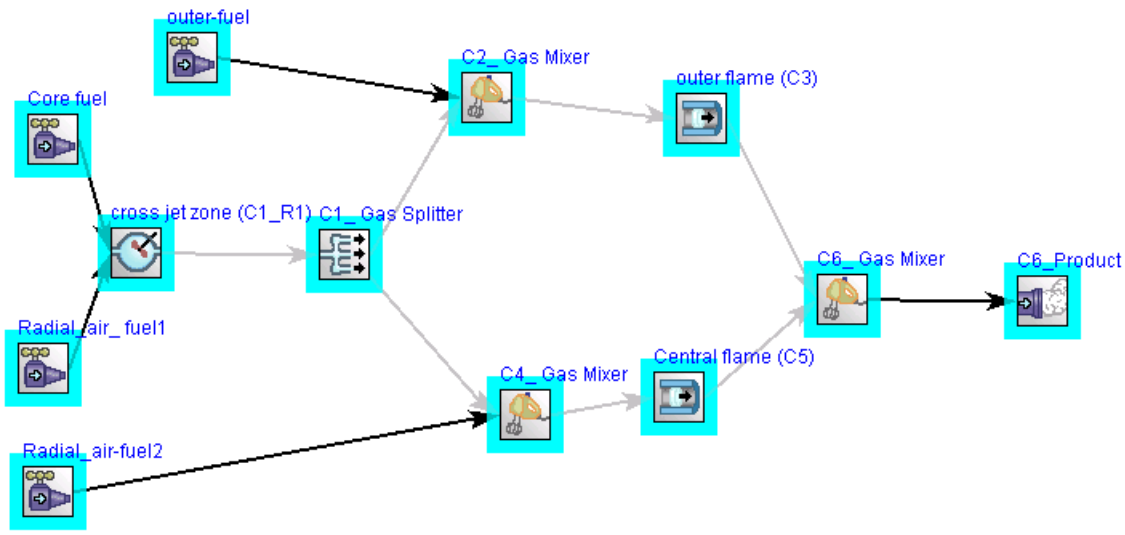

6.3 Results

Figure 52 shows the results of CRN model in terms of NO_x emission. The detailed chemical reaction mechanism used was GRI3.0. The results are shown corrected to 3 percent oxygen to allow comparison with the previously presented measured results. The simulation result shows a trend which is consistent with observations in the tests. The emission level reduces as EA increases. Given a constant heat input, the addition of propane into natural gas causes increase in NO_x emission.

Figure 52 Results of CRN Model in Terms of NO_x Emission, Compared to Measured Data

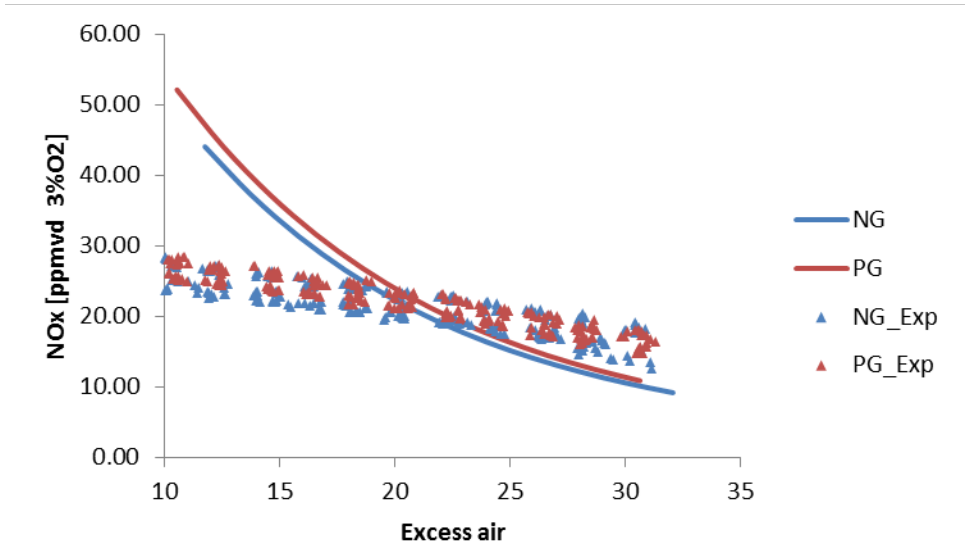

However, the current model is not applicable for all cases with various values of EA. This is mainly due to the dynamic response of reactor inputs to the change of EA. For example, while EA decreases, the fuel flow rate is kept unchanged to ensure the constant heat input. Therefore, the core and outer fuel flow remain the same whereas the radial flow rate decreases. Such variation may yield greater penetration of the cross jet zone into the radial flow. As a result, greater portion of the radial flow is mixed with the core fuel. Meanwhile, the decrease of momentum of radial flow results in larger portion of the exhaust gas from C1_PSR reactor feed into the outer flame. Therefore, to correct the overestimated value in the small EA zone, the split ratio of radial mixture is increased from 50:50 percent to 55:45 percent, for example 55 percent of the radial flow is mixed with core fuel in cross jet zone. Likewise, the split ratio of C1_gas mixer is changed from 50:50 percent to 55:45 percent. Figure 53 presents the corrected data by changing split ratios. NO_x emission drops significantly in low EA side if split ratio is modified according to inlet condition change. It indicates that split ratio substantially affects the prediction performance and the dynamic response should be taken into account while changing EA in the CRN model.

Figure 53 Data Correction by Changing Split Ratios

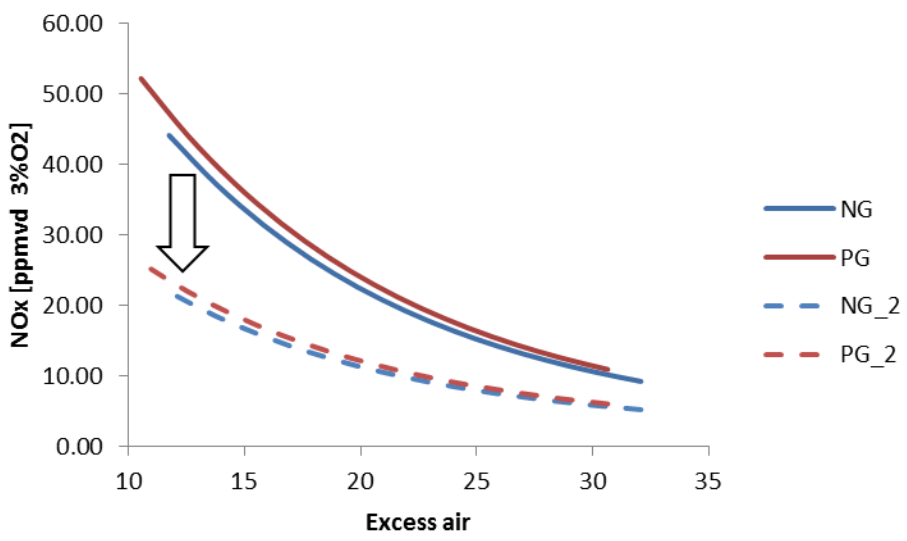

In summary, a CRN model was constructed according to the CFD results. A detailed and comprehensive reaction kinetic was incorporated to predict NO_x emission. The trends were reproduced that addition of propane and lower EA both yield higher NO_x emission level. The fixed split ratio cannot work universally for all tested cases. A correction strategy was demonstrated to deal with this limitation. It points out a need for future work by establishing a CRN model with dynamic reactor parameters.

CHAPTER 7: Conclusions

The following conclusions are drawn from the work:

- For the same operating condition (FS/EA) and heating load, natural gas blended with large amounts of propane produce more NOx than blends with less propane or none at all. To counteract this problem, blends with high amounts of propane must operate at higher EA conditions than the natural gas baseline case. For this reason fuel flexible technology becomes necessary to meet regulation and performance standards.
- A methodology based on a combination of CFD and CRN is able to generally predict the emissions trends as a function of fuel composition. As a result, further affirmation that this methodology can successfully infer how fuel composition impacts emissions has been established.
- A speed of sound sensor can accurately predict the composition, Wobbe Index, and C/H ratio of a binary mixture of natural gas and propane. The ultrasonic sensor was demonstrated to work very well in predicting the composition of a binary mixture; however, if a multi-constituent gas mixture was used (i.e. addition of other hydrocarbon fuels or inert gases such as carbon dioxide) additional sensors such as CO_2 and thermal conductivity sensors would be required.
- Flame luminosity data are linearly correlated to NO_x emissions for natural gas-propane blends burned at the same heating load and is fuel independent. A strong correlation (R^2 = 0.94) was found between these two parameters for blends of 100-0, 95-5, and 92.5-7.5 NG PG. The data presented were only for a specific heating load. Fuel flows with different heating loads were not extensively studied and thus no remarks can be made on trends for these scenarios.
- Oscillations in flame luminosity can quantify the instability of a flame. A high frequency (>1000 Hz) fiber optic reading must be used to accurately measure this parameter in order to capture the fast dynamics of the flame.
- For this Coen scaled Quantum Low NO_x burner, the optimal operating condition for low NO_x is at positive FS and high EA. At these same points the flame is the most unstable. For positive fuel splits the air to fuel ratio at the main combustion zone (Core + Radial) is leaner than negative fuel split operation. This produces an overall cooler flame which produces less NO_x.
- For static data (NF simulations) PDS and DHS algorithms perform relatively the same. The DHS algorithm appeared to have a slight advantage in average number of function computations, but proved to fail slightly more at finding an acceptable NO_x operating condition than the PDS algorithm.

- For static data with fuel transitions (WF simulations) the DHS algorithm found the optimal operating conditions much faster than the PDS algorithm. The PDS algorithm requires many function computations to be taken when using the hill-climbing subroutine. Therefore, even though the initial point for the PDS algorithm is near the new gas blend's optimal condition it must still do a thorough search of the area to converge.
- For noisy data (SNNF simulations) the PDS algorithm took on an order of 4 to 5 times longer to reach an optimal condition than the DHS algorithm, but had a lower NO_x failure rate. If it is desirable to lower the error in the convergence value then more data must be taken in order to be confident in the answer. An inverse relation between speed and accuracy is thus created.
- For noisy data with fuel transitions (SNWF simulations) the DHS algorithm was the most efficient and fastest algorithm in finding an optimal condition. This result follows the same result from the WF simulation. The DHS algorithm has the ability to quickly converge depending on the coefficient values (alpha, beta, and gamma). Once the simplex begins to contract it is very difficult for the simplex to expand back to original size or larger. Thus the DHS algorithm has a faster convergence time, but this also means the convergence can result in a non-optimal condition.
- The DHS algorithm requires significant adjustments in initial simplex size and cycle coefficients. The DHS algorithm can do well for one scenario but does not guarantee it will do well using the same gains for a drastically different scenario (ex: NF to SNNF simulations). This algorithm requires significant interaction with the system and engineer to fine tune the gains of the system. This is an unappealing situation since it would be desirable to have an algorithm that is able to adapt to any situation and require no further interaction with the designer once written.
- The PDS algorithm requires minimal prior information and requires very little adjustment for drastically different scenarios. This algorithm is simple to follow and simple to implement. The PDS algorithm can take significantly more time to converge than the DHS algorithm, but ultimately it can find an acceptable optimal point with fewer errors.

GLOSSARY

Terms	Definition
AFT	Adiabatic Flame Temperature
AVG	Average
BAAQMD	Bay Area Air Quality Management District
Btu	British Thermal Unit
CARB	California Air Resources Board
CEC	California Energy Commission
CFD	Computational Fluid Dynamics
Corr	Corrected
Core (C)	Inner fuel line for quantum burner
CRN	Chemical Reactor Network
DHS	Downhill Simplex
EA	Excess Air
Eff	Efficiency
EIA	Energy Information Administration
EPA	Environmental Protection Agency
FGR	Flue Gas Recirculation
FS	Fuel Split
HHV	Higher heating value
Hr	Hour
Hz	Hertz
lb.	Pound
LNG	Liquid Natural Gas
MBTu	One Thousand British Thermal Units
MFC	Mass Flow Controller
MMBTU	One Million British Thermal Units

MW	Molecular Weight
NF	No Fluctuations
NG	Natural Gas
NGC	Natural Gas Council
NPT	National Pipe Thread
Outer (O)	Outside fuel line in Quantum burner
PDF	Probability Density Function
PDS	Powell's Direction Set
PFR	Plug Flow Reactor
PG	Propane gas
PIER	Public Interest Energy Research
PkPk	Peak to Peak – change between largest magnitude values in signal
PPMvd	parts per million by volume, dry basis
PSI	Pounds Per Square Inch
PSR	Perfectly Stirred Reactor
Radial (R)	Middle fuel line of Quantum Burner
RD&D	Research, Development, and Demonstration
RPS	Renewable Portfolio Standards
SCAQMD	South Coast Area Air Quality Management District
SCF	Standard Cubic Feet
SCFM	Standard Cubic Feet Per Minute
SG	Specific Gravity
SNNF	Simulated Noise with No Fluctuations
SNWF	Simulated Noise with Fluctuations
SOS	Speed of Sound
VYCOR	High temperature glass produced by Corning Inc.
WF	With Fluctuations

AGA	American Gas Association
ANOVA	Analysis of variance

Symbols and Subscripts	Definition
A	Array that holds fifth order approximations set by recorded data
C	Speed of Sound
C/H	Carbon to Hydrogen
CH^*	Methylidyne radical
CH_4	Methane
C_3H_8	Propane
CO	Carbon Monoxide
CO_2	Carbon Dioxide
H	High Rank Point used in Downhill Simplex Method
HCN	Hydrogen Cyanide
J	Performance Index
K	Kelvin, measure of temperature
L	Low Rank Point in downhill simplex method
M	Middle Rank Point in downhill simplex method
N	Number of function computations taken from the initial point to the final optimal value
P	Vertices of "simplex" in downhill simplex method
P	Point on a line used in direction set algorithm
$\bar{P}$	Centroid used in downhill simplex method
R	Random number between 1 and zero set for direction set algorithm and used to define the direction α_o (see above in glossary)
NH	Amine
NH_3	Amonia
NO	Nitric Oxide
NO_2	Nitrogen Dioxide
NO_X	Nitrogen Oxides

N_2	Nitrogen
N_2O	Nitrous Oxide
O	Oxygen
O_2	Oxygen
OH	Hydroxyl
OH*	Hydroxyl Radical
S′	Swirl Intensity
T	Temperature
a	Initially set variable for first point of objective function in direction set algorithm
b	Initially set variable for second point of objective function in direction set algorithm. Initially set to q (see definition for q further below)
c	Initially set variable for third point of objective function in direction set algorithm. Initial variable setting depends on value of first and second objective function. In 5th order approximation m-file used for NO_X data taken at corresponding fuel split (FS) and excess air (EA) testing scenarios
C_w	Specific Heat of Water
abs	Absolute value
d	Turning value in direction set algorithm which is used to predict the possible minimum of an objective function. Function of a,b, and c and corresponding objective functions of those variables.
D_{gas}	Distance in Specific Gas
D_{air}	Distance in Air
e	Accuracy to which minimum is required
exp	Exponential function
f(x)	Objective function used in direction set algorithm
F	Cost Function used in downhill simplex method
%F_global	Percent Error Between Final Converged F and global F for given fuel case
H_1	Reflection Point used in downhill simplex method

Hz	Unit of frequency (1/s)
m	Upper bound to length of step along a line used in direction set algorithm
$\dot{m}_f$	Mass flow rate of fuel
$\dot{m}_w$	Mass flow rate of water
%NO_x Fail	Percentage of how many initial conditions did not converge to an acceptable NO_x Value
q	Order of magnitude of length of step along a line, used in direction set algorithm.
R^2	Coefficient of determination, number that indicates how well data fits a statistical model
tol	Value used to test for convergence of values between function value f(H) and f(L) set in downhill simplex algorithm
w	Weight
X	Position used in direction set algorithm
α_o	Initial direction set in direction set algorithm
α	Constant
β	Contraction Coefficient
η_B	Boiler Efficiency
η_c	Combustion efficiency
η_{EA}	Efficiency Based on Excess Air
$gamma\ (\gamma)$	Expansion Coefficient used in downhill simplex algorithm to solve for the expansion point H
$\boldsymbol{\gamma}$	Specific Heat Ratio – used in speed of sound calculation
λ	Placeholder for variable input into objective function used in direction set algorithm. Term used to minimize objective function f(x) used in direction set algorithm
Φ	Equivalence Ratio
ξ	Direction of a line in direction set algorithm

REFERENCES

Bay Area Air Quality Management District REGULATION 9 INORGANIC GASEOUS POLLUTANTS RULE 7 NITROGEN OXIDES AND CARBON MONOXIDE FROM INDUSTRIAL , INSTITUTIONAL AND COMMERCIAL BOILERS , STEAM GENERATORS AND PROCESS HEATERS (2011).

Brouwer, D. (1996). *Characterization and Design Optimization of a Scaled, UltraLow-NOx Burner*. University of California, Irvine.

Davis, N. T. (1995). *Active Duty Cycle Optimization of Gas Turbine Combustor Performance*. University of California, Irvine.

Davis, N. T., and Samuelsen, G. S. (1996). Optimization of gas turbine combustor performance throughout the duty cycle. *Symposium (International) on Combustion*, *26*(2), 2819–2825. doi:10.1016/S0082-0784(96)80121-4

Demayo, T. (2001). *Robust Active Combustion Control for the Optimization of Environmental Performance and Energy Efficiency*. University of California, Irvine.

EIA. (2013). *Annual Energy Outlook 2013*. Retrieved from www.eia.gov/forecasts/aeo

Faravelli, T., Bua, L., Frassoldati, A., Antifora, A., Tognotti, L., and Ranzi, E. (2001). A new procedure for predicting NOx emissions from furnaces. *Computers & chemical engineering*.

Ferguson, D., Richard, G., and Straub, D. (2008). Fuel Interchangeability for Lean Premixed Combustion in Gas Turbine Engines. *ASME Turbo Expo 2008: Power for Land, Sea, and Air*, *3*(Combustion, Fuels and Emissions).

Ferguson, D., Straub, D., Richards, G., and Robey, E. (2007). Impact of Fuel Variability on Dynamic Instabilities in Gas Turbine Combustion, 1–11.

Flores, M., McDonell, V., and Samuelsen, G. S. (2003). Impact of ethane and propane variation in natural gas on the performance of a model gas turbine combustor. *Journal of Engineering for Gas Turbines and Power*, *125*.

Hack, R., and McDonell, V. (2008). Impact of ethane, propane, and diluent content in natural gas on the performance of a commercial microturbine generator. *Journal of Engineering for Gas Turbines and Power*, *130*.

Hill, S., & Douglas Smoot, L. (2000). Modeling of nitrogen oxides formation and destruction in combustion systems. *Progress in Energy and Combustion Science*, *26*(4-6), 417–458. doi:10.1016/S0360-1285(00)00011-3

Jackson, M. D., and Agrawal, A. K. (1999). Active Control of Combustion for Optimal Performance. *Journal of Engineering for Gas Turbines and Power*, *121*.

Lefebvre, A., and Ballal, D. (2010). *Gas Turbine Combustion: Alternative Fuels and Emissions* (Third Edit.).

Lieuwen, T., McDonell, V., Petersen, E., and Santavicca, D. (2008). Fuel flexibility influences on premixed combustor blowout, flashback, autoignition, and stability. *Journal of Engineering for Gas Turbines and Power*, *130*.

Loubar, K., Rahmouni, C., Le Corre, O., and Tazerout, M. (2007). A combustionless determination method for combustion properties of natural gases. *Fuel*, *86*(16), 2535–2544. doi:10.1016/j.fuel.2007.02.024

Lueptow, R. M., and Phillips, S. (1994). Acoustic sensor for determining combustion properties of natural gas. *Measurement Science and Technology*, *5*(11), 1375–1381. doi:10.1088/0957-0233/5/11/010

Miyasato, M. (2005). Active optimization of the performance of a gas-turbine combustor. *Combustion science and ….* Retrieved from http://www.tandfonline.com/doi/abs/10.1080/00102200590959396

Nelder, J., and Mead, R. (1965). A simplex method for function minimization. *The computer journal*. Retrieved from http://comjnl.oxfordjournals.org/content/7/4/308.short

Padmanabhan, K. T., Bowman, C. T., and Powell, J. D. (1995). An Adaptive Optimal Combustion Control Strategy, *2180*(1), 101–110.

Powell, M. (1964). An efficient method for finding the minimum of a function of several variables without calculating derivatives. *The computer journal*. Retrieved from http://comjnl.oxfordjournals.org/content/7/2/155.short

Press, W., Teukolsky, S., Vetterling, W., and Flannery, B. (2007). *Numerical Recipes: The Art of Scientific Computing* (3rd Editio.). Cambridge University Press.

Rios, L. M., and Sahinidis, N. V. (2012). Derivative-free optimization: a review of algorithms and comparison of software implementations. *Journal of Global Optimization*, *56*(3), 1247–1293. doi:10.1007/s10898-012-9951-y

Samuelsen, G., and Miyasato, M. (2000). Active control for reducing the formation of nitrogen oxides in industrial gas burners and stationary gas turbines. *Californian Energy Commision*. Retrieved from http://scholar.google.com/scholar?hl=en&btnG=Search&q=intitle:ACTIVE+CONTROL+FOR+REDUCING+THE+FORMATION+OF+NITROGEN+OXIDES+IN+INDUSTIAL+GAS+BURNERS+AND+STATIONARY+GAS+TURBINES#0

Scott, D., King, G., and Laurendeau, N. (2002). Chemiluminescence Based Feedback Control of Equivalence Ratio for a Continuous Combustor. *Journal of Propulsion and Power*, *18*(2).

South Coast Air Quality Management District Rule 1146.2: Emissions of Oxides of Nitrogen from Large Water Heaters and Small Boilers and Process Heaters (2006).

St. John, D. (1994). *Active Optimization of a Natural Gas-Fired Research Burner for the Control of Nitrogen Oxides*. University of California, Irvine.

Turns, S. R. (2000). *An introduction to combustion. System* (Vol. 499, p. 411). McGraw-Hill. Retrieved from http://sutlib2.sut.ac.th/sut_contents/H89404.pdf

Appendix A:
5th Order Approximation Code (Approx.m)

```
%% 5th Order Approximation of NOx and LPkPk data
clear
clc
clf
%% Read in data
% Name of the file to be analyzed
datafile = 'Masterdata_clean.xlsx';
% Which sheet to be analyzed
% 1 = 100-0 NG-PG
% 2 = 95-5 NG-PG
% 3 = 92.5-7.5 NG-PG
sheet = 1;

% Read the selected file with the data wanting to be processed
[data,text] = xlsread(datafile,sheet);

[M,N] = size(data);

%% Column descriptions
% 1: time
% 2: O2%
% 3: CO2%
% 4: NOx ppm (uncorrected)
% 5: CO ppm
% 6: Fuel SCFM
% 7: Air SCFM
% 8: EA
% 9: FS
% 10: %CH4
% 11: %C3H8
% 12: Boiler Eff % (HHV)
% 13: Volt SOS
% 14: Temp SOS [F]
% 15: Light AVG
% 16: Light PkPk
% 17: NOx corr ppm
% 18: AFT [K]

EA = data(:,8);
FS = data(:,9);
NOx = data(:,17);
LPKPK = data(:,16);

%% 5th order approximation using EA and FS as inputs
a1 = EA;
a2 = EA.^2;
a3 = EA.^3;
a4 = EA.^4;
a5 = EA.^5;
a6 = EA.^6;
```

```
a7 = EA.^7;
b1 = FS;
b2 = FS.^2;
b3 = FS.^3;
b4 = FS.^4;
b5 = FS.^5;
b6 = FS.^6;
b7 = FS.^7;
A = [a1 a2 a3 a4 a5 b1 b2 b3 b4 b5];

%% Pick either NOx or LPkPk to be approximated
% c = NOx;
c = LPKPK;

%% Compute coefficients
t = inv(A'*A)*A'*c

%% Generate contour to compare results
[X,Y] = meshgrid(10:2:30,5:-1:-5);
J =
X*t(1)+X.^2*t(2)+X.^3*t(3)+X.^4*t(4)+X.^5*t(5)+Y*t(6)+Y.^2*t(7)+Y.^3*t(8)+Y.^
4*t(9)+Y.^5*t(10);
figure(1)
contourf(X,Y,J)

%% Results for different blends
% 100-0 NG-PG:
%  tN = [7.93177779324310;-0.902274401458070;0.0478340422873351;-
0.00121880800974382;1.18789269200147e-05;-
1.08307858944469;0.00586717278470460;0.0387732936657552;0.000568334217205021;
-0.000533436838726728;]
%  tLP = [0.0335030593848174;-0.00145774320008373;-1.45022193282395e-
05;1.86621134258038e-06;-1.94633555466442e-
08;0.00399549142843718;0.000247510011601515;7.47970104533188e-05;-
1.04607771039703e-05;-8.58620451711344e-06;]

% 95-5 NG-PG:
%  tN = [8.99638668167019;-1.07165304769635;0.0602374672786870;-
0.00163945591069701;1.71184168714840e-05;-0.581138363858844;-
0.0168671651894008;0.0278380315148987;-4.76649020158523e-05;-
0.000873716021811252;]
%  tLP = [0.0474525155915965;-0.00352220176077741;7.48316286564009e-
05;1.70944098404558e-06;-5.50874787867381e-08;-2.73294256721041e-
05;0.000386920505896207;0.000184514739444561;-1.04934913926238e-05;-
4.56485301318641e-06;]

% 92.5-7.5 NG-PG:
%  tN = [8.56181241038290;-0.942313331237765;0.0496271997527366;-
0.00128958942050401;1.30453196839340e-05;-0.754752362235309;-
0.0829871838649132;0.0358121616712557;0.00357693537044549;-
0.000644835135734785;]
%  tLP = [0.0411155367440790;-0.00218145722351296;-1.48915488811781e-
05;4.21216011396967e-06;-8.09595673016770e-08;0.00383534944745931;-
0.000263690942895408;-0.000312059763775139;6.28501778128069e-
06;7.91214943459426e-06;]
```

Contour Generation Code (Fmap.m)

```
function [J] = Fmap(NG,wmap)
%Generates contours of cost function, NOx, and LPkPk for the three gases
%Uses the tN and tLP values from Approx.m

if NG == 100
% 100-0 NG-PG
 tN = [7.93177779324310;-0.902274401458070;0.0478340422873351;-
0.00121880800974382;1.18789269200147e-05;-
1.08307858944469;0.00586717278470460;0.0387732936657552;0.000568334217205021;
-0.000533436838726728;];
 tLP = [0.0335030593848174;-0.00145774320008373;-1.45022193282395e-
05;1.86621134258038e-06;-1.94633555466442e-
08;0.00399549142843718;0.000247510011601515;7.47970104533188e-05;-
1.04607771039703e-05;-8.58620451711344e-06;];
elseif NG == 95
% 95-5 NG-PG
 tN =[8.99638668167019;-1.07165304769635;0.0602374672786870;-
0.00163945591069701;1.71184168714840e-05;-0.581138363858844;-
0.0168671651894008;0.0278380315148987;-4.76649020158523e-05;-
0.000873716021811252;];
 tLP =[0.0474525155915965;-0.00352220176077741;7.48316286564009e-
05;1.70944098404558e-06;-5.50874787867381e-08;-2.73294256721041e-
05;0.000386920505896207;0.000184514739444561;-1.04934913926238e-05;-
4.56485301318641e-06;];
else
% 92.5-7.5 NG-PG
 tN = [8.56181241038290;-0.942313331237765;0.0496271997527366;-
0.00128958942050401;1.30453196839340e-05;-0.754752362235309;-
0.0829871838649132;0.0358121616712557;0.00357693537044549;-
0.000644835135734785;];
 tLP = [0.0411155367440790;-0.00218145722351296;-1.48915488811781e-
05;4.21216011396967e-06;-8.09595673016770e-08;0.00383534944745931;-
0.000263690942895408;-0.000312059763775139;6.28501778128069e-
06;7.91214943459426e-06;];
end

%% Compute cost function
[Z,Y] = meshgrid(10:2:30,5:-.25:-5);

NOx =
Z*tN(1)+Z.^2*tN(2)+Z.^3*tN(3)+Z.^4*tN(4)+Z.^5*tN(5)+Y*tN(6)+Y.^2*tN(7)+Y.^3*t
N(8)+Y.^4*tN(9)+Y.^5*tN(10);
LPk =
Z*tLP(1)+Z.^2*tLP(2)+Z.^3*tLP(3)+Z.^4*tLP(4)+Z.^5*tLP(5)+Y*tLP(6)+Y.^2*tLP(7)
+Y.^3*tLP(8)+Y.^4*tLP(9)+Y.^5*tLP(10);
NOxlim = 20;
LPklim = .3;
w = 1/3;
J = w*((NOx/NOxlim).^2+exp(NOx/NOxlim)/exp(1)-1)+w*(LPk/LPklim)+w*sqrt(Z/30);

%% Generate desired contour
if wmap == 1 %Cost function contour
 figure1 = figure(1);
```

```
 % Create axes
 axes1 = axes('Parent',figure1,'Layer','top','CLim',[.88 1.45]);
 box(axes1,'on');
 hold(axes1,'all');
 % Create contour
 contourf(Z,Y,J,'LineColor',[0 0 0],'Fill','on','Parent',axes1);
 % Create title
 title('EA vs Fuel Split Contour Plot: Cost Function');
 % Create xlabel
 xlabel('EA');
 % Create ylabel
 ylabel('Fuel Split');
 % Create colorbar
 colorbar('peer',axes1);
 % Create textbox
 annotation(figure1,'textbox',[0.01029 0.0619 0.08257 0.1038],...
    'String',{'More','Radial'},...
    'FitBoxToText','off');
 % Create textbox
 annotation(figure1,'textbox',[0.01886 0.869 0.07757 0.1024],...
    'String',{'More','Outer'},...
    'FitBoxToText','off');
 % Create textbox
 annotation(figure1,'textbox',[0.9125 0.481 0.09107
0.1024],'String',{'F'},...
    'FitBoxToText','off',...
    'LineStyle','none');
 hold on
elseif wmap == 2 %NOx contour
 hold off
 figure2 = figure(2);
 % Create axes
 axes2 = axes('Parent',figure2,'Layer','top','CLim',[15 30]);
 box(axes2,'on');
 hold(axes2,'all');
 % Create contour
 contourf(Z,Y,NOx,'LineColor',[0 0 0],'Fill','on','Parent',axes2);
 % Create title
 title('EA vs Fuel Split Contour Plot: NOx corr. 3%O2');
 % Create xlabel
 xlabel('EA');
 % Create ylabel
 ylabel('Fuel Split');
 % Create colorbar
 colorbar('peer',axes2);
 % Create textbox
 annotation(figure2,'textbox',[0.01029 0.0619 0.08257 0.1038],...
    'String',{'More','Radial'},...
    'FitBoxToText','off');
 % Create textbox
 annotation(figure2,'textbox',[0.01886 0.869 0.07757 0.1024],...
    'String',{'More','Outer'},...
    'FitBoxToText','off');
 % Create textbox
 annotation(figure2,'textbox',[0.9125 0.481 0.09107
0.1024],'String',{'NOx','ppmvd 3%O2'},...
    'FitBoxToText','off',...
```

```
    'LineStyle','none');
 hold on
else %LPkPk contour
 hold off
 figure3 = figure(3);
 % Create axes
 axes3 = axes('Parent',figure3,'Layer','top','CLim',[.15 .4]);
 box(axes3,'on');
 hold(axes3,'all');
 % Create contour
 contourf(Z,Y,LPk,'LineColor',[0 0 0],'Fill','on','Parent',axes3);
 % Create title
 title('EA vs Fuel Split Contour Plot: LPkPk');
 % Create xlabel
 xlabel('EA');
 % Create ylabel
 ylabel('Fuel Split');
 % Create colorbar
 colorbar('peer',axes3);
 % Create textbox
 annotation(figure3,'textbox',[0.01029 0.0619 0.08257 0.1038],...
    'String',{'More','Radial'},...
    'FitBoxToText','off');
 % Create textbox
 annotation(figure3,'textbox',[0.01886 0.869 0.07757 0.1024],...
    'String',{'More','Outer'},...
    'FitBoxToText','off');
 % Create textbox
 annotation(figure3,'textbox',[0.9125 0.481 0.09107
0.1024],'String',{'LPkPk'},...
    'FitBoxToText','off',...
    'LineStyle','none');
 hold on
end
end
```

Cost Function Code (objfcn.m)

```
function [F, X] = objfcn(NG, P, SN)
%Objective function
%Each time this function runs it simulates a data point being taken
NOxlim = 20; %NOx limit [ppm]
LPlim = .3; %LPkPk limit
muEA = 30; %EA upper bound
mlEA = 10; %EA lower bound
muFS = 5; %FS upper bound
mlFS = -5; %FS lower bound


%% Select gas blend to be analyzed
% t's are 5th order approximations of the data gathered from experiments
% See m-files "NOxApprox.m" and "LPkPkApprox.m" for further details on
calculations
```

```
% How to use t's to approx NOx (tN) and LPKPK (tLP):
% NOx =
EA*tN(1)+EA^2*tN(2)+EA^3*tN(3)+EA^4*tN(4)+EA^5*tN(5)+FS*tN(6)+FS^2*tN(7)+FS^3
*tN(8)+FS^4*tN(9)+FS^5*tN(10)
%  or in matrix notation:
%   NOx = [EA EA^2 EA^3 EA^4 EA^5 FS FS^2 FS^3 FS^4 FS^5]*tN
% LPKPK =
EA*tLP(1)+EA^2*tLP(2)+EA^3*tLP(3)+EA^4*tLP(4)+EA^5*tLP(5)+FS*tLP(6)+FS^2*tLP(
7)+FS^3*tLP(8)+FS^4*tLP(9)+FS^5*tLP(10)
%  or in matrix notation:
%   LPKPK = [EA EA^2 EA^3 EA^4 EA^5 FS FS^2 FS^3 FS^4 FS^5]*tLP

if NG == 100
% 100-0 NG-PG
 tN = [7.93177779324310;-0.902274401458070;0.0478340422873351;-
0.00121880800974382;1.18789269200147e-05;-
1.08307858944469;0.00586717278470460;0.0387732936657552;0.000568334217205021;
-0.000533436838726728;];
 tLP = [0.0335030593848174;-0.00145774320008373;-1.45022193282395e-
05;1.86621134258038e-06;-1.94633555466442e-
08;0.00399549142843718;0.000247510011601515;7.47970104533188e-05;-
1.04607771039703e-05;-8.58620451711344e-06;];
elseif NG == 95
% 95-5 NG-PG
 tN =[8.99638668167019;-1.07165304769635;0.0602374672786870;-
0.00163945591069701;1.71184168714840e-05;-0.581138363858844;-
0.0168671651894008;0.0278380315148987;-4.76649020158523e-05;-
0.000873716021811252;];
 tLP =[0.0474525155915965;-0.00352220176077741;7.48316286564009e-
05;1.70944098404558e-06;-5.50874787867381e-08;-2.73294256721041e-
05;0.000386920505896207;0.000184514739444561;-1.04934913926238e-05;-
4.56485301318641e-06;];
else
% 92.5-7.5 NG-PG
 tN = [8.56181241038290;-0.942313331237765;0.0496271997527366;-
0.00128958942050401;1.30453196839340e-05;-0.754752362235309;-
0.0829871838649132;0.0358121616712557;0.00357693537044549;-
0.000644835135734785;];
 tLP = [0.0411155367440790;-0.00218145722351296;-1.48915488811781e-
05;4.21216011396967e-06;-8.09595673016770e-08;0.00383534944745931;-
0.000263690942895408;-0.000312059763775139;6.28501778128069e-
06;7.91214943459426e-06;];
end

%% Compute the objective function F
Ap = [P(1,1) P(1,1)^2 P(1,1)^3 P(1,1)^4 P(1,1)^5 P(1,2) P(1,2)^2 P(1,2)^3
P(1,2)^4 P(1,2)^5];
X = [Ap*tN Ap*tLP]; %NOx and LPKPK

if SN == 1
 % Add noise to system
 XNOx = -0.2 + (0.2 - (-0.2))*rand(1);
 XLPk = -0.02 + (0.02 - (-0.02))*rand(1);
 X = X + [XNOx XLPk];
 EAsn = P(1,1)-0.2 + (0.2 - (-0.2))*rand(1);
```

```
end

w = 1/3;
F = w*((X(1,1)/NOxlim)^2+exp(X(1,1)/NOxlim)/exp(1)-1) + w*X(1,2)/LPlim +
w*sqrt(P(1,1)/muEA);

% If point is out of bounds make very large F value
if P(1,1) > muEA || P(1,1) < mlEA || P(1,2) > muFS || P(1,2) < mlFS
  F = F + 100;
end

end
```

Hill-Climbing Code (hillclimb.m)

```
function [lam n] = hillclimb(Pl,Epl,NG,SN)
%% Search for minimum along search direction using hill-climbing technique
%Setup
muEA = 30; %EA upper bound
mlEA = 10; %EA lower bound
muFS = 5; %FS upper bound
mlFS = -5; %FS lower bound
ex = 0;
lp = 1;
n = 0;
lam = 0;
s = 1;
trn = 0;
bv = 0;

P2 = Pl + lam*Epl;
[F2(lp,1) X2] = objfcn(NG,P2,SN);
n = n + 1;

while ex == 0
 lp = lp+1;
 lam = lam + sign(s)*1;
 P2 = Pl + lam*Epl;
 %Compute objective function at point
 [F2(lp,1) X2] = objfcn(NG,P2,SN);
 if F2(lp,1) >= 50
     n = n;
 else
     n = n + 1;
 end

 %Compare current F to previous F
 if F2(lp,1) > F2(lp-1,1)
   trn = trn+1;
   s = -1*sign(s);
 end
```

```
 %Convergence check
  if trn >= 3
    ex = 1;
    if bv == 0
    lam = lam + sign(s)*1;
    end
  end

end

end
```

Powell's Direction Set Algorithm for Single Point (PDS_single.m)

```
%% Powell's Direction-Set Algorithm
% The following algorithm is outlined in Chapter 2
clear
clc
clf

% Initial Gas
NG = 100; %Gas blends: 100-0, 95-5, 92.5-7.5 NG-PG...use NG value to declare

% Cost Function topology for given NG
J = Fmap(NG,1);

% Simulated noise on SN = 1 or off SN = 0
SN = 0;

%% Initialization
% Initial Position:
% P(run,EA/FS,iteration) = P(1,:,1) = [EAi FSi]
% X(run,NOx/LPKPK,iteration) = X(1,:,1) = [NOxi LPKPKi]
% Random points:
% EAi = 10 + (30-10).*rand(1);
% FSi = -5 + (5-(-5)).*rand(1);
% Specific points:
EAi = 14;
FSi = -2;

P(1,:,1) = [EAi FSi]; %Initial position
[F(1,1,1) X(1,:,1)] = objfcn(NG,P(1,:,1),SN); %Initial F value

% Initial Search Directions: Ep(run,sEA/sFS,iteration) = Ep(1,:,1) = [sEA 0],
Ep(2,:,1) = [0 sFS]
sEA = 1; %Step length in EA
sFS = .5; %Step length in FS
Ep(1,:,1) = [sEA 0]; %Direction-set 1
Ep(2,:,1) = [0 sFS]; %Direction-set 2
```

```
win = 0; %Logical arguement for algorithm being completed or not
nit = 0; %Number of data points taken
it = 0; %Number of iterations of algorithm
tol = 0.0005; %Convergence tolerance
while win == 0
it = it + 1;

%% Search for minimum along search direction
%First Search Direction
[lam1 n] = hillclimb(P(1,:,it),Ep(1,:,it),NG,SN);
P(2,:,it) = P(1,:,it)+lam1*Ep(1,:,it);
[F(2,1,it) X(2,:,it)] = objfcn(NG,P(2,:,it),SN);
nit = nit + n;
L(1,1,it) = lam1;
%Second Search Direction
[lam2 n] = hillclimb(P(2,:,it),Ep(2,:,it),NG,SN);
P(3,:,it) = P(2,:,it)+lam2*Ep(2,:,it);
[F(3,1,it) X(3,:,it)] = objfcn(NG,P(3,:,it),SN);
nit = nit + n;
L(2,1,it) = lam2;
%Third Search Direction
Ep(3,:,it) = P(3,:,it)-P(1,:,it);
if (Ep(3,:,it)) == 0 %No expansion has occurred
  F(4,1,it) = F(3,1,it);
  P(4,:,it) = P(3,:,it);
  X(4,:,it) = X(3,:,it);
else
 Ep(3,:,it) = Ep(3,:,it)/sqrt(Ep(3,1,it)^2+Ep(3,2,it)^2);
 [lam3 n] = hillclimb(P(3,:,it),Ep(3,:,it),NG,SN);
 P(4,:,it) = P(3,:,it)+lam3*Ep(3,:,it);
 [F(4,1,it) X(4,:,it)] = objfcn(NG,P(4,:,it),SN);
 nit = nit + n;
 L(3,1,it) = lam3;
end
%% Check Convergence
cnv = abs(F(1,1,it)-F(3,1,it));
if cnv <= tol && win == 0
    win = 1;
    J1 = F(4,1,it);
end
%% Create new search directions
if lam1 == 0 || lam2 == 0
  Ep(1,:,it+1) = Ep(1,:,1);
  Ep(2,:,it+1) = Ep(2,:,1);
else
  Ep(1,:,it+1) = Ep(2,:,it);
  Ep(2,:,it+1) = Ep(3,:,it);
end
%% Create new initial position for next iteration
if win == 0
P(1,:,it+1) = P(4,:,it);
F(1,1,it+1) = F(4,1,it);
X(1,:,it+1) = X(1,:,it);
end
end

% Plotting statement
```

```
if it == 1
 plot(P(:,1,1),P(:,2,1),'m-x',P(4,1,1),P(4,2,1),'c-x')
else
 plot(P(:,1,1),P(:,2,1),'m-x',P(:,1,2),P(:,2,2),'c-x')
end

% Percent error in cost function from global value
J2 = abs(min(min(J))-J1)/min(min(J))*100;

%% Results from run
Results(1,1) = nit; % number of data points taken
Results(1,2) = P(1,1,1); % initial EA
Results(1,3) = P(1,2,1); % initial FS
Results(1,4) = P(4,1,it); % final EA
Results(1,5) = P(4,2,it); % final FS
Results(1,6) = J1; % final cost function value
Results(1,7) = J2; % percent error from global cost function value
Results(1,8) = X(4,1,it); % NOx at final position

Results

%% Plots of NOx and LPkPk with PDS route overlaid

Jn = Fmap(NG,2);
plot(P(:,1,1),P(:,2,1),'m-x',P(:,1,2),P(:,2,2),'c-x')

Jn = Fmap(NG,3);
plot(P(:,1,1),P(:,2,1),'m-x',P(:,1,2),P(:,2,2),'c-x')


%% Finished
display('done')
```

Powell's Direction-Set Algorithm for Full FS/EA Map (PDS_Full.m)

```
%% Powell's Direction-Set Algorithm
% The following algorithm is outlined in Chapter 2
clear
clc
clf

% Initial Gas
NG = 100; %Gas blends: 100-0, 95-5, 92.5-7.5 NG-PG...use NG value to declare

% Cost Function Topology for given NG
J = Fmap(NG,1);
```

```
% Simulated noise on SN = 1 or off SN = 0
SN = 0;

rit = 0;
for EAi = 10:1:30
  for FSi = -5:.5:5
  rit = rit+1;

%% Initialization
% Initial Position:
% P(run,EA/FS,iteration) = P(1,:,1) = [EAi FSi]
% X(run,NOx/LPKPK,iteration) = X(1,:,1) = [NOxi LPKPKi]

P(1,:,1) = [EAi FSi]; %Initial position
[F(1,1,1) X(1,:,1)] = objfcn(NG,P(1,:,1),SN);

% Initial Search Directions: Ep(run,sEA/sFS,iteration) = Ep(1,:,1) = [sEA 0],
Ep(2,:,1) = [0 sFS]
sEA = 1; %Step length in EA
sFS = .5; %Step length in FS
Ep(1,:,1) = [sEA 0];
Ep(2,:,1) = [0 sFS];

win = 0; %Logical arguement for algorithm being completed or not
nit = 0; %Number of data points taken
it = 0; %Number of iterations of algorithm
tol = 0.0005; %Convergence tolerance
while win == 0
it = it + 1;

%% Search for minimum along search direction
%First Search Direction
[lam1 n] = hillclimb(P(1,:,it),Ep(1,:,it),NG,SN);
P(2,:,it) = P(1,:,it)+lam1*Ep(1,:,it);
[F(2,1,it) X(2,:,it)] = objfcn(NG,P(2,:,it),SN);
nit = nit + n;
L(1,1,it) = lam1;
%Second Search Direction
[lam2 n] = hillclimb(P(2,:,it),Ep(2,:,it),NG,SN);
P(3,:,it) = P(2,:,it)+lam2*Ep(2,:,it);
[F(3,1,it) X(3,:,it)] = objfcn(NG,P(3,:,it),SN);
nit = nit + n;
L(2,1,it) = lam2;
%Third Search Direction
Ep(3,:,it) = P(3,:,it)-P(1,:,it);
if (Ep(3,:,it)) == 0 %No expansion has occurred
  F(4,1,it) = F(3,1,it);
  P(4,:,it) = P(3,:,it);
  X(4,:,it) = X(3,:,it);
else
 Ep(3,:,it) = Ep(3,:,it)/sqrt(Ep(3,1,it)^2+Ep(3,2,it)^2);
 [lam3 n] = hillclimb(P(3,:,it),Ep(3,:,it),NG,SN);
 P(4,:,it) = P(3,:,it)+lam3*Ep(3,:,it);
 [F(4,1,it) X(4,:,it)] = objfcn(NG,P(4,:,it),SN);
 nit = nit + n;
```

```
 L(3,1,it) = lam3;
end
%% Check Convergence
cnv = abs(F(1,1,it)-F(3,1,it));
if cnv <= tol && win == 0
    win = 1;
    J1 = F(4,1,it);
end
%% Create new search directions
if lam1 == 0 || lam2 == 0
  Ep(1,:,it+1) = Ep(1,:,1);
  Ep(2,:,it+1) = Ep(2,:,1);
else
  Ep(1,:,it+1) = Ep(2,:,it);
  Ep(2,:,it+1) = Ep(3,:,it);
end
%% Create new initial position for next iteration
if win == 0
P(1,:,it+1) = P(4,:,it);
F(1,1,it+1) = F(4,1,it);
X(1,:,it+1) = X(1,:,it);
end
end

% Percent error in cost function from global value
J2 = abs(min(min(J))-J1)/min(min(J))*100;

% Results from run
Results(rit,1) = nit; % number of data points taken
Results(rit,2) = P(1,1,1); % initial EA
Results(rit,3) = P(1,2,1); % initial FS
Results(rit,4) = P(4,1,it); % final EA
Results(rit,5) = P(4,2,it); % final FS
Results(rit,6) = J1; % final cost function value
Results(rit,7) = J2; % percent error from global cost function value
Results(rit,8) = X(4,1,it); % NOx at final position
  end
end

%% Finished
display('done')
```

Downhill Simplex Algorithm for Single Point (DHS_Single.m)

```
%% Downhill Simplex Algorithm
% The following algorithm is outlined in Chapter 2
clear
clc
clf

% Initial Gas
NG = 100; %Gas blends: 100-0, 95-5, 92.5-7.5 NG-PG...use NG value to declare
```

```
% Cost Function topology for given NG
J = Fmap(NG,1);

% Simulated noise on SN = 1 or off SN = 0
SN = 0;

%% Gains
alpha = 1.5;
beta = .4;
gamma = 1.65;

%% Initialization
muEA = 30; %EA upper bound
mlEA = 10; %EA lower bound
muFS = 5; %FS upper bound
mlFS = -5; %FS lower bound

% Initial Position:
% P(vertex,EA/FS,iteration) = P(1,:,1) = [EAi FSi]
% X(vertex,NOx/LPKPK,iteration) = X(1,:,1) = [NOxi LPKPKi]

%Initial random point, right angle triangle generation for two other points
% EAi = 10 + (30-10).*rand(1);
% FSi = -5 + (5-(-5)).*rand(1);
EAi = 14;
FSi = -2;
P(1,:,1) = [EAi FSi]; %Initial position 1

st = 4; %EA direction
P(2,:,1) = [P(1,1,1)+st P(1,2,1)]; %Initial position 2
if P(2,1,1) > muEA || P(2,1,1) < mlEA || P(2,2,1) > muFS || P(2,2,1) < mlFS
  P(2,:,1) = [P(1,1,1)-st P(1,2,1)];
end

st = 2.5; %FS direction
P(3,:,1) = [P(1,1,1) P(1,2,1)+st]; %Initial position 2
if P(3,1,1) > muEA || P(3,1,1) < mlEA || P(3,2,1) > muFS || P(3,2,1) < mlFS
  P(3,:,1) = [P(1,1,1) P(1,2,1)-st];
end

win = 0; %Logical arguement for algorithm being completed or not
nit = 0; %Number of data points taken
it = 0; %Number of iterations of algorithm
tol = 0.0005; %Convergence tolerance
while win == 0
it = it + 1;
%Block 1: Find Centroid, compute F's, rank point H,M,L
Pc(it,:) = (P(1,:,it)+P(2,:,it)+P(3,:,it))/3; %Centroid position
F(1,1,it) = objfcn(NG,P(1,:,it),SN); %F vertex 1
F(2,1,it) = objfcn(NG,P(2,:,it),SN); %F vertex 2
F(3,1,it) = objfcn(NG,P(3,:,it),SN); %F vertex 3
if it == 1
 nit = nit + 3; %Further iterations have already computed vertices' F's
end
[Fh, hi] = max(F(:,1,it));
H = P(hi,:,it);
```

```
[Fl, li] = min(F(:,1,it));
L = P(li,:,it);
if (hi == 1 && li == 2) || (hi == 2 && li == 1)
 M = P(3,:,it);
 Fm = F(3,:,it);
elseif (hi == 1 && li == 3) || (hi == 3 && li == 1)
 M = P(2,:,it);
 Fm = F(2,:,it);
else
 M = P(1,:,it);
 Fm = F(1,:,it);
end

%Block 2: Reflection
H1 = (1+alpha)*Pc(it,:) - alpha*H;
Fh1 = objfcn(NG,H1,SN); %F reflection vertex
nit = nit + 1;

if Fh1 < Fl
 %Block 3: Expansion
  H2 = gamma*H1 + (1-gamma)*Pc(it,:);
  Fh2 = objfcn(NG,H2,SN); %F expansion vertex
  nit = nit + 1;
  if Fh2 < Fh1
   H = H2;
  else
   H = H1;
  end

else
 if Fh1 < Fm
   H = H1;
 else
 %Block 4: Single Contraction
  H3 = beta*H + (1-beta)*Pc(it,:);
  Fh3 = objfcn(NG,H3,SN); %F contraction vertex
  nit = nit + 1;

  if Fh3 < Fh
   H = H3;
  else
  %Block 5: Double Contraction
   M = (M+L)/2;
   Fm = objfcn(NG,M,SN); %F mid contraction vertex
   nit = nit + 1;
   H = H3;
  end

 end
end

%Block 6: Convergence check
Fh = objfcn(NG,H,SN);
cnv = abs(Fh - Fl);
if cnv <= tol
 win = 1;
```

```
 [J1 xi] = min([Fh Fm Fl]);
 Pc(it+1,:) = (H+M+L)/3;
 if xi == 1
    pr = H;
 elseif xi == 2
    pr = M;
 else
    pr = L;
 end

 P(1,:,it+1) = H;
 P(2,:,it+1) = M;
 P(3,:,it+1) = L;
 Pc(it+1,:) = (P(1,:,it+1)+P(2,:,it+1)+P(3,:,it+1))/3; %Centroid position

else
 P(1,:,it+1) = H;
 P(2,:,it+1) = M;
 P(3,:,it+1) = L;
end
end

% Plotting statement
% Plots initial simplex and then only shows centroid movement
plot(Pc(:,1),Pc(:,2),'m-x')
plot(P(1,1,1),P(1,2,1),'k-x',P(2,1,1),P(2,2,1),'k-x',P(3,1,1),P(3,2,1),'k-x')

% Percent error in cost function from global value
J2 = abs(min(min(J))-J1)/min(min(J))*100;
% Calculates the NOx value at final position
[J3 X] = objfcn(NG,pr,SN);

%% Results from run
Results(1,1) = nit; % number of data points taken
Results(1,2) = P(1,1,1); % initial EA
Results(1,3) = P(1,2,1); % initial FS
Results(1,4) = pr(1); % final EA
Results(1,5) = pr(2); % final FS
Results(1,6) = J1; % final cost function value
Results(1,7) = J2; % percent error from global cost function value
Results(1,8) = X(1,1); % NOx at final position

Results

%% Plots of NOx and LPkPk
Jn = Fmap(NG,2);
plot(Pc(:,1),Pc(:,2),'m-x')
plot(P(1,1,1),P(1,2,1),'k-x',P(2,1,1),P(2,2,1),'k-x',P(3,1,1),P(3,2,1),'k-x')

Jn = Fmap(NG,3);
plot(Pc(:,1),Pc(:,2),'m-x')
plot(P(1,1,1),P(1,2,1),'k-x',P(2,1,1),P(2,2,1),'k-x',P(3,1,1),P(3,2,1),'k-x')


%% Finished
display('done')
```

Downhill Simplex Algorithm for Full FS/EA Map (DHS_Full.m)

```
%% Downhill Simplex Algorithm
% The following algorithm is outlined in Chapter 2
clear
clc
clf

% Initial Gas
NG = 100; %Gas blends: 100-0, 95-5, 92.5-7.5 NG-PG...use NG value to declare

% Cost Function topology for given NG
J = Fmap(NG,1);

% Simulated noise on SN = 1 or off SN = 0
SN = 0;

%% Gains
alpha = 1.5;
beta = .4;
gamma = 1.65;

rit = 0;
for EAi = 10:1:30
  for FSi = -5:.5:5
  rit = rit+1;
%% Initialization
muEA = 30; %EA upper bound
mlEA = 10; %EA lower bound
muFS = 5; %FS upper bound
mlFS = -5; %FS lower bound

% Initial Position:
% P(vertex,EA/FS,iteration) = P(1,:,1) = [EAi FSi]
% X(vertex,NOx/LPKPK,iteration) = X(1,:,1) = [NOxi LPKPKi]

%Initial random point, right angle triangle generation for two other points
P(1,:,1) = [EAi FSi]; %Initial position 1

st = 4; %EA direction
P(2,:,1) = [P(1,1,1)+st P(1,2,1)]; %Initial position 2
if P(2,1,1) > muEA || P(2,1,1) < mlEA || P(2,2,1) > muFS || P(2,2,1) < mlFS
  P(2,:,1) = [P(1,1,1)-st P(1,2,1)];
end

st = 2.5; %FS direction
P(3,:,1) = [P(1,1,1) P(1,2,1)+st]; %Initial position 2
if P(3,1,1) > muEA || P(3,1,1) < mlEA || P(3,2,1) > muFS || P(3,2,1) < mlFS
  P(3,:,1) = [P(1,1,1) P(1,2,1)-st];
end

win = 0; %Logical arguement for algorithm being completed or not
nit = 0; %Number of data points taken
```

```
it = 0; %Number of iterations of algorithm
tol = 0.0005; %Convergence tolerance
while win == 0
it = it + 1;
%Block 1: Find Centroid, compute F's, rank point H,M,L
Pc(it,:) = (P(1,:,it)+P(2,:,it)+P(3,:,it))/3; %Centroid position
F(1,1,it) = objfcn(NG,P(1,:,it),SN); %F vertex 1
F(2,1,it) = objfcn(NG,P(2,:,it),SN); %F vertex 2
F(3,1,it) = objfcn(NG,P(3,:,it),SN); %F vertex 3
if it == 1
 nit = nit + 3; %Further iterations have already computed vertices' F's
end
[Fh, hi] = max(F(:,1,it));
H = P(hi,:,it);
[Fl, li] = min(F(:,1,it));
L = P(li,:,it);
if (hi == 1 && li == 2) || (hi == 2 && li == 1)
 M = P(3,:,it);
 Fm = F(3,:,it);
elseif (hi == 1 && li == 3) || (hi == 3 && li == 1)
 M = P(2,:,it);
 Fm = F(2,:,it);
else
 M = P(1,:,it);
 Fm = F(1,:,it);
end

%Block 2: Reflection
H1 = (1+alpha)*Pc(it,:) - alpha*H;
Fh1 = objfcn(NG,H1,SN); %F reflection vertex
nit = nit + 1;

if Fh1 < Fl
 %Block 3: Expansion
  H2 = gamma*H1 + (1-gamma)*Pc(it,:);
  Fh2 = objfcn(NG,H2,SN); %F expansion vertex
  nit = nit + 1;
  if Fh2 < Fh1
   H = H2;
  else
   H = H1;
  end

else
 if Fh1 < Fm
   H = H1;
 else
 %Block 4: Single Contraction
  H3 = beta*H + (1-beta)*Pc(it,:);
  Fh3 = objfcn(NG,H3,SN); %F contraction vertex
  nit = nit + 1;

  if Fh3 < Fh
   H = H3;
  else
  %Block 5: Double Contraction
```

```
    M = (M+L)/2;
    Fm = objfcn(NG,M,SN); %F mid contraction vertex
    nit = nit + 1;
    H = H3;
   end

  end
 end

%Block 6: Convergence check
Fh = objfcn(NG,H,SN);
cnv = abs(Fh - Fl);
if cnv <= tol
 win = 1;
 [J1 xi] = min([Fh Fm Fl]);
 Pc(it+1,:) = (H+M+L)/3;
 if xi == 1
    pr = H;
 elseif xi == 2
    pr = M;
 else
    pr = L;
 end

 P(1,:,it+1) = H;
 P(2,:,it+1) = M;
 P(3,:,it+1) = L;
 Pc(it+1,:) = (P(1,:,it+1)+P(2,:,it+1)+P(3,:,it+1))/3; %Centroid position

else
 P(1,:,it+1) = H;
 P(2,:,it+1) = M;
 P(3,:,it+1) = L;
end
end

% Percent error in cost function from global value
J2 = abs(min(min(J))-J1)/min(min(J))*100;
% Calculates the NOx value at final position
[J3 X] = objfcn(NG,pr,SN);

% Results from run
Results(rit,1) = nit; % number of data points taken
Results(rit,2) = P(1,1,1); % initial EA
Results(rit,3) = P(1,2,1); % initial FS
Results(rit,4) = pr(1); % final EA
Results(rit,5) = pr(2); % final FS
Results(rit,6) = J1; % final cost function value
Results(rit,7) = J2; % percent error from global cost function value
Results(rit,8) = X(1,1); % NOx at final position

  end
end


%% Finished
```

```
display('done')
```